THERMAL, MECHANICAL AND DIELECTRIC PROPERTIES OF ETHYLENE-CO-VINYL ACETATE BASED COMPOSITES

Thesis submitted to
the University of Calicut in partial fulfilment of
the requirements for the award of the degree of

DOCTOR OF PHILOSOPHY IN CHEMISTRY

by

ANNIE STEPHY

Under the supervision of
DR. TANIA FRANCIS

DEPARTMENT OF CHEMISTRY
ST. JOSEPH'S COLLEGE (AUTONOMOUS) DEVAGIRI,
CALICUT, KERALA – 673008
(Affiliated to University of Calicut)
JANUARY 2024

DEPARTMENT OF CHEMISTRY
ST. JOSEPH'S COLLEGE (AUTONOMOUS) DEVAGIRI
CALICUT - 673 008, KERALA, INDIA.
'College with potential for excellence',
Accredited by **NAAC** with Grade **A**$^{++}$
Affiliated to University of Calicut

Dr. Tania Francis
Assistant Professor & Head

Tel: +91 9496928889; 9895726068
Email: francistania76@gmail.com

Date:.....

CERTIFICATE

This is to certify that the thesis entitled **"THERMAL, MECHANICAL AND DIELECTRIC PROPERTIES OF ETHYLENE-CO-VINYL ACETATE BASED COMPOSITES"** is an authentic record of the research work carried out by Ms. **Annie Stephy**, under my supervision and guidance in partial fulfilment of the requirements for the award of the degree of **Doctor of Philosophy in Chemistry** under the **Faculty of Science**, University of Calicut, Kerala. The contents of the thesis have been checked for plagiarism using the software '***iThenticate***' and the similarity index falls under permissible limit. I further certify that the contents of this thesis have not been submitted elsewhere for any other degree or diploma.

I also certify that the corrections/ suggestions recommended by the adjudicators have been incorporated in the thesis.

Kozhikode **Dr. Tania Francis**

DECLARATION

I hereby declare that the work presented in the thesis entitled **"THERMAL, MECHANICAL AND DIELECTRIC PROPERTIES OF ETHYLENE-CO-VINYL ACETATE BASED COMPOSITES"** is based on the original work done by me under the guidance of **Dr. Tania Francis**, Assistant Professor & Head, Department of Chemistry, St. Joseph's College (Autonomous) Devagiri, Calicut and has not been included in any other thesis submitted previously for the award of any degree. The contents of the thesis are undergone plagiarism check using '***iThenticate'*** software at C.H.M.K. Library, University of Calicut, and the similarity index found within the permissible limit. I also declare that the thesis is free from AI generated contents.

Kozhikode **Annie Stephy**
Date

Signature of the Supervising teacher:
Name:

ACKNOWLEDGEMENTS

As I reach towards the finale of my days as a PhD scholar the feeling of ecstasy and pride is equally overwhelming. It feels surreal to finally reach this milestone. However, the realisation of all that I have achieved at this juncture of my life is not just through my own work makes me humble and grateful. There have been many individuals that acted as catalysts during the course of my PhD life and this thesis would be incomplete without bestowing my gratitude and respect to them.

Like every other person, I've also had my highs and lows. ***Dr. Tania Francis****, my guide and supervisor, stayed as a strong pillar for me throughout this period. She has always pushed me to achieve better results and accomplishments by providing insightful suggestions and critiques. During my lows she stayed as a strong shoulder for me to lean on and extended her hand to pull me through the falls. She is not just my research supervisor; she is practically family. We say that we shouldn't thank our family. However, I would like to tender her my gratitude with utmost sincerity.*

It was not just my supervisor who encouraged me during the course of my PhD. I was fortunate enough to have an eminent person like ***Dr. Akshay Pottathil*** *in my life as a mentor and brother. His constant encouragement and motivation helped me finish my research work despite the hurdles I had to face.*

I acknowledge the research scholars and staff of Department of Polymer Science and Rubber Technology, Cochin University of Science and Technology (CUSAT) helping me from the sample preparation to sample analysis, especially ***Dr. Honey John*** *for her guidance during the small tenure while I worked with her under ASPIRE fellowship.*

I extend my special gratitude to the Manager, Fr. Fr. Biju K Isacc CMI, to the Principal, Dr. Boby Jose and also to Dr. Sateesh George (Principal in-charge). I would also like to remember former manager, Late Fr. Joseph Paikada CMI, and along with the former managers and Principals Dr. Sibichen M Thomas, Dr. Sabu K Thomas, Dr. Jose John Mallikasseri of St. Joseph's College (Autonomous) Devagiri. I'm grateful towards former Heads of the Department of Chemistry, Dr. Joy Joseph and Dr. Babu I Maliakkal for their support during my research tenure. I also would like to thank all the teaching and non-teaching staff of St. Joseph's College (Autonomous) Devagiri for their wishes and co-operation.

Special thanks to Dr. Abraham Joseph, Dr. N K Renuka and Dr. M T Ramesan members of the Research Advisory Committee for their critique and encouragement throughout my research period

I acknowledge the Department of Collegiate Education, Government of Kerala for ASPIRE- Scholarship, and St. Joseph's College (Autonomous) Devagiri for financial support under Rashtriya Uchchatar Shiksha Abhiyan (RUSA).

I acknowledge all the research scholars of St. Joseph's College (Autonomous) Devagiri particularly Dr. Meril Shelly, Ms. Bashpa P and Ms. Sini K S for making the tiresome research period a lot bearable.

It is with immense humility and respect I thank the two most important people in my life, my parents, ***Joy Valavil*** *and* ***Saly Joy****. They have supported me through thick and thin and allowed me to follow my interests throughout. Without them I would not be able to achieve the things in my life. I feel luck and am proud to be their daughter. Along with my parents I'd like to offer my heartful gratitude towards my friends for putting up with my emotional roller coasters and helping me to not fall lack of confidence.*

From the countless hours spent working to the moments of self-doubt, I weathered every storm that came my way with the aid from God Almighty. No words would be enough to express my gratefulness towards the grace he provided me with.

I bid farewell to the familiar halls of academia and step into the vast arena of possibilities. This whole journey was a huge chapter of the book of my life

Annie Stephy

Dedicated to

My Appan & Amma

ABSTRACT

The selection of a material for a specific application is carried out by analysing the performance under different mechanical, thermal and electrical conditions for any material. In this aspect polymer composites become a unique group whose properties can be tuned in accordance with the applications. The present research work carries out an extensive study on composites of ethylene-co-vinyl acetate (EVA) with modified chitosan as fillers keeping in mind the necessity of waste to energy goal.

As an initial step towards the development of composites, modification of chitosan via graft polymerization is carried out. These modified chitosans namely, chitosan-g-PANi, chitosan-g-MMA, chitosan-g-HEMA and chitosan/phytic acid polyelectrolyte complex, were used as fillers in the polymer composites that were processed via melt-mixing. The processed polymer composites were characterized using infrared spectroscopy, mechanical and thermogravimetric analysis. The ones that comprised of chitosan-g-PANi were further explored for their dielectric properties. The thermal degradation kinetics and thermodynamic parameters were calculated for the developed materials. Non-isothermal model free methods viz, Flynn-Wall-Ozawa (FWO), Kissinger-Akahira-Sunose (KAS), Starink, Tang, Friedman (FR) and Vyazovkin were employed for the calculation. The activation energy values obtained by the differential FR method shows an increase compared to the integral methods like FWO, KAS, Starink

and Tang. This is due to the lack of assumptions and approximations employed during the calculations via FR method.

The mechanical testing showed that the composites other than EVA/chitosan-g-PANi showed decrease in tensile strength with increase filler content. Samples with grafted PANi showed increased tensile strength with increase in filler concentration. The model-free kinetic methods pointed towards the endothermic nature of the degradation process progressed by the formation of activated complexes for all four systems. The study signifies the need for better understanding towards the degradation properties which will aid in developing methods in industrial scale recycling of similar materials. Further the developed materials can be investigated towards flame retardant and food packaging applications.

Keywords: EVA based composites, grafting, degradation kinetics, mechanical, dielectrics

സംഗ്രഹം

ഏതെങ്കിലും മെറ്റീരിയലിന്റെ വ്യത്യസ്ത മെക്കാനിക്കൽ, തെർമൽ, ഇലക്ട്രിക്കൽ സാഹചര്യങ്ങളിൽ പ്രകടനം വിശകലനം ചെയ്തുകൊണ്ടാണ് ഒരു നിർദ്ദിഷ്ട ആപ്ലിക്കേഷനായി ഒരു മെറ്റീരിയൽ തിരഞ്ഞെടുക്കുന്നത്. ഈ വശത്ത്, പോളിമർ കോമ്പോസിറ്റുകൾ ഒരു അദ്വിതീയ ഗ്രൂപ്പായി മാറുന്നു, അവയുടെ ഗുണവിശേഷതകൾ ആപ്ലിക്കേഷനുകൾക്ക് അനുസൃതമായി ട്യൂൺ ചെയ്യാൻ കഴിയും. ഊർജ്ജ ലക്ഷ്യത്തിലേക്കുള്ള മാലിന്യത്തിന്റെ ആവശ്യകത കണക്കിലെടുത്ത് ഫില്ലറുകളായി പരിഷ്കരിച്ച ചിറ്റോസൻ ഉപയോഗിച്ച് എഥിലീൻ-കോ-വിനൈൽ അസറ്റേറ്റ് (ഇവിഎ) സംയുക്തങ്ങളെക്കുറിച്ചുള്ള വിപുലമായ പഠനം നിലവിലെ ഗവേഷണ പ്രവർത്തനങ്ങൾ നടത്തുന്നു.

കമ്പോസിറ്റുകളുടെ വികസനത്തിലേക്കുള്ള പ്രാരംഭ ഘട്ടമെന്ന നിലയിൽ, ഗ്രാഫ്റ്റ് പോളിമറൈസേഷൻ വഴി ചിറ്റോസന്റെ പരിഷ്ക്കരണം നടത്തുന്നു. ചിറ്റോസാൻ-ജി-പാനി, ചിറ്റോസാൻ-ജി-എംഎംഎ, ചിറ്റോസാൻ-ജി-ഹീമ, ചിറ്റോസാൻ/ഫൈറ്റിക് ആസിഡ് പോളി ഇലക്ട്രോലൈറ്റ് കോംപ്ലക്സ് എന്നിങ്ങനെയുള്ള പരിഷ്ക്കരിച്ച ഈ ചിറ്റോസാനുകൾ, മെൽറ്റ്-മിക്സിംഗ് വഴി

സംസ്കരിച്ച പോളിമർ കോമ്പോസിറ്റുകളിൽ ഫില്ലറുകളായി ഉപയോഗിച്ചു. ഇൻഫ്രാറെഡ് സ്പെക്ട്രോസ്കോപ്പി, മെക്കാനിക്കൽ, തെർമോഗ്രാവിമെട്രിക് വിശകലനം എന്നിവ ഉപയോഗിച്ചാണ് പ്രോസസ്സ് ചെയ്ത പോളിമർ കോമ്പോസിറ്റുകളുടെ സവിശേഷത. ചിറ്റോസാൻ-ജി-പാനി അടങ്ങിയവ അവയുടെ വൈദ്യുത ഗുണങ്ങൾക്കായി കൂടുതൽ പര്യവേക്ഷണം ചെയ്തു. വികസിപ്പിച്ച മെറ്റീരിയലുകൾക്കായി താപ ഡീഗ്രേഡേഷൻ ചലനാത്മകതയും തെർമോഡൈനാമിക് പാരാമീറ്ററുകളും കണക്കാക്കി. ഫ്ലിൻ-വാൾ-ഒസാവ (എഫ്ഡബ്ല്യുഒ), കിസിംഗർ-അകാഹിറ-സുനോസ് (കെഎഎസ്), സ്റ്റാറിങ്ക്, ടാങ്, ഫ്രീഡ്മാൻ (എഫ്ആർ), വ്യാസോവ്കിൻ എന്നീ നോൺ-ഐസോതെർമൽ മോഡൽ ഫ്രീ രീതികളാണ് കണക്കുകൂട്ടലിനായി ഉപയോഗിച്ചത്. എഫ്ഡബ്ല്യുഒ, കെഎഎസ്, സ്റ്റാറിങ്ക്, ടാങ് തുടങ്ങിയ അവിഭാജ്യ രീതികളുമായി താരതമ്യപ്പെടുത്തുമ്പോൾ ഡിഫറൻഷ്യൽ എഫ്ആർ രീതിയിലൂടെ ലഭിക്കുന്ന ആക്റ്റിവേഷൻ എനർജി മൂല്യങ്ങൾ വർദ്ധനവ് കാണിക്കുന്നു. എഫ്ആർ രീതിയിലൂടെയുള്ള കണക്കുകൂട്ടലുകളുടെ സമയത്ത് ഉപയോഗിച്ച അനുമാനങ്ങളുടെയും ഏകദേശങ്ങളുടെയും അഭാവമാണ് ഇതിന് കാരണം.

മെക്കാനിക്കൽ പരിശോധനയിൽ EVA/chitosan-g-PANi ഒഴികെയുള്ള സംയുക്തങ്ങൾ

ഫില്ലർ ഉള്ളടക്കം വർദ്ധിപ്പിക്കുന്നതിനനുസരിച്ച് ടെൻസൈൽ ശക്തി കുറയുന്നതായി കാണിച്ചു. ഗ്രാഫ്റ്റ് ചെയ്ത പാനി ഉപയോഗിച്ചുള്ള സാമ്പിളുകൾ ഫില്ലർ കോൺസൺട്രേഷൻ വർദ്ധിപ്പിച്ചുകൊണ്ട് വർദ്ധിച്ച ടെൻസൈൽ ശക്തി കാണിച്ചു. നാല് സിസ്റ്റങ്ങൾക്കുമായി സജീവമാക്കിയ കോംപ്ലക്സുകളുടെ രൂപീകരണത്തിലൂടെ പുരോഗമിച്ച ഡീഗ്രഡേഷൻ പ്രക്രിയയുടെ എൻഡോതെർമിക് സ്വഭാവത്തിലേക്ക് ചൂണ്ടിക്കാണിച്ച മോഡൽ രഹിത ചലനാത്മക രീതികൾ. സമാന വസ്തുക്കളുടെ വ്യാവസായിക തലത്തിൽ പുനരുപയോഗം ചെയ്യുന്നതിനുള്ള രീതികൾ വികസിപ്പിക്കുന്നതിന് സഹായിക്കുന്ന ഡീഗ്രഡേഷൻ പ്രോപ്പർട്ടികളെ കുറിച്ച് നന്നായി മനസ്സിലാക്കേണ്ടതിന്റെ ആവശ്യകതയെ പഠനം സൂചിപ്പിക്കുന്നു. കൂടുതൽ വികസിപ്പിച്ച വസ്തുക്കൾ ഫ്ലേം റിട്ടാർഡന്റ്, ഫുഡ് പാക്കേജിംഗ് ആപ്ലിക്കേഷനുകൾ എന്നിവയിലേക്ക് അന്വേഷിക്കാവുന്നതാണ്.

സൂചകപദങ്ങൾ: EVA അടിസ്ഥാനമാക്കിയുള്ള സംയുക്തങ്ങൾ, ഗ്രാഫ്റ്റിംഗ്, ഡീഗ്രഡേഷൻ കൈനറ്റിക്സ്, മെക്കാനിക്കൽ, ഡൈഇലക്ട്രിക്സ്

CONTENTS

LIST OF TABLES

LIST OF FIGURES

LIST OF ABBREVIATIONS

EVA	:	Ethylene-co-Vinyl Acetate
CHM	:	chitosan-g-HEMA
CMM	:	chitosan-g-MMA
CPS	:	chitosan-g-PANi
CS	:	Chitosan
Ea	:	Activation Energy
EC	:	EVA/chitosan
ECHM	:	EVA/ chitosan-g-HEMA
ECMM	:	EVA/ chitosan-g-MMA
ECP	:	EVA/chitosan-g-PANi
ECPE	:	EVA/PEC
FESEM	:	Field Emission Scanning Electron Microscopy
FITR	:	Fourier-Transform Infrared
FR	:	Friedman
FWO	:	Flynn-Wall-Ozawa
HEMA	:	2-Hydroxy Ethyl Methacrylate
Hz	:	Hertz
KAS	:	Kissinger-Akahira-Sunose
MMA	:	Methyl Methacrylate
PA	:	Phytic Acid
PANi	:	Polyaniline

PEC	:	Polyelectrolyte complex
TGA	:	Thermogravimetric Analysis
TS	:	Tensile Strength
UTM	:	Universal Testing Machine
α	:	Conversion rate
β	:	Heating rate

Preface

Polymers especially plastics are an inevitable part of our day-to-day life. The question whether they are a boon or bane has opened the door to a wide area of research. Starting from developing a lesser detrimental material to designing better and viable methods of recycling are hot topics in the research fraternity. Polymer composites are one such material where in-depth studies regarding their production and degradation methods need to be investigated. The current research problem stems from the afore mentioned ideas.

The thesis entitled **"THERMAL, MECHANICAL AND DIELECTRIC PROPERTIES OF ETHYLENE-CO-VINYL ACETATE BASED COMPOSITES"** comprise of 9 chapters. **Chapter 1** deals with the general idea of polymer composites, the types of fillers and the significance of ethylene-co-vinyl acetate and chitosan. A meticulous and updated review of the literature has been carried out to identify the research gaps on the said topic. The chapter is concluded by mentioning the objectives and scope of the work.

Chapter 2 details the materials used for the modification of chitosan via graft polymerization using polyaniline, methylmethacrylate, 2-hydroxy methacrylate and chitosan/phytic acid polyelectrolyte. It also consists of the detailed explanation on the characterization of the formed chitosan grafts via FTIR, SEM and TGA techniques.

Chapter 3 deals with the methods used to extensively analyse the thermal, mechanical and dielectric behaviour of the materials developed. To get better understanding of these methods, an extensive survey of recent literature is also included in the chapter.

Chapter 4 describes the thermal degradation kinetics of fillers developed such as chitosan grafted with polyaniline (PANi), chitosan grafted methylmethacrylate (MMA), chitosan grafted 2-hydroxy ethyl methacrylate (HEMA) and chitosan/phytic acid polyelectrolyte has been carried out by employing data obtained from thermogravimetric analysis. Isoconversional model free methods such as Flynn-Wall-Ozawa (FWO), Kissinger-Akahira-Sunose (KAS), Starink, Tang, Friedman (FR) and Vyazovkin has been employed to calculate activation energies of various conversions from 0.1 to 0.9. Furthermore, thermodynamic parameters were also calculated for the said materials.

Chapter 5, Chapter 6 and Chapter 7 collectively details the analysis of mechanical properties using UTM, the thermal properties using TGA and the dielectric properties with dielectric broadband spectroscopy. These chapters also extensively describe the decomposition kinetics of pyrolysis of the developed composites along with their thermodynamic parameters.

Chapter 8 concludes the studies and points out the major outcomes of the overall work. The future prospect of the present research is summarised in **Chapter 9** as recommendations

Chapter 1
Introduction

This chapter illustrates a general overview on the fabrication of polymer composites keeping the focus on ethylene-co-vinyl acetate (EVA). An extensive review of literature was carried out to detail the necessity of polymer composites. The descriptions are split into various heads vis-a-vis types of composites, a brief note about the various kinds of fillers and literature review on the role of different types of fillers in polymer composites with EVA matrix. The literature review brings forth the research gaps. The gaps pave the way for the present work focusing on the development of polymer composites with matrix as EVA and chitosan-based fillers. The scope and objectives have also been defined.

1.1. Polymer Composites

Composites are a class of materials which -lay a vital role on a global scale from the humble household to space technology (Lebreton *et al.*, 2017; Bhagabati, 2020; Matta *et al.*, 2021). Figure 1.1 presents a general classification of various composites.

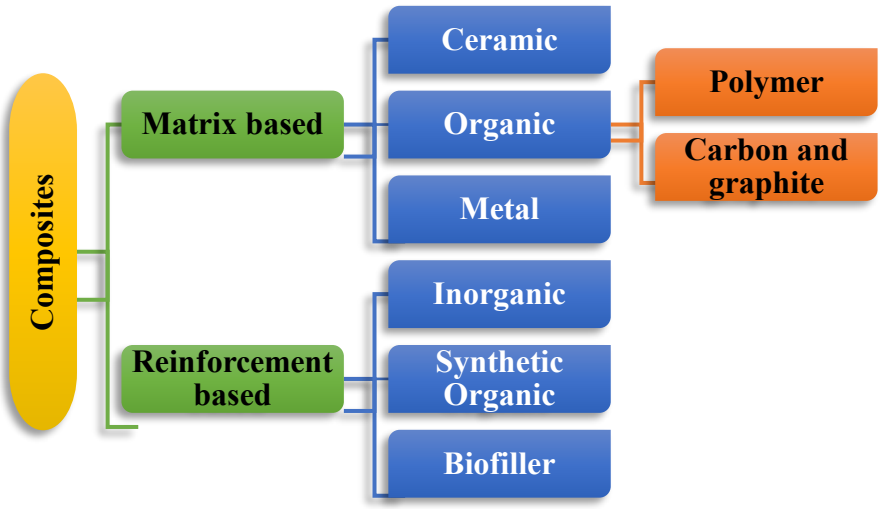

Figure 1.1: General classification of composites

Among these, Polymer composites are one of the most easily manufacturable and inexpensive types of composites that can be formulated. They are ubiquitous. There can be a vast array of fillers/reinforcements that are added to the polymer matrices to tune the character according to the needs and applications. The formulation, characterization, properties, and applications of polymer composites is a growing area of research in material science. Figure 1.2 depicts the comparison of the projection of global usage of polymer matrix with

other matrices. The global value of polymers as the most used composite matrix has been projected to about USD 8.80 billion by 2033, from USD 4.96 billion in 2023 as per the statistics of 2023 (Aboughaly *et al.*, 2023). This gives an idea about the appeal of focusing materials production using polymer composites.

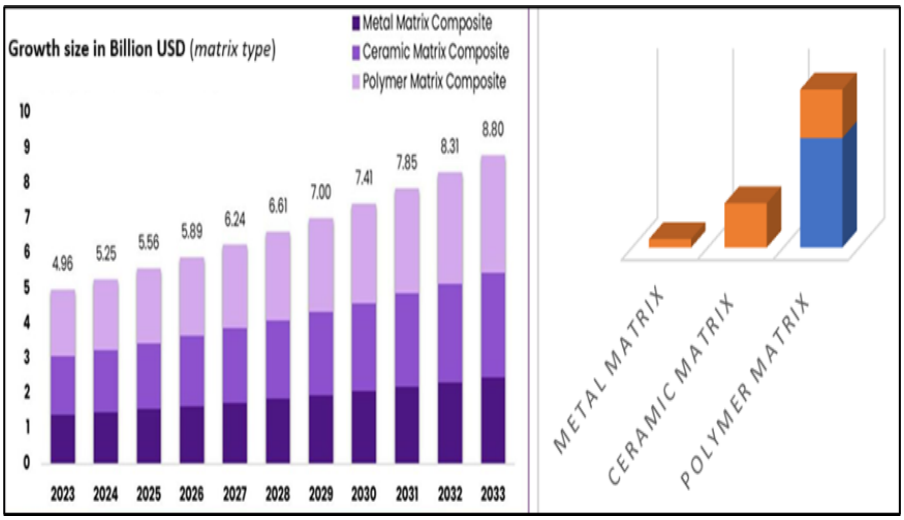

Figure 1.2: Market forecast for matrices in composites 2023-2033

1.2. Ethylene-co-vinyl acetate (EVA)

Ethylene copolymers, such as ethylene-co-vinyl acetate (EVA), ethylene vinyl alcohol (EVOH), Polyvinyl acetate (PVA), polyvinyl alcohol (PVOH), ethylene acrylic acid (EAA) and ionomers, make a large volume of the plastics industry wherein the lion-portion is taken up by EVA. Figure 1.3 depicts the major players in the polymer sector.

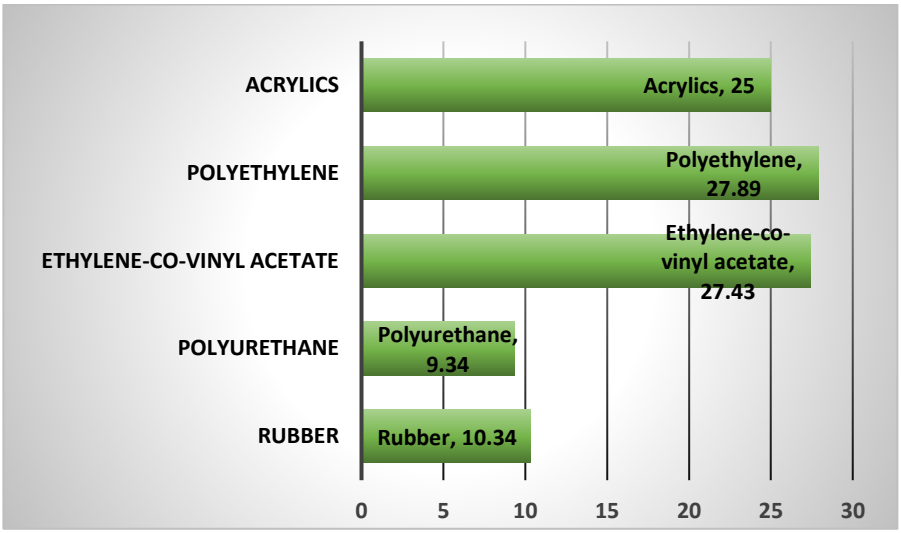

Figure 1.3: Market share of polymers by type (in percentage)

Ethylene with vinyl acetate forms the copolymer EVA. The properties of EVA depend on the vinyl acetate content - usually varies from 10 to 40 wt % - controls its character. Although the copolymer acts similar to LDPE (low density polyethylene) at low vinyl acetate content, it displays the physical behaviour and processing performances of thermoplastics which are tougher than LDPE. This ability to show the tendencies similar to rubber, thermoplastic elastomers and plastics with the variation of vinyl content makes it an exceptional material for composite formation. This tuneable capacity of the copolymer qualifies EVA to have fascinating properties such as better adhesion, printability, electrical, mechanical and compatibility with other materials (polymers, metals or biomaterials) (Azizi *et al.*, 2018; Omastová, Číková and Mičušík, 2019; Xiao *et al.*, 2020; Xu *et al.*, 2021).

The ease of fabrication and the transparent nature of this category of polymers led them to become a commercial hit. These heat processible odourless copolymers are flexible, comparatively inexpensive and show promising UV and ozone resistance.

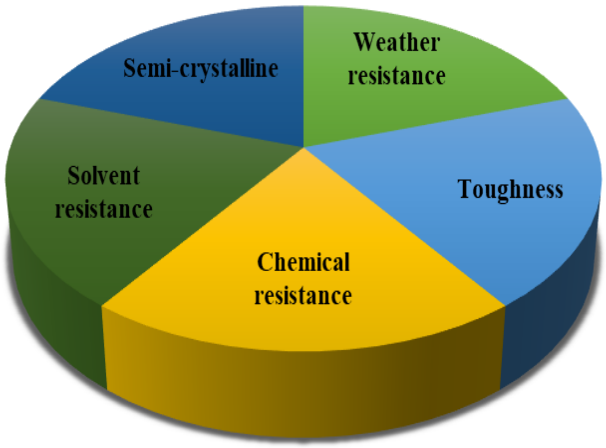

Figure 1.4: Properties of EVA

EVA also exhibits better flexibility and durability at low temperatures. Also, it is recognized as a material with improved resistance towards stress/cracking and adhesion characteristics. Owing to its low permeability to gases and organic vapours EVA falls in to the category of high barrier materials. Even though EVA is a highly resistant polymer to dilute mineral acids, alkalis, fats, oil and detergents, they do tend to react with concentrated mineral acids, ketones and aromatic or chlorinated hydrocarbons and strong oxidizing agents. Halogen attack on EVA tends to make it embrittled but solutions of chlorine and other bleaching agents hardly affect the material.

The development of the polymer into desired end applications can be carried out by various processing techniques such as coating, solvent evaporation, moulding, melt extrusion and a variety of emulsion and solution casting. These polymers can be made to have tailorable electrical, mechanical and thermal properties by utilizing them as matrix material in the fabrication of composites.

1.3. Types of fillers

As can be seen from Figure 1.1, there is a huge array of fillers from which we can choose to use in the development of novel composites. The reinforcements are classified generally into inorganic, synthetic organic and biofillers.

1.3.1. Non-Biofiller Composites

The tunability and availability of inorganic fillers make them the go to materials for composite development. Better modulus, chemical resistance and impact resistance, have been demonstrated by EVA with inorganic fillers. The range of fillers include substances such as metals, semiconductors, carbon nanotubes, and magnetic nanoparticles.

Synthetic fillers such as carbon fibers, nylon, polyester, aramid, and glass fibers are some of the frequently sourced reinforcements in the fabrication of composites that helps tackle overreliance on chemicals derived from fossil fuels. For example, albeit its several shortcomings, the conventional glass fiber is used as an improvement of the stiffness and strength of plastics. However, Glass fiber production requires a great deal of energy with a steep processing temperature. They tend to abrade the equipment for processing and increase the density of the

processed material. Table 1.1 depicts the effect of composites with certain synthetic materials as fillers with EVA.

Over the course of time, the particles that are left over from the polymeric materials eventually find their way into food products forming a link in food chains. The existence of these particles endangers people's health and well-being whilst polymer microparticles less than 10 μm can enter the lung. (Lebreton *et al.*, 2017).

Reduction of the waste generated or to completely liquidate the same with the use of preventive techniques and methods is the primary goal of circular economy. In order to close the loop, two types of cycles can be identified: biological cycle and technical cycle. The latter deals with the oversight of non-renewable resources, encompassing their recovery and reuse, while the former is concerned with the stream of biodegradable materials. (Navare *et al.*, 2021; Wojnarowska, Sołtysik and Guzik, 2021).

Table 1.1: EVA composites with inorganic/non-biofiller composites

Sl No	Type of reinforcement	Processing type	Inference	Reference
1	Aluminium hydroxide (ATH) and melamine cyanurate (MCA)	Blending	MCA addition increased the compatibility and thermal stability of the EVA-ATH composites. The combustion results and limiting oxygen index (LOI) value indicated that the composite with 60 phr ATH and 40 phr MCA addition to EVA (EVA-60-40) depicted the optimal isolated layer favouring the fire resistance and incombustible character.	(Xu *et al.*, 2021)
2	Carbon black (CB) and graphene	Solvent casting and melt compounding	The EVA composites containing the additives CB and graphene, recorded a marginal rise in thermal conductivity compared to pure EVA. The filler orientation, distribution and dispersion were found to influence the thermal and electrical conductivities.	(Azizi *et al.*, 2018)
3	Multi-walled carbon nanotubes (MWCNT)	Extrusion (twin screw extruder)	The enquiry of rheological properties depicted that at low shear flow, the composite is of Newtonian behavior and at higher filler addition the behavior turns to non-Newtonian. In addition, a linear dependency with the increase on filler wt %	(Stan, Stanciu and Fetecau, 2017)

			is shown for viscosity. Also, the dependence of shear viscosity on temperature is consistent with the Arrhenius equation	
4	Copper nanowire (Cu NW) and multi-walled carbon nanotubes	Solvent Casting	The well connected Cu NWs welded by chemical steam reduction method becomes the reason for the electrical conductivity of the formed foam. The addition of MWCNTs not only improves the adhesion between Cu NWs and flame-retardant EVA (FR-EVA) but also helps in keeping oxidation of Cu wires at bay.	(Y. Wang *et al.*, 2021)
5	Magnesium hydroxide (MH), zeolite imidazole frame (ZIF-67) on the surface of attapulgite (ATP)	Open mixing	The addition of ZIF-67 to the EVA/MH composite improves its flame-retardancy and thermal stability. There was also an improvement in the elongation at break values while no significant change in the tensile and impact values.	(Ma *et al.*, 2022)
6	Ultra-high molecular weight polyethylene fibres (UHMWPE) and aluminium oxide (Al_2O_3)	Fibre impregnation	Various filler combinations depicted a significant improvement on the modulus of elasticity leading to diverse types of composite failures. A brittle failure was shown by the highest modulus of elasticity for composite with alumina anoparticles (Al_2O_3/EVA/UHMWPE)	(Zec *et al.*, 2018)
7	Conductive silver	Screen printing	Composites show potential towards printable electronics. The composite with	(Y. Shen *et al.*, 2019)

			55% of the filler has low volume resistivity and bendable properties.	
8	Multi walled carbon nanotubes (MWCNT)	Electrospinning	A homogeneous dispersion of MWCNTs by the addition of compatibilizer was achieved which inturn led to the better thermally stable electrospun composites. The amount was kept to a max of 3 wt % for MWCNTs.	(Omastová, Číková and Mičušík, 2019)
9	Magnesium hydroxide ($Mg(OH)_2$), zinc borate (ZB) and bismuth oxide (BO)	Mechanical blending method	A rise in the filler content lowered the tensile strength and elongation of the EVA composites, whereas they showed better flame-retardant property.	(Guo-hui et al., 2019)
10	Fluorographene (FG)	Ball milling	Composite films with different thermal conductivity can be achieved by tuning the type of FG and the mass ratio of FG and EVA.	(Han *et al.*, 2022)
11	Aluminium hypophosphite (AHP), melamine cyanurate (MCA) and molyMoS$_2$	Melt blending	EVA composites with AHP and MCA exhibited excellent flame retardancy. After the addition of 30 wt % AHP and MCA to the composites, the limiting oxygen index (LOI) rose to 35.5%, and with a V-0 rating the material qualified the UL-94 test. The results of cone calorimeter test showed that heat release rate (HRR), total heat release (THR) values were largely diminished owing to the continuous char layer acting as isolating barriers to heat transfer and flame	(Zhou *et al.*, 2016)

			propagation.	
12	$Ti_3C_2T_x$ (MXene)	Solution casting	Among the composites prepared, the composite with 8 wt % of $Ti_3C_2T_x$ exhibited higher dielectric properties with low dielectric loss. The high dielectric properties are due to improved electrical conductivity which can be the result of proper filler dispersion and synergistic interaction between the filler and the matrix.	(Jena *et al.*, 2021)
13	Magnesium hydroxide (MH) and Hexaphenoxycyclotriphosphazene (HPCTP)	Blending (two roll mill)	HPCTP via a bridging effect improves the processability of EVA–MH–HPCTP composite. It also acts as a synergistic flame retardant.	(L. Shen *et al.*, 2019)
14	Biochar	Twin screw extruder	Biochar at higher loadings enhanced the forced combustion behavior of the composites which was evident by the decrease of peak of HRR and THR Also, the stiffness increased with the increase in amount of biochar loading.	(Matta *et al.*, 2021)
15	Paraffin/expanded graphite (EG)	Melting	The leakage rate of the composites was about 3 % with the EVA content. Presence of EG accelerated the phase change of the materials considerably. During initial stages of melting, high average velocity values of the melt were exhibited by the paraffin/EG/EVA composites with a high	(Cai *et al.*, 2020)

			mass fraction. However, during the progress of the melting, there was a decrease in velocity and finally the composites with a low mass fraction of EG showed high average velocity	
16	Mg/Al/Fe ternary layered double hydroxides (Mg/Al/Fe-LDHs)	Melt blending	The LDH reinforcement can enhance the flame-retardant properties of composites by catalyzing EVA carbonization. At low temperatures, TG-FTIR results indicated a reduction the release of toxic gases which promote decomposition of composites by the introduction of LDHs. Further, at an elevated temperature a delay in the decomposition rate of the composites was noted.	(Qian, Jiang and Li, 2019)
17	Carbonized wood fiber (CWF)	Melt blending	The increasing addition of CWF caused the drop in mechanical properties and mass swell percentages for EVA composites. The attraction between CWF and EVA promotes the establishment of conductive networks within the system thus improving the conductivity. 10 phr of CWF loading was used to determine the CWF percolation threshold in the EVA matrix. An improvement in the thermal stability with the increase in CWF content was observed.	(Hanif *et al.*, 2017)

			The addition of CWF instigated a reduction in crystal orientation ratio and d-spacing in EVA/CWF composites.	
18	Calcium carbonate and ammonium polyphosphate (APP)	Melt mixing	In mass loss calorimeter studies, the combination of APP with partially and fully hydrated calcium oxide resulted in more effective flame-retardant effect than in the system with carbonated calcium.	(Laoutid *et al.*, 2021)
19	Silver-calcined scallop shell (Ag-CS)	Wet phase inversion	Compared to raw EVA, the prepared composite with 6 wt % Ag-CS showed better tensile strength and improved thermal properties. The prepared composite displayed photocatalytic property with a pseudo first order kinetics which is attributed to the incorporation of Ag-CS to EVA polymer matrix. The filler also contributes towards the antibacterial property of the formed composite.	(Manoj *et al.*, 2021)
20	trans-polyisoprene (TPI)	Two roll milling	The composite shows shape memory property. Addition of DCP as compatibilizer improved the shape memory nature and gave a smooth structure at higher DCP content. As the concentration of DCP increased, the crosslinking density increased as well, preventing molecular mobility and impeding crystallization.	(Ma *et al.*, 2022)

1.3.2. Biocomposites

"Biocomposite" by definition refers to a polymer composite that contains one or more environmentally beneficial, green additive/s, which are primarily sourced from nature. The base polymer matrix can either be a petroleum-based nondegradable or degradable polymer or it could be a bioderived degradable or nondegradable polymer. Thus, a "biocomposite" is a mixture of at least two of these materials that includes one or more phases that are derived from nature.

Certain other reasons for the emergence of biocomposites are their eco-friendly properties with diversity, simplicity and cost effectiveness. Those materials that are naturally occurring organic polymers can be divided into the following as shown in Figure 1.5

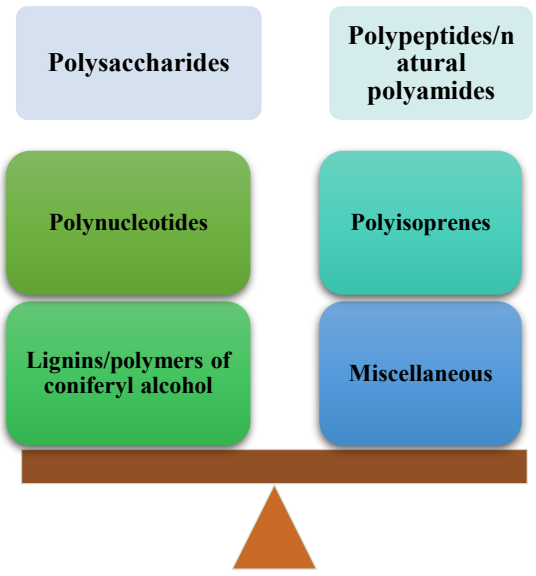

Figure 1.5: Types of natural/organic fillers

The technologies related to natural filler reinforced composites are well established. In order to develop products of commercial nature, strict targets for industrial ecology and adherence to environmental protection laws should be followed. The guidelines and strict legislations for the development of commercial products include stringent sustainability goals toward industrial ecology and should comply with regulations related to environmental protection (Bhagabati, 2020). At this juncture, natural fibers and organic fillers are exclusively used for the fabrication of polymer composites. The plant fibers demonstrate itself as a substitute fiber to its synthetic counterparts. But, biofibers are extremely hydrophilic in nature, so proper chemical treatments are required to enhance the composite durability (Hemalatha *et al.*, 2011; Bari and Mishra, 2017). Focus of the current study is on the grafting aspect of the chemical treatment procedures are described later in Chapter 2. Utilization of fillers for waste management through biodegradation and bioconversion has turned more significant. Bio-fillers are also very sensitive to the environmental factors. So, various chemical modifications through functionalization of the major functional groups have also been done in this work to enhance the overall properties of the composite.

Here, the matrix is a polymer and biomaterials are used as reinforcing fillers. Table 1.2 depicts briefly some of the recent literature that involves mainly cellulosic fibers that are used in their native conditions like sisal, coir, jute, flax, cotton, and paper as reinforcement for various matrices of thermoplastic nature. Amongst the number of mentioned lignocellulosic materials, bast fibers (jute) contains comparatively higher proportion of stiff bio-derived cellulose. This lignocellulosic bast fiber (jute) has been studied at length by blending

it with synthetic polymers for reinforcing polymeric materials. Research on environmentally friendly composite polymers has been attempted to generate more affordable, biodegradable, and innovative materials on a global scale. (Chaudhuri and Chakraborty, 2013). Traditionally, synthetic non-biodegradable polymers, such as polypropylene, polyethylene, polyester etc., are being explored as matrices in order to use them in arenas like automobiles and buildings. Future biocomposites will be made feasible by biodegradable polymers if they are obtainable in adequate quantities and at affordable prices. From the environment perspective, when both or either matrix and fillers being biodegradable, biocomposites become attractive products. Nevertheless, lack of broad and reliable data on composites with natural filler and/or on bio-composite makes it challenging to design product with these materials. As soon as the database is accessible, design and manufacture of products with natural fiber composites and bio-composites offer newer opportunities and concerns. Therefore, the general goal of a researcher is to make a polymer composite with acceptable physical, mechanical and thermal properties.

1.4. Chitosan as filler reinforcement

Of late, a growing interest has been driven towards development of biodegradable plastics that encompasses a wide range of applications in agriculture, food packaging, health and biomedical fields. India being a country with vast coastal area around it, has fishing and related occupations as a major player in its economy especially in coastal regions like Gujarat, Kerala, West Bengal, Maharashtra etc. Hence, Governments extend their hands of support for betterment of the financial and livelihood security of the people of these areas thereby introducing initiatives generating large quantities of aquatic waste

materials (Agarwal Professor, Chaudhary Associate Professor and Singh, 2015; Lebreton *et al.*, 2017). As a result of which over 60,000 and 80,000 tonnes of marine waste products containing chitinous materials, shrimp, crab and squid are produced annually (Oyatogun *et al.*, 2020). In this thesis an attempt to use modified chitosan, grafted chitosan per-say, as filler is made. As foliage have cellulose exterior, organisms such as crustaceans and insects have chitin as their exoskeleton which is a close relative of polysaccharide - cellulose. Chitin and cellulose take up the lion's share of biopolymers on earth.

Chitosan, the deacetylated product of chitin, is more reactive than its parent chitin, biodegradable, non-toxic and biocompatible. It is also known as Poliglusam in the medical community (Soleimani, Vaseghi and Loconte, 2019).

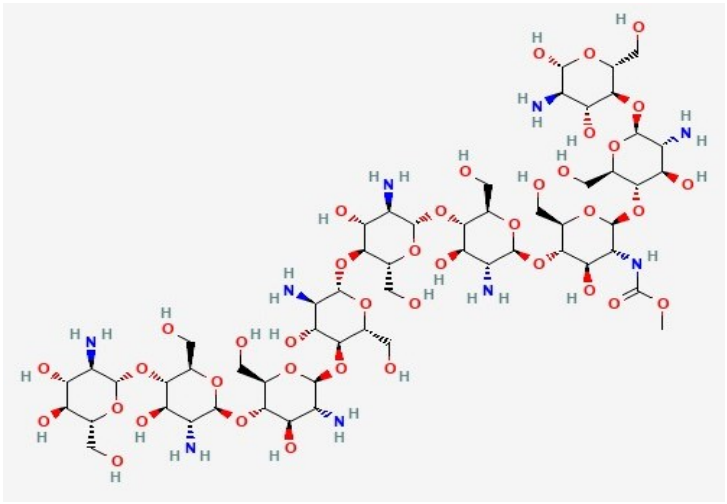

Figure 1.6: Structure of Chitosan or Poliglusam

It has better properties of film formation, chelation and absorption. As a consequence, to all these properties chitosan has been widely used

for various applications. Figure 1.7 collectively depicts the preparation route, properties and applications of chitosan. As can be observed from figure 1.6 chitosan has a unique structure wherein it can be modified via physical or chemical methods.

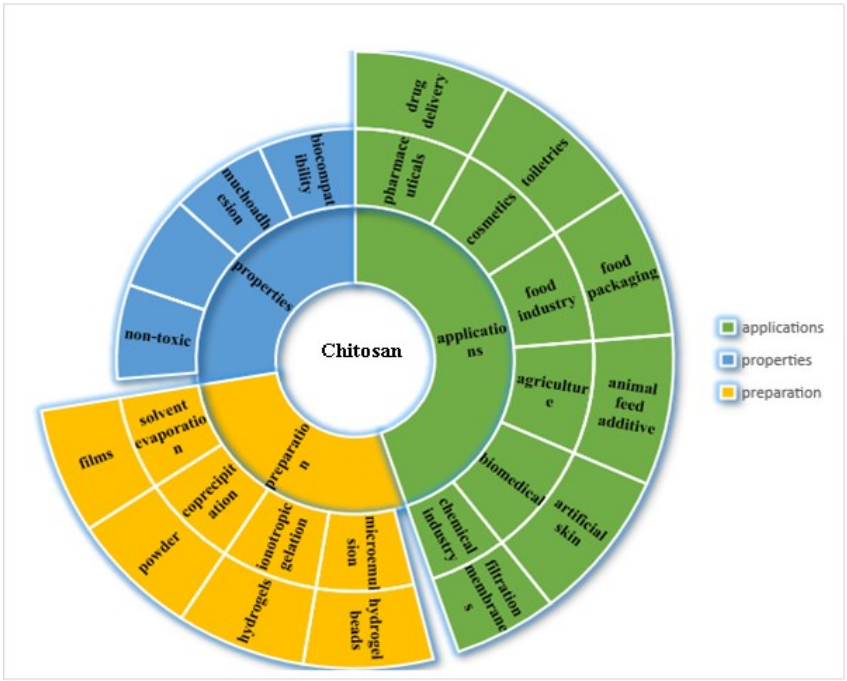

Figure 1.7: Methods of preparation, properties and applications of chitosan

A popular technique to manufacture novel materials with desired qualities is melt-compounding, which is used for manufacturing polymer blends and composites. Main advantages of this method are elimination of complicated processes (eg. polymerization reactions, gradient copolymerization, partial block or graft copolymerization etc) and application of commercially available components. A wide range of possible selections of polymeric material compositions and their processing conditions can be a useful tool for easy tailoring of their

respective properties. Furthermore, melt-compounding is usually performed in extruders commonly used in the industry. Extrusion is one of the fastest developing methods of polymer processing, owing to its quick processing time, better efficiency towards mixing, high capacity, good quality of the resultant products, diversity and adaptability. As a result, research focusing on biodegradable polymer blends and composites obtained via melt-compounding enjoys growing interest among many academic and industrial research groups (Formela *et al.*, 2018).

Table 1.2: EVA composites with organic/biofiller composites

Sl No	Type of reinforcement	Processing type	Inference	Reference
1	Polysaccharides	Melt compounding	α-1,3 glucan offers high purity, consistency, better crystallinity, low density, and thermal stability as a reinforcing material. Addition of the filler brings about enhancement in key properties such as modulus, toughness, wear resistance and hardness. The reason for this is due to the interaction between the hydroxyl (−OH) moieties of polysaccharides and the carbonyl (–C=O) of vinyl acetate via hydrogen bonds.	(Esmizadeh, Tzoganakis and Mekonnen, 2020)
2	Hemp derived biochar fibers (HFB)	Melt mixing	Biochar fibers have no significant effect on the thermal behavior of EVA whereas it improves the crystallinity degree. The increase in thermo-oxidative nature was observed with increase in HFB. The prepared composites show better stiffness and lower ductility. Also, higher thermal conductivity and microwave electrical conductivity are attained for the high concentrations of HFB.	(Di Maro *et al.*, 2020)
3	Kenaf fiber	Twin screw extruder	Intumescent systems utilize the mechanism of foaming and carbonization for flame retardancy. Addition of kenaf as a filler improves the mechanical and flame-retardant properties which makes it a better composite as intumescent material.	(Park *et al.*, 2018)

4	Carbonised wood fiber	Melt mixing	The inclusion of CWF surface modified with $ZnCl_2$ (CWF-$ZnCl_2$) resulted in a reduced the organic solvent (toluene) diffusion capacity of the composite. The mechanical, thermal and electrical stability of the composites with modified CWF was better than the one with unmodified filler. Porous structure of the CWF upon surface modification resulted in the could be the reason	(Pisal *et al.*, 2021)
5	Microcrystalline cellulose	Roll milling	The decline in the deformation properties and the strength of the composite is a result of increase in the number of VA groups and the less the molecular weight of the EVA polymer.	(Shelenkov, Pantyukhov and Popov, 2020)
6	Leather fiber	Two roll milling	The scrap/discarded leather wastes could be utilized to develop the leather buffing dust/recycled EVA polymer composites. Composites with a higher amount leather waste, 1:1, depicted better mechanical properties. The filler also behaved similarly when used in elastomer composites	(Sharma *et al.*, 2022)
7	Wood flour	Two roll milling	Composites with EVA of different VA content and different trademark EVA were prepared. The prepared composites can be used as superconcentrates in manufacturing products. EVA with low melt flow index (MFI) are most durable. Also, optimal combination of characteristics (tensile strength, elongation at break and MFI) is found in the	(Shelenkov, Pantyukhov and Popov, 2018)

			composites based on EVA 28025, which indicates the prospect of using this EVA trademark for manufacturing of superconcentrates.	
8	Olive husk flour (OHF)	Single screw extruder	Neat EVA/OHF displayed no notable property changes. This stability was further enhanced with addition of a compatibilizer. This behaviour is suspected by the crosslinking at the fifth cycle of extrusion	(Dehouche, Kaci and Kaid, 2019)
9	Lignin and magnesium hydroxide	Melt processing	Regardless of its nature, the inclusion of lignin, induced reduction of thermal stability towards the composite during TGA analysis as well as considerable decrease of the time to ignition (TTI) in cone calorimeter test. Furthermore, no chemical modification of lignin is required for this behaviour.	(Laoutid *et al.*, 2019)
10	Poly(lactic acid)/cellulose	Melt mixing	An enhancement in adhesion and dispersion of fibres were showed by the composites. The miscibility of the materials controlled the crystallization and morphology of the composite materials. By varying the blend composition and the concentration of fibres the properties can be altered. Ternary composites that include PLA display advantageous processability and mechanical properties	(Pracella *et al.*, 2016)
11	Grafted kenaf	Melt mixing	DSC data revealed that with the addition of 30% grafted and ungrafted kenaf fibers the crystallinity of	(Bakar *et al.*, 2015)

			the EVA decreased. Upon grafting the composites, TGA and DTG curves displayed an increase in the thermal stability. DMA studies reveals that with the addition of the filler, the glass transition temperature shifter to elevated temperatures for the PVC and EVA in the PVC/EVA/kenaf composites.	
12	Chitosan, iprodione loaded poly(ethylene glycol)-poly(ε-caprolactone) PEG-PCL) [IPP micelles]	Solvent casting	The fabricated films have better controlled drug release ability and permeability than neat chitosan. Therefore, the self-prepared IPP micelles-loaded EVA/CS nanocomposite films have wide applications in the arena of sustainable agriculture by reducing the use of pesticide and artificial bagging.	(Xiao *et al.*, 2020)
13	Cellulose	Solution casting	At large concentrations of cellulose the degree of crystallinity varied. The storage modulus obtained from the DMA analysis depicted inverse proportionality towards the cellulose content. This indicated an increase in the rigidity of the material by the introduction of cellulose dispersion as a reinforcement.	(Aragão Melo *et al.*, 2018)
14	Starch nanocrystals (SNCs)	Microextruder	During melt-processing no loss of crystallinity of SNCs was observed. Moreover, by the addition of SNCs the mechanical and thermal properties of the neat matrix improved which is attributed to the strong hydrogen bond between the surface of the nanofillers and the acetate groups of the matrix. An increase of	(Sessini *et al.*, 2019)

			the thermal stability of about 10 °C compared to the neat matrix also was observed by the SNCs addition	
15	Cassava starch and polyolefin elastomer (POE)	Two roll milling	The composite was prepared to investigate its use in footwears. The POE content in EVA/starch composites influenced positively both the density and abrasion resistance. However, properties such as tensile strength, elongation at break, and permanent set properties decreased on increasing POE content. EVA 80 phr, starch 20 phr and POE 20 phr displayed the best composition of foamed EVA/cassava starch/POE composites for footwear materials.	(Lestari, Priambodo and Nurhajati, 2021)
16	Starch	Twin screw extruder	The compatibility between EVA/starch composites improved by addition of either polyethylene-grafted maleic anhydride (PE-g-MA), or by reactive extrusion with maleic anhydride (MA) and benzoyl peroxide (PBO). An increase in crystallinity was observed for the non-compatibilized composites with the amount of starch added. The addition of PE-g-MA increased the crystallinity of the composites (up to 20 wt% of starch). The thermal stability of EVA/starch composites decreased on increasing the starch content. The addition of the compatibilizer was found to improve the thermal stability of the composite. For composites with higher starch content, the in-situ grafting with MA and PBO led to increased thermal	(Hamadache et al., 2019)

			stability.	
17	*Luffa Cylindrica*	Moulding	EVA/*Luffa Cylindrica* (EVLc) were formulated for usage in mouth guards (PPE). Similar to previous literature, low tensile strength values compared to EVA resistance ranges was observed. SEM images of the material confirmed good adhesion between the reinforcement and matrix without surface treatment. The descriptive statistical analysis indicated an intrinsic variation within the material processed.	(Carmona and Colorado Lopera, 2022)
18	Hemp stem powder	Mixing	Introduction of hemp leads to the decrease in hardness and density of the composite system, improve the resilience and the deformation rate of compression. It also introduces excellent moisture absorption, quick drying and antibacterial properties. The results show that for the application in shoes. The better mechanical properties were exhibited by systems containing 10% - 20% of hemp stem powder.	(Guo-hui et al., 2019)
19	a-1,3glucan polysaccharide	Melt processing	The incorporation of α-1,3 glucan resulted in better mechanical properties, such as toughness, modulus, wear resistance, and hardness making the tailored polysaccharides as better reinforcements. The reason for these observations is inferred towards the association between the−OH moieties of polysaccharides and –C=O of vinyl acetate via hydrogen bond.	(Esmizadeh, Tzoganakis and Mekonnen, 2020b)

20	Banana Fiber and Wood Flour	Single-screw corotating extruder	The reinforcements act as nucleating agents which affect the stability of cells during the construction of the cellular structure. Cellular density, fiber content and density of the have significant impact on the mechanical properties of expanded composites. An intermediate thermal stability was observed for composites with either filler compared to their respective constituents.	(Zimmermann *et al.*, 2014)

1.5. Objectives

The objectives of the current studies are given below:

1. To develop composite systems of EVA with fillers such as,
    - Chitosan
    - Chitosan grafted polyaniline
    - Chitosan grafted Methylmethacrylate
    - Chitosan grafted 2-Hydroxyethylmethacrylate
    - Chitosan/Phytic acid Polyelectrolyte
2. To carry out the mechanical (tensile & elongation at break) properties, thermal profile (using TGA) and to investigate the dielectric properties of the newly developed composites.
3. To utilize the obtained thermal data to further comprehend the thermal degradation kinetics of the composites with various isoconversional methods namely, Flynn-Wall-Ozawa (FWO), Kissinger-Akahira-Sunose (KAS), Starink, Tang, Friedman (FR) and Vyazovkin methods.
4. To determine the thermodynamic parameters with the activation energy obtained from the model free methods.

1.6. Scope of the present study

The kinetics of thermal degradation is a vital tool as it comprises of the different aspects of understanding and categorising the degradation process. Major areas that fall within the scope of thermal degradation kinetics are:

- **Analysis of Degradation Kinetics:** In this the probable pathway of the kinetics of reaction, the steps in which the degradation occurs and the presence of intermediates (if any) formed are identified.

- **Activation Energy Determination**: Determining the activation energy is an essential aspect of kinetics of thermal degradation. The activation energy provides insights into the energy barrier that needs to be surmounted for the degradation process to occur. It helps understand the temperature dependence of the reaction rate and stability of the material.

- **Evaluation of Thermal Stability:** At higher temperatures, the stability and the possibility of occurrence of hazardous by-products and reactions can be evaluated by studying the thermal degradation behaviour.

- **Lifetime Prediction:** The estimation of life-time under any given temperature is relevant. A better perception of the kinetics of degradation and reaction mechanism helps to predict the rate and thus ascertain the shelf life and recommend proper storage methods.

- **Kinetic Modelling:** The degradation behaviour based on experimental results leads to the development of mathematical models. The kinetic triplets namely activation energy, pre-exponential factor and reaction order can be estimated by fitting the data to suitable kinetic models.

- **Design and Optimization of Materials:** Understanding the degradation behavior and kinetics helps to create better heat-resistant materials, to improve process conditions, and to reduce degradation at the time of storage and manufacture.

Thus, the scope of kinetics of thermal degradation extends across various industries, including pharmaceuticals, polymers, chemicals, food, and materials science. A productive evaluation of crucial processes such as pyrolysis and heat assisted oxidation of polymers and fuels, thermal stabilization of polymeric materials and further analysis of pyrolytic conversion of polymer (fossil-fuel based) waste to energy applications, thermal optimization of development and storage conditions of high temperature composites for aircraft and aerospace usage are also the scope of kinetic degradation via TG data.

Chapter 2
MATERIALS AND THEIR CHARACTERIZATION

This chapter involves the description of the materials involved in the modification of chitosan using grafting technique and the methodology in which the grafts are synthesized. The characterization techniques and equipment used to analyse the filles using Fourier-transform infrared (FTIR) spectroscopy, Field emission scanning electron microscopy (FESEM) and Thermogravimetric Analysis (TGA) are detailed in this section. The general scheme of reactions for the grafting methodology that are already reported is also depicted.

2.1. Materials

2.1.1 Ethylene-co-vinyl acetate (EVA)

Ethylene-co-vinyl acetate (EVA-40) with 40 % vinyl acetate content was supplied by Sreenivasa polymers, Chennai, India. Table 2.1 depicts the properties of EVA 40 from technical data sheet.

Table 2.1 Properties of EVA from technical data sheet

Property	Test Method	Unit	Typical Value
Vinyl acetate Content	FTIR (internal method)	% .- wt.	40
Melt Flow Index	ISO 1133 / ASTM D1238	g/10min	55
Density	ISO 1193 / ASTM D150	g/cm3	0.94
Vicat Softening Temperature	ISO 306 / ASTM D1525	°C	<40
Elongation at Break	ISO 527-2 / ASTM D638	%	1100
Ring & Ball Temperature	ASTM E28 / NF EN 1238	°C	97

2.1.2. Chitosan

Chitosan with a degree of deacetylation of 82% was obtained from India Sea Foods, Kochi, Kerala, India, and Table 2.2 represents the values provided.

Table 2.2: Properties of chitosan

Property	**Approximate Value**
Appearance	Off white powder
Ash	< 1%
Deacetylation	> 85%
Moisture	< 10%
Viscosity (1%)	> 50 cps

2.1.3. Aniline

Table 2.3. depicts the physical properties of aniline procured from Merck, India. Aniline was used to modify chitosan to prepare chitosan-g-PANi.

Table 2.3: Properties of aniline

Property	**Approximate Value**
Physical state	Liquid
Colour	Light brown
Molecular weight	93.13 g/mol
Initial boiling point and boiling range	184 °C at 1.013 hPa 70 - 71 °C at 13 hPa
Density	1,021 g/cm3 at 20 °C

2.1.4. Ammonium persulphate

The peroxide initiator Ammonium persulphate APS was used in the grafting of polyaniline on to chitosan. It was procured from Merck; India and the physical properties are given in Table 2.4.

Table 2.4: Properties of Ammonium persulphate

Property	**Approximate Value**
Physical state	Solid
Colour	White
Molecular weight	228.20 g/mol
Melting point/freezing point	Decomposes before melting
Density	1,980 g/cm^3

2.1.5. Phytic acid

Phytic acid is used in the preparation of the polyelectrolyte complex. The physical properties obtained from the material safety data sheet (msds) is depicted in Table 2.5.

Table 2.5: Properties of Phytic acid

Property	**Approximate Value**
Physical state	Liquid
Colour	Yellow
Molecular weight	660.03 g/mol
Boiling point	105 °C
Vapour density	22.7
Specific gravity	1.37

Chitosan being versatile biomaterial has its own short comings especially regarding its mechanical properties, solubility and shelf-life. Several methods can be employed in order to improve its properties. The most convenient and apt technique for modifying the innate characteristics of natural polymers with polysaccharide and -like structures is graft polymerization. Chitosan contains two reactive

functional groups, an amino group and a hydroxyl group. The hydroxyl group acts as the point of initiation of the graft copolymerization leading to the formation of a bond on to chitosan skeleton (Yu *et al.*, 2020).

The modification can be carried out by utilizing non-vinyl and vinyl graft polymerization methods. The polymers to graft on to the chitosan skeleton can be chosen according to the applications intended. Polyaniline (PANi) is one of the most promising organic conducting polymers that is well known for its conducting as well as mechanical ability. Grafting of this particular polymer can help impart its properties on to the formed copolymer. Grafting of PANi onto chitosan is carried out via non-vinyl grafting can be carried forward by peroxide initiators like potassium persulfate (KPS) and ammonium persulfate (APS) (Hosseini, Simiari and Farhadpour, 2009; Abbasian *et al.*, 2017). These grafts can be utilised for their electrical properties and stability. Another method to introduce grafts onto chitosan is via graft polymerization of vinyl monomers. The grafting takes place in such a way that initially a free radical is generated on chitosan spine and these radicals aid as macro initiators for the vinyl (or acrylic) monomer. The free radical initiated grafting leads to the formation of highly branched high molecular weight grafts (Radhakumary *et al.*, 2005)

2.2. Methods of Characterization

2.2.1. Fourier Transform Infra-Red spectroscopy (FTIR)

The Fourier transform infrared spectroscopy of the chitosan derivatives was carried out using a Thermo Nicolet, Avatar 370 spectrometer. The wavenumber range of 400–4000 cm^{-1} was employed to record the

powder-pressed KBR pellets. The number of scans with a resolution of 4 cm^{-1} were set to 32.

2.2.2. Field Emission Scanning electron microscopy (FESEM)

The surface morphology of the prepared samples was investigated with FE-SEM (TESCAN-MIRA 3 LMH, 2014) operated at the accelerating voltage ranging from 50 V to 30 kV in steps of 10 V.

2.2.3. Thermogravimetric Analysis

The prepared samples were analysed for their thermal properties using Thermogravimetric Analyser (Hitachi, STA720 thermal analysis system). The scanning temperature ranged from ambient to 600 ºC at a heating rate of 10 ºC/min under N_2 atmosphere (flowrate 100 cm^3/min). TGA data has been utilised for establishing degradation kinetics of the materials developed. About ~3 mg of samples was heated at four different heating rates namely, 5, 10, 15 and 20 ºC/min in order to carry out the kinetic studies.

2.3. Grafting of polyaniline onto Chitosan

The grafting methodology adopted involved taking calculated amount of chitosan dried in the oven at 60 ºC and dissolved in 100 mL, 2 wt % acetic acid by stirring using a magnetic stirrer for 30 minutes till homogenized. To this solution 2 mL aniline mixed in 15 mL 1 M HCl was added and continuously stirred in an ice bath for 1 hour. Further 3g ammonium persulphate (APS) dissolved in 15 mL 1 M HCl was dropped in to the reactive medium and continued to stir for 4 hours. The obtained dark green coloured product was washed, dried and used for characterization

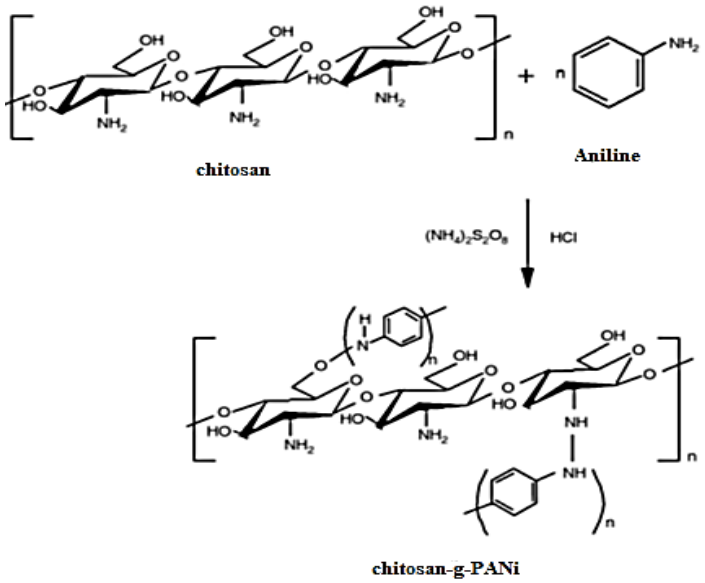

General Scheme 2.1: Chitosan-g-PANi synthesized through the oxidative-radical graft copolymerization (Tiwari and Singh, 2007; Sajjad, 2014)

2.4. Characterisation of chitosan grafted polyaniline

2.4.1. FTIR

FTIR spectra of chitosan-g-PANi (CPS) (Figure 4.1) exhibits characteristic peaks of PANi as well as chitosan. The broad peak between 3300 and 3400 cm^{-1} points to the combination of NH stretching with hydrogen bonded amino groups and the free –OH stretching vibrations (Hosseini, Simiari and Farhadpour, 2009; Khairkar and Raut, 2014). The peaks 2923 and 2850 cm^{-1} is due to aliphatic C–H stretching and the peak at ~1653 cm^{-1} is due to C=O stretching of carbonyl group (typical saccharide absorption). At ~1530 cm –1 and ~1460 cm^{-1} the peaks are indications of C=C stretching of quinoid and C=C stretching vibration of benzenoid rings respectively.

At ~1290 cm^{-1} a peak due to C–N stretching is observed. The absorption band at 1106 cm–1of N=C=N bending vibration shift towards the lower wave number indicating the grafting of PANi on to Chitosan. Also, the hydrogen bonding between the chitosan and imine group in the grafted chain of PANi is responsible for the peak at 1130 cm^{-1} band to shift to a lower wave number (Stephy, Antony and Francis, 2021).

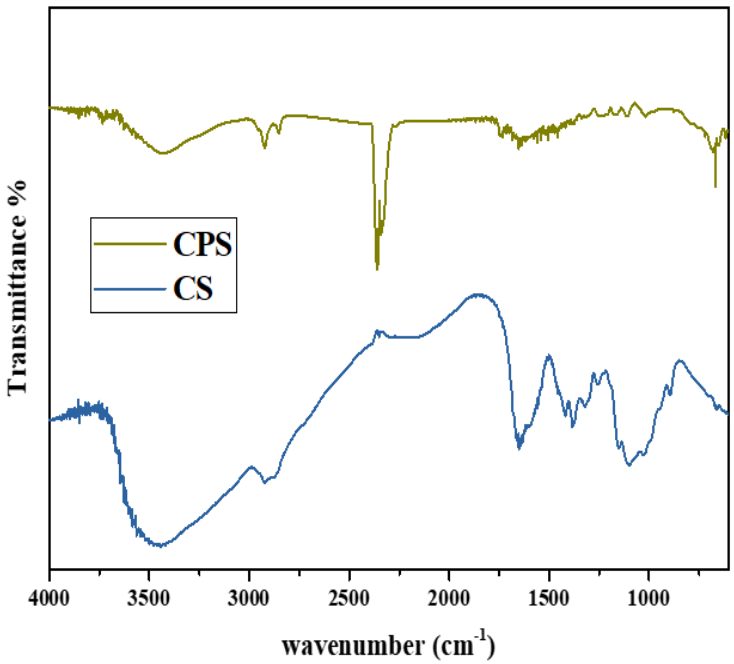

Figure 2.1: Infrared spectra of chitosan and chitosan-g- PANi (CPS)

2.4.2. Surface Morphology

The SEM image shows CPS like accumulated globules in contrast to the interior structures and showed a porous surface. In contrast to chitosan which had cotton-like aggregation and had an uneven form, it reveals the porosity of the globular surface in the grafted chitosan.

Hence, the surface evidence supports the homogeneity of the grafting of PANi on to the chitosan.

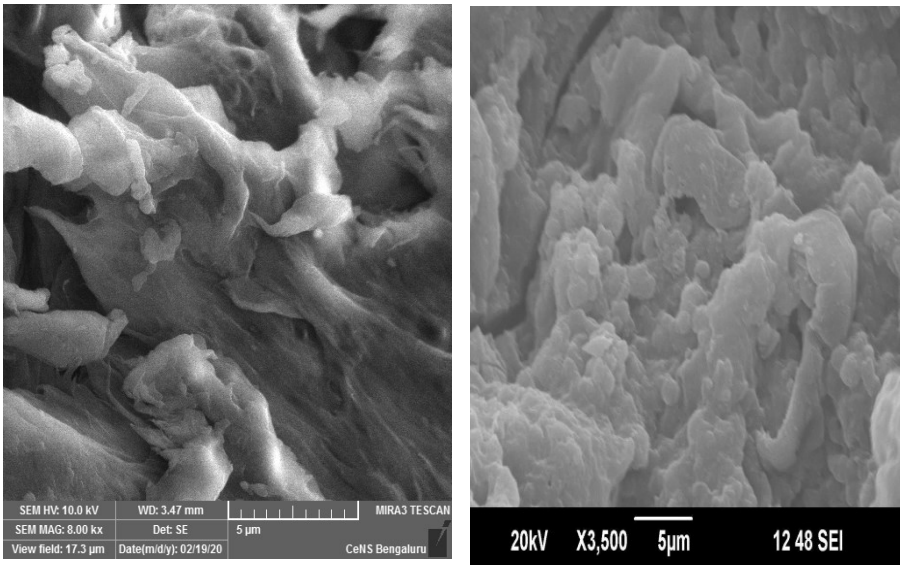

Figure 2.2: SEM micrographs of chitosan and chitosan-g-PANi (CPS)

2.4.3. Thermal properties

The loss of adsorbed water, elimination of impurities and un-reacted monomers becomes the reason for initial loss of weight at temperature up to 250 ℃ for CPS. In the subsequent stage temperature ranging from 250 to 400 ℃ is associated with the loss of chitosan and main polymer chain (Pal and Katiyar, 2017). The weight loss from 400 to 600 ℃ for CPS is due to the loss of chitosan side chain polymers. At the end of the experiment, the increase in residue compared to raw chitosan is a clear indication that CPS exhibits highest thermal stability over chitosan (Al-Allaq, Al-Lami and Al-Mowali, 2019).

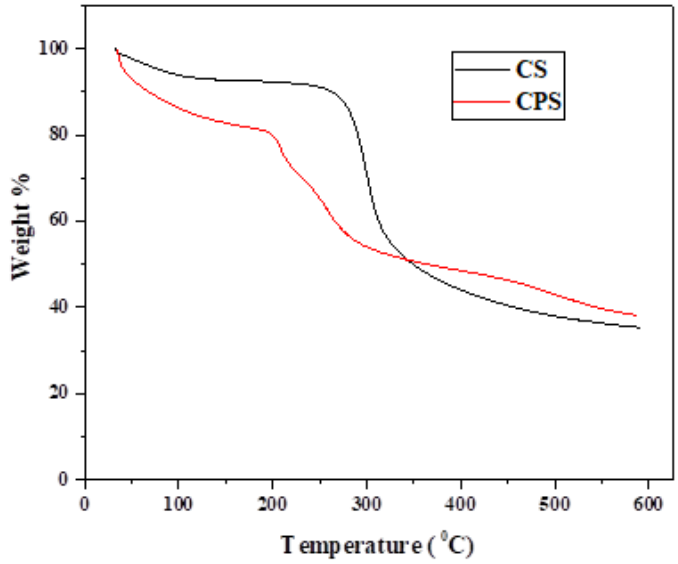

Figure 2.3: TGA thermograms of chitosan and chitosan-g-PANi

2.5. Chitosan grafted with MMA and HEMA

2.5.1. Preparation of Ce(IV) initiated Chitosan grafted with methyl methacrylate

A 2 % w/v solution of chitosan was prepared in 2 % aqueous acetic acid. To the dissolved chitosan, 0.1 M Ceric Ammonium Nitrate (CAN) solution in 10 mL of 1 N nitric acid followed by drop-by-drop addition of 16 mL MMA with continuous stirring. The reaction was carried out at 70 °C in inert atmosphere. After a specified time, the reaction was stopped and the thus obtained product was precipitated using 30 mL of 10 % sodium hydroxide solution with vigorous stirring. The precipitate was washed with distilled water, filtered and the homopolymer was extracted from the grafted product using acetone as solvent in a Soxhlet extractor (Radhakumary, Nair and Mathew,

2005). The formation of the grafted copolymer was confirmed using FTIR, thermal and SEM studies.

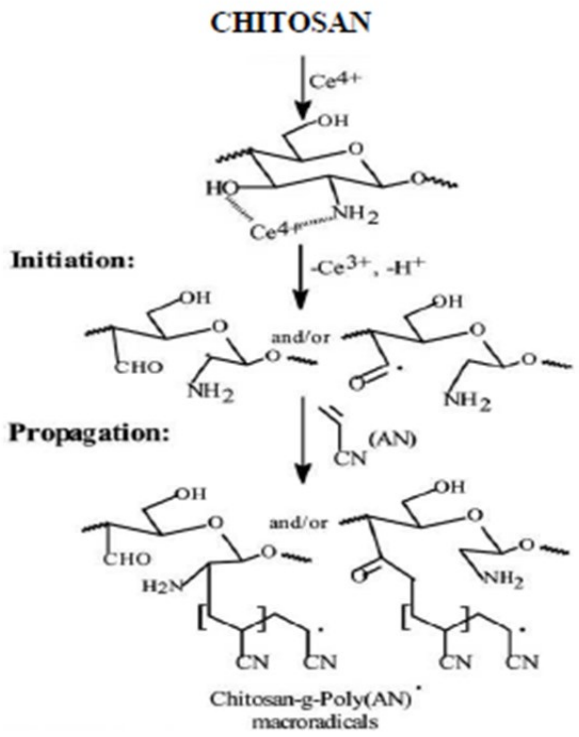

General Scheme 2.2: Reported mechanism for ceric-initiated graft copolymerization of a typical vinyl monomer, acrylonitrile (AN), onto chitosan (Radhakumary *et al.*, 2003, 2005)

2.5.2. Preparation of Ce(IV) initiated Chitosan grafted with 2-hydroxy ethyl methacrylate

2 % chitosan (homogenous solution) was created by stirring the mixture in 2 % acetic acid for 48 h at room temperature. 100 mL of this solution was placed in a three-necked round bottomed flask, fitted with a condenser and stirrer. 0.1 M Ceric Ammonium Nitrate (CAN) in 5 mL of 2 N nitric acid as the initiator followed by 15g HEMA. The

reaction with constant stirring was carried out at 70 ^{o}C for 5 h under nitrogen atmosphere. Subsequently, 30 mL of 10 % NaOH was added while the mixture was being vigorously stirred to precipitate the result. After being filtered, the precipitate was repeatedly washed with distilled water. The homopolymer was removed from the grafted product by Soxhlet extraction using methanol until the methanol extract was devoid of free HEMA (Radhakumary *et al.*, 2003).

2.6. Characterization of chitosan grafted with vinyl monomers

2.6.1. FTIR

FTIR spectroscopy are very useful for the confirmation of the grafting between chitosan and the vinyl monomers. The carbonyl absorption peak appeared at 1724 cm^{-1} for the homopolymer PMMA. In the graft copolymer the presence of the carbonyl absorption peak at 1724, confirmed the grafting reaction between chitosan and MMA. Amide I and Amide II bands of pure chitosan are located at 1648 and 1587 cm^{-1} respectively (Radhakumary *et al.*, 2005).

The FTIR peak at 1710 cm^{-1} of the graft ascertained the grafting of HEMA onto chitosan. Amide I and Amide II bands of pure chitosan are located at ~1640 cm^{-1} and 1550 cm^{-1}, respectively (Singh and Ray, 1998; Radhakumary *et al.*, 2003). The carbonyl band of the HEMA is reported at ~1717 cm^{-1}. On the other hand, the carbonyl absorption band of the graft copolymer shifted to 1710 cm^{-1}. Ahn *et al.* noted a similar lower frequency shifting of the carbonyl peak for poly acrylic acid–chitosan complex (Ahn, Choi and Cho, 2001). This is ascribed to the hydrogen bonding of the carbonyl with the amino and hydroxyl groups of chitosan.

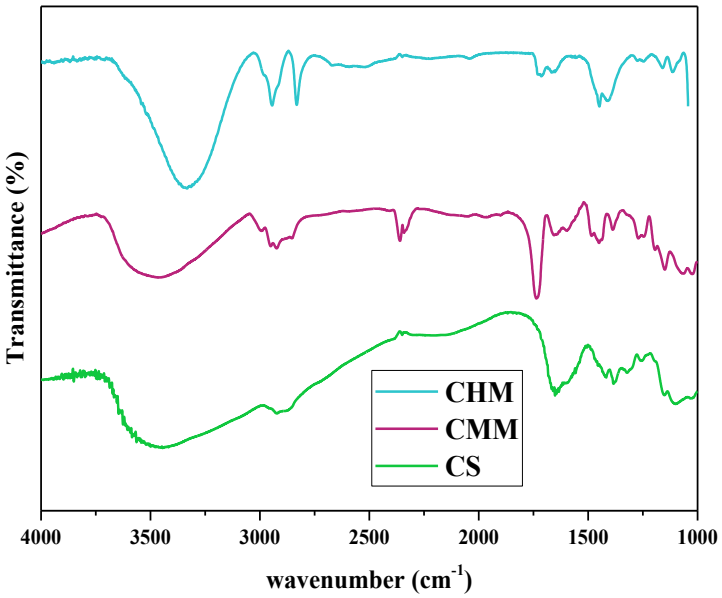

Figure 2.4: Infrared spectra of chitosan (CS), chitosan-g-MMA (CMM) and chitosan-g-HEMA (CHM)

2.6.2. Surface Morphology

Graft copolymerization considerably modifies chitosan morphology. Figure 2.5 shows the SEM micrographs of non-grafted chitosan and grafted chitosan respectively. The PMMA and HEMA are strongly attached onto the chitosan surface and the difference can be observed on the surface grafted chitosan. The micrographs of the grafted chitosan appeared more towards globular structure which is different from the neat flaky chitosan.

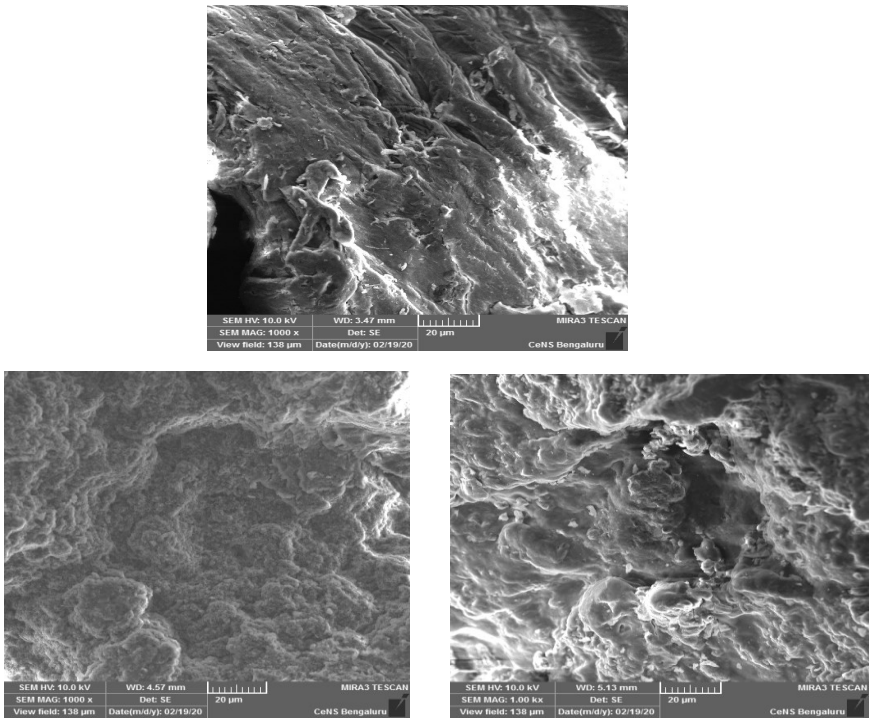

Figure 2.5: SEM micrographs of CS, CMM AND CHM

2.6.3. Thermal properties

The thermal stabilities of chitosan, CMM and CHM is depicted in the figure. The grafting modification with the vinyl monomers is indicated by the two-stage decomposition temperature of the copolymers compared to the single stage decomposition of neat chitosan. Water molecules in the samples may have evaporated, which would account for the weight decrease at temperatures between 100 and 150 ºC. Weight loss between 200 and 400 ºC could be due to the degradation of chitosan main chains. Grafting has increased the initial decomposition temperature, as can be seen plainly from the CMM TGA curve. The higher decomposition temperature of PMMA may be the reason improved thermal stability of CMM. It is already been

reported that PMMA envelops the chitosan surface and thus increased the overall thermal stability of the grafted chitosan.

The grafting with HEMA enhanced the thermal stability of chitosan as seen from the TGA of the polymers. In pure chitosan, the first decomposition temperature was observed at ~240 ºC. It is observed that the copolymer decomposes into two stages, one for the graft and one for the core. However, the overall decomposition temperature of the graft copolymers is elevated with regards to pure chitosan. The second stage of decomposition occurring at ~400 ºC is attributed to the HEMA segments (Figure 2.6). This is attributed to the thermal stabilization of the core-ring by way of H-bonding with the pendant grafts.

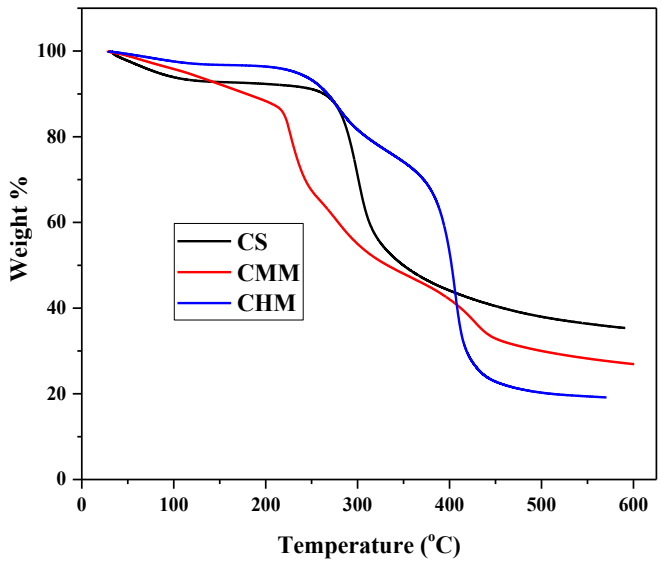

Figure 2.6: TGA thermograms of CS, CMM and CHM

2.7. Preparation of chitosan/phytic acid polyelectrolyte complex

A homogeneous solution of 2 % w/v of chitosan in 2 % acetic acid was prepared by stirring it overnight. The pH of the solution was adjusted to 1.5 using 5 M HCl or NaOH. The phytic acid solution was prepared as 4 wt % concentration using deionized water and the pH was adjusted to 1.5 using 5 M NaOH or HCl (Zhang *et al.*, 2014). The prepared phytic acid was added dropwise to yield a white precipitate. The precipitate was washed till neutral, filtered and dried at 60 °C. The characterization was carried out via FTIR and TGA

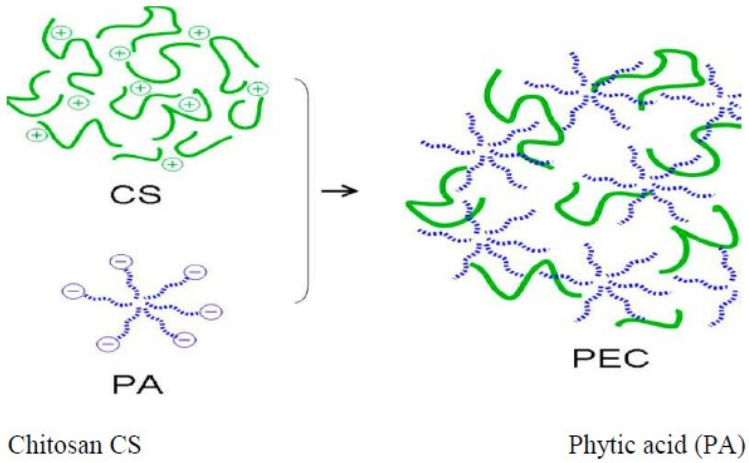

General scheme 2.3: Chitosan/phytic acid polyelectrolyte complex (Zhang *et al.*, 2014)

2.8. Characterization of Chitosan/phytic acid polyelectrolyte complex

2.8.1. FTIR

Figure 2.7 depicts the FTIR spectra of chitosan, phytic acid and chitosan. The characteristic peaks of chitosan at ~1636 (amide I), 3132 (OH stretching) and ~1400 cm^{-1} (CH_2 bending). In the PEC spectrum,

the shoulder amide peak at around 1644 cm^{-1} decreased and shifted to ~1630 cm^{-1}, signifying the formation of an interaction between CS and PA(Zhang *et al.*, 2014). Comparatively, PEC exhibits a novel absorption band at 1540 cm^{-1}, which is attributed to the NH_3^+ vibrational mode. This could be the result of partially protonated NH_2 from the addition of HCl, which complexes positively charged CS and negatively charged PA(Stephy, Antony and Francis, 2023). Also, the band near 1067 cm^{-1} (stretching mode of $(PO_3)^{2-}$) is depicted by the formed PEC.

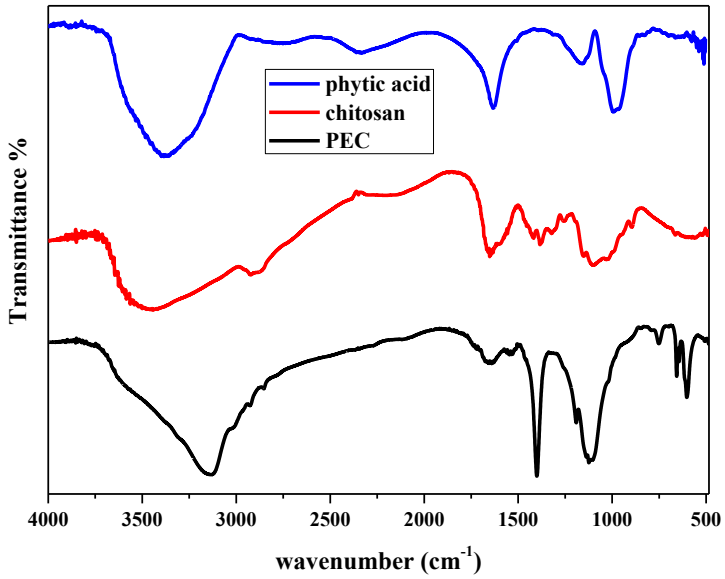

Figure 2.7: Infrared spectra of chitosan, phytic acid and PEC

2.8.2. Surface Morphology

It can be observed that there is a distinct variation in the appearance of the polyelectrolyte complex in comparison with chitosan which appears to be. Also, the presence of Phosphorous was confirmed by

EDX data (Stephy, Antony and Francis, 2023). These observations are similar to the previously reported literature (Zhang *et al.*, 2014).

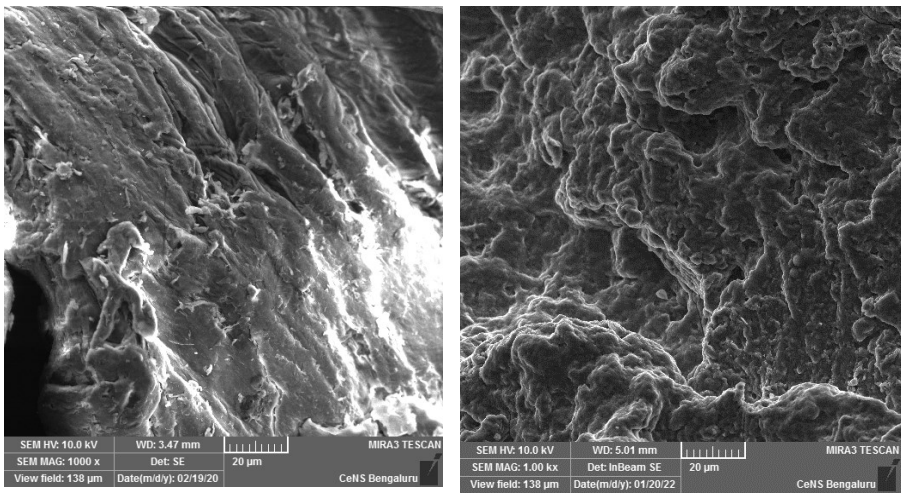

Figure 2.8: SEM image of chitosan and PEC

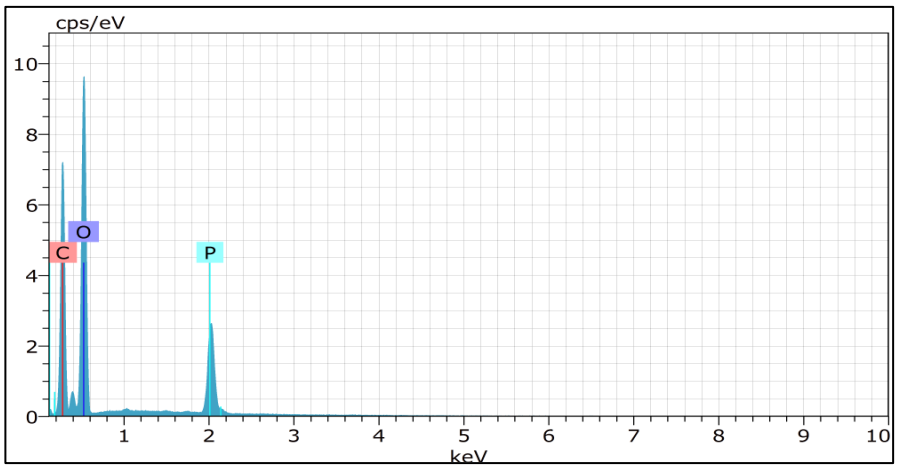

Figure 2.9: EDX image of PEC

2.8.3. Thermal Properties

Figure 2.10 depicts the information about the thermal degradation behavior of phytic acid, chitosan and PEC under nitrogen atmosphere and Table 2.6 represents the initial degradation temperatures of the materials.

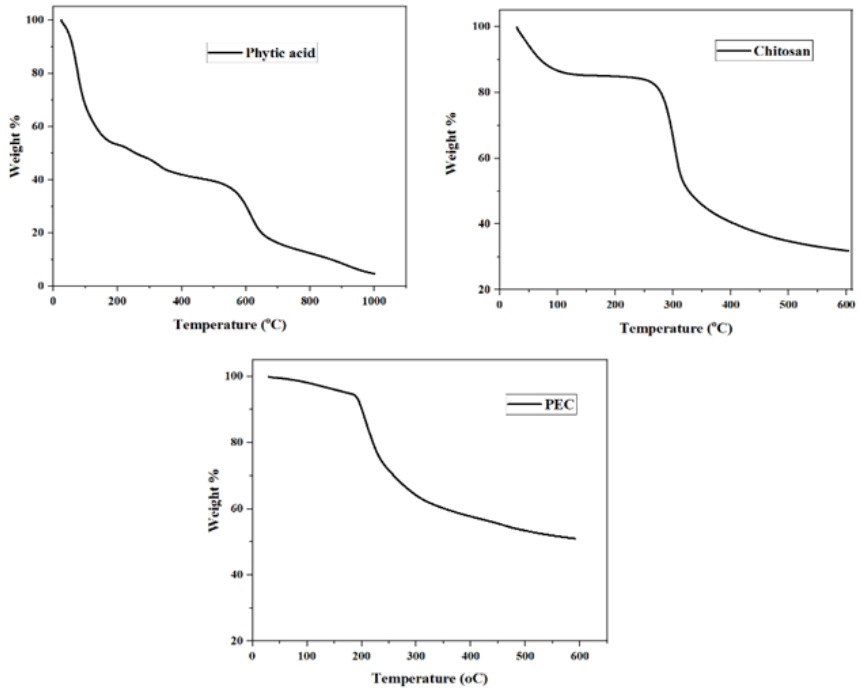

Figure 2.10: TGA thermograms of chitosan and PEC

When compared to raw chitosan, the lower value for the initial decomposition of PEC shows the role of PA in initiating earlier degradation because of the phosphorus-containing groups(Stephy, Antony and Francis, 2023).

Table 2.6. Degradation temperatures of the materials

Sample code	Initial degradation temperature (°C)
CS	251
PA	181
PEC	194

In comparison to pure chitosan, the residue increased, suggesting that PEC has better thermal stability and char formation, both of which are facilitated by the acidic sites of phytic acid(Stephy, Antony and Francis, 2023).

Chapter 3
Composite Fabrication and Characterization Methodology

This chapter deals in detailed the methodologies involved in the investigation of the properties of the composites prepared. The formulations and the methods that are used in for the development of the composites, ie; melt mixing with Brabender is described. The elaborate study on the mechanical properties using UTM, the thermal properties using TGA and the dielectric properties with dielectric broadband spectroscopy is carried out. The recent literature involving the same has also been reviewed.

3.1. Methods

3.1.1. Composite Development

One of the most effective methods for the fabrication of the polymer composites is the melt mixing method wherein the mixing occurs inside a chamber which is fitted with a roller rotor. The rotation of these rotors in the opposite direction introduces the shearing force on the samples. Since this solvent free technique leads to the production of lesser by-products, it is considered to be a cost-effective, sustainable method. The processing was executed in a in Brabender Plasticoder Model PL 3S with a volumetric capacity of 40 cm^3.

Figure 3.1 Brabender Plasticoder Model PL 3S

The general process was carried out as follows, the instrument is preheated to a desired temperature. A heat as a result of mechanical dissipation is thus developed in the gaps of the chamber and the rotors which helps in the melting of the constituents. EVA was initially

added, allowed to melt and followed by the addition of the filler. The automatic cut-off feature of the instrument comes into play when the temperature rises above the set limit.

In this work EVA is used as the matrix and chitosan grafts are taken as fillers. the formulation used during mixing has been given in the respective chapters

3.2. Characterization techniques

3.2.1. Mechanical characterizations

The mechanical characterization was studied using stress-strain measurements of the developed composites. The films that are cut into dumbbell shape was used to carry out the test for tensile properties on a 'Shimadzu Autograph AG-X series' Universal Testing Machine (UTM) at a cross head speed of 50 mm/min. Between the clamps the distance was fixed to 40 mm at the start of each test. An average of 5 - 6 concordant measurements were done for each composition and taken to represent each data. A digital thickness gauge was used to measure the thickness of the narrow portion. The standard test piece is gripped at both ends in the jaws of UTM, which slowly exerts an axial pull so that the sample is stretched and finally it breaks. The tensile strength, elongation at break and Young's modulus was determined from the stress-strain analysis.

Tensile strength (σ) is defined as a stress that can be described as force per unit area. Generally, a change in cross-sectional area is observed after the stress-strain analysis. Hence the area used in the calculation is the un-deformed cross-sectional area, A.

$$\sigma = \frac{Force}{Area} \quad (1)$$

Strain (ε) is measured as the change in length (L) to the initial length (L_0) of the sample.

$$\text{Strain } (\varepsilon) = \frac{L}{Lo} \quad (2)$$

The deformation of the material depends upon the magnitude of the external stress imposed on it. At a lower stress level, strain is directly proportional to stress (Hooke's Law). The majority of the specimen undergoes a linear stress - strain relationship, where the material shows an elastic behavior. Beyond the linear region, the deformations are not elastic and do not return to the original length.

Young's Modulus / Modulus of elasticity/ tensile modulus (E) is the slope of the linear portion of the stress – strain curve. It measures the stiffness of the material.

$$E = \frac{\sigma}{\varepsilon} \quad (3)$$

The effect of concentration of filler on the mechanical properties of the developed EVA based composites were explored. Further the impact of chemical modification of the fillers were also determined. Table 3.1 shows the literature reviewed on the mechanical properties of some of the polymer composites.

Table 3.1: Literature review on mechanical studies of polymer composites

Sl No	Material Type	Inference	Reference
1	Low density polyethylene and ethylene vinylacetate (LDPE–EVA) blends with alumina trihydrate (ATH)	With the increase of MMT loading from 5 -10 phr, the tensile strength of all un-irradiated ATH added LDPE–EVA blends remains unchanged. However, with the increase in MMT loading from 10 - 20 phr the tensile strength of un-irradiated samples was gradually increased.	(Bee *et al.*, 2013)
2	EVA/Bacterial cellulose nano fibers (BC)	Modified BC nano-fibres imparts better mechanical and barrier properties to the EVA films. The results were attributed to the different chemical functional groups on the surface of cellulose fibres	(Yuwawech, Wootthikanokkhan and Tanpichai, 2015)
3	EVA/hydroxyapatite (HAP)	The influence of size of HAP particles were explored. The higher values of mechanical properties like tensile modulus, flexural modulus, and impact strength were shown by composites with HAP of smaller size. Further the interaction between the filler and matrix was found to be mechanical rather than a chemical bond.	(Sunny *et al.*, 2011)
4	EVA/ magnesium hydroxide/ cerium oxide (EVA/MDH/CeO_2)	The addition of CeO_2 into the EVA/MDH composites improved the tensile properties such as elongation at break (~52.25%) and Young's modulus (~6.85%).	(Hobson *et al.*, 2022)

		Additionally, the incorporation of the rare earth oxide significantly increased the flame retardancy and anti-UV ageing properties.	
5	EVA//carbon fibers (EVA/CF)	The influence of electron beam radiation on the mechanical properties of EVA/CF composites was carried out. Although there was an increase in the modulus and shear stress, the creep value tends to decrease with the increase in filler content and irradiation. This trend indicated the better interaction and cross-linking	(Hamid, Svoboda and Svobodova, 2020)
6	EVA/microcrystalline cellulose (MCC)	Composites with varying VA composition and MCC were studied. Increase of VA group concentration leads to an increase in the elongation at break of the composites. Also, a reduction in mechanical properties was observed with the increase in melt flow index (MFI) of EVA.	(Shelenkov, Pantyukhov and Popov, 2020)
7	EVA/Graphene	The simulated results and the experimental values of that the glass transition temperature, modulus, yield strength, and ultimate strength of the nanocomposites are higher than that of pristine EVA. The improvement of mechanical properties of EVA/ graphene composites were attributed to the limited movement of the EVA chains due to the strong interfacial interaction between	(Shi *et al.*, 2020)

		graphene and EVA.	
8	EVA/ halloysite nanotubes (HNTs)	An increase in tensile modulus and elongation of 100 % was seen with the increase in filler (HNTs) concentration. This was attributed to the reinforcing effect of the HNT towards the EVA matrix	(Zubkiewicz *et al.*, 2020)
9	Chitosan/Polyvinyl Alcohol (PVA)	PVA improved tensile strength (TS) and elongation at break of the prepared chitosan films. The presence of chemicals to modify the material imparted an increase in the film strength for all samples prepared.	(Wardhono *et al.*, 2022)
10	Chitosan (CS)-based functional film/cellulose nanofiber (CNF)/ammonium polyphosphate (APP)/ branched polyethyleneimine (BPEI)	The inherent toughness and the availability of hydroxyl groups on the surface of CNF imparted a better mechanical strength towards the formed composite film.	(Chen *et al.*, 2022)

3.2.2. Non-isothermal degradation kinetics

In order to acquire a better understanding and information of thermal degradation non-isothermal degradation kinetics was explored with model-free and model-fitting methods. These methods are widely used for the kinetic analysis of biomass (Ahmad *et al.*, 2017; Çepelioğullar *et al.*, 2018; Naqvi *et al.*, 2018). For all types of non-isothermal kinetic investigations, the degradation response can be described by,

$$\frac{d\alpha}{dt} = \mathrm{k(T)f(\alpha)} \tag{4}$$

where, k(T), f (α), α denote the rate constant, reaction model and conversion rate (degree), respectively.

The conversion α of materials can be calculated by,

$$\alpha = \frac{(m_0 - m_t)}{(m_0 - m_f)} \tag{5}$$

where, m_o, is the initial weight of the sample, m_t is the weight of the sample at time (t) and m_f is the final weight of the sample (Stephy, Antony and Francis, 2021).

The rate constant k(T) in equation (4) obeys the Arrhenius equation

$$\mathrm{k(T)} = Aexp\left(\frac{-E_a}{RT}\right) \tag{6}$$

where, E_a is the activation energy (kJ/mol), R is the universal gas constant (8.314 $Jmol^{-1}K^{-1}$), T is the absolute temperature (K) and A is the pre-exponential factor (min^{-1}).

The constant heating rate (β) for the dynamic analysis of the non-isothermal data obtained from the TGA experiments is defined as follows:

$$\beta = \frac{dT}{dt} \tag{7}$$

By combining the value of k(T) and β, we can rewrite equation (7) as

$$\frac{d\alpha}{dT} = \frac{A}{\beta} exp\left(\frac{-E_a}{RT}\right) f(\alpha) \tag{8}$$

Equation (8) represents the expression to estimate the activation energy (E_a) based on TGA kinetics data for rate of degradation developed materials (Stephy, Antony and Francis, 2021, 2023). The following equations were used in this work to evaluate the activation energies from various methods.

Table 3.2: Formulas used in the modelling of pyrolysis kinetics

Equation No	Method	Expressions
9	FWO	$\ln(\beta) = const - 1.052(\frac{E_a}{RT})$
10	KAS	$\ln\left(\frac{\beta}{T^2}\right) = \frac{E_a}{RT} - \ln\left(\frac{AR}{E_a}\right)$
11	Tang	$\ln\left(\frac{\beta}{T^{1.8947}}\right) = const - 1.0015\left(\frac{E_a}{RT}\right)$
12	Starink	$\ln\left(\frac{\beta}{T^{1.92}}\right) = const - 1.0008\left(\frac{E_a}{RT}\right)$
13	Friedman	$\ln\left[\frac{d\alpha}{dt}\right] = \ln[Af(\alpha)] - \frac{E_a}{RT}$
14	Vyazovkin	$\int_0^{\alpha} \frac{dy}{f(y)} = A\int_0^{t} exp\left(-\frac{E_a}{RT}\right)dt$

3.2.3. Thermodynamic parameters

In this work, the thermodynamic parameters such as change in enthalpy (ΔH), change in entropy (ΔS), and Gibbs free energy (ΔG) were determined using the following equations from the estimated kinetic parameter values.

$$\Delta H = E_a - RT \tag{15}$$

$$\Delta G = E_a + RT_p \, ln\left(\frac{K_B T_P}{hA}\right) \tag{16}$$

$$\Delta S = \frac{\Delta H - \Delta G}{T_P} \tag{17}$$

where K_B (1.3819 x 10^{-23} J/K) and h (6.6269 x 10^{-34} Js) are the Boltzmann and Planck constants, respectively.

To reduce interaction effects, the value Tp (the DTG peak temperature) value was calculated based on the lowest heating rate i.e., 5 °C/min (Parthasarathy *et al.*, 2022). The previous literature regarding the thermal behaviour of polymeric materials is given in Table 3.3.

Table 3.3: Literature on thermal degradation kinetics of materials

Sl No	Modelling type		Material type	Inference	Reference
	Model-free/ model-fitting/ computational	**Model name**			
1	Model-free	Friedman, KAS, FWO, iterative, Vyazovkin, Vyazovkin AIC	Pinewood	Pyrolysis of pinewood depicted multistep kinetics that was deduced from isoconversional methods. Till conversion value 0.7, the pyrolysis tends to follow diffusion mechanism followed by 1 ½ order reaction	(Mishra, Kumar and Bhaskar, 2015)
2	Model-free	Kissinger, Ozawa, Kissinger-Akira-Sunose, Friedman	Lignite coal	Studies pointed that Friedman method is best for solid state mechanism like pyrolysis of coal.	(Heydari, Rahman and Gupta, 2015)
3	Model-free	Friedman, KAS, FWO, Vyazovkin	Saw mill waste	Similar activation energy profile was observed for all the methods and the mechanism pointed to two-dimensional diffusion.	(Bonilla, Salazar and Mayorga, 2019)

4	Model-free	FWO and in-house developed software	Bio-sourced substrates	The activation energies obtained for carbohydrate based substrates were on par with the FWO method than the in-house method. However, the E_a values should be considered as apparent.	(Thomas *et al.*, 2020)
5	Model free & model fitting	Coats-Redfern (CR), DAEM, FWO, Vyazovkin	Cattle manure	CR and DAEM methods presented are more in agreement with the experimental data as compared to the model-free methods. The power law (P_3) reaction model is proper to describe the experimental behavior of cattle manure. When compared with FWO, the Vyazovkin method displayed the better results for decomposition.	(Chen *et al.*, 2017)
6	Model free	Friedman, KAS, FWO, Popescu, Artificial Neural Network (ANN)	High-ash sewage sludge (HASS)	The pyrolysis of HASS is endothermic and the DG and DS values pointed towards non-spontaneity.	(Naqvi *et al.*, 2018)
7	Computational	ANN	Lignocellulosic forest residue (LFR) and olive oil residue	At $\alpha > 0.7$, ANN predicted data started to show deviations from the experimental data but the E_a values are	(Çepelioğullar *et al.*, 2018)

			(OOR)	closer to the experimental ones. This depicted that ANN can be coined as good method to determine Ea	
8	Model free	Friedman, KAS	Sodium Lauroyl Isethionate	The correlation between predicted and measured degradation supports the utilisation of the modelling methods in analysis of complex organic systems. In these metallic associations were found to lead to a greater complexity in atomic composition, polarity and coulombic interactions.	(Jeraal *et al.*, 2019)
9	Model free and model fitting	FWO, KAS, CR	Bayan Obo rare earth (BORE) concentrate	The calculation of E_a which were similar was carried out by FWO and KAS methods. The Avrami−Erofeev mechanism, was predicted using CR method.	(Zou *et al.*, 2018)
10	Model fitting	Parallel reaction model (PRM), Avrami-Erofeev model, DAEM	Saw dust	The isothermal and non-isothermal pyrolysis of the material was studied. The non-isothermal pyrolysis of the system was described by DAEM which was in concurrence with PRM. Avrami-Erofeev model explained the isothermal pyrolysis.	(Zhang *et al.*, 2019)

11	Computational	Discrete DAEM	Bio-oil derived from cedar wood	Activation energy studies showed significant variation predicting the multistep kinetic nature of the reaction. Discrete DAEM results showed the prominence of weight fraction on the reaction profiles.	(Chen *et al.*, 2019)
12	Model free	FWO, KAS, Friedman, Cai, Vyazovkin	Glass fibre-reinforced epoxy resin composites	It was found that both linear and non-linear isoconversional methods gave similar outcome for the activation energy estimation. The use of DEAM and IPR models depicted a highly predictable system that had only a slight deviation. These results pointed that pyrolysis is a better method to dispose epoxy-based resins.	(Yousef *et al.*, 2021)
13	Model free and model fitting	FWO, KAS, Kissinger, CR, Criado	PLA/talc/Opuntia Ficus Indica flour (OFI-F) composite	The results indicated activation energy values of the PLA/OFI-F biocomposites are lower than the neat PLA. Also, addition of talc did not show any significant change in the E_a values. The kinetic model was predicted by Coats-Redfern and Criado methods. The thermal degradation follows a second-order reaction mechanism.	(Gharsallah *et al.*, 2021)

14	Model free and model fitting	FWO, Kissinger, Friedman	PLA with ZnO, TiO_2, AgNPs	Friedman and Kissinger methods were used to calculate the E_a of non-isothermal cold crystallization. The addition of metal oxide nanofillers affected the thermal stability of PLA by a decrease in the E_a values.	(Tarani *et al.*, 2021)
15	Model-free	KAS, Friedman	Cellulose cryogel	The estimation of degradation kinetics and lifetime prediction of biomass cellulose cryogels (BC) reinforced by cellulose pyrolysis waste and by graphene nanoplatelets (NPG) was carried out. The two-step degradation and high E_a values depicted better thermal stability of the said composites. Also, lifetime prediction indicated the CC cryogel became more stable on standing, maintaining almost 80% of the mass at an exposure of 1 year at 180 °C.	(Lazzari *et al.*, 2022)

3.2.4. Dielectric properties

Dielectric measurements can be taken using an LCR meter or using broadband dielectric spectroscopy. The electrical properties of the composites were studied using broadband dielectric spectroscopy (BDS). The measurements using the Novocontrol Alpha A Analyzer in the broad frequency range (10^{-2} to 10^{7} Hz) were carried out at room temperature. The samples were sandwiched between two parallel gold-plated electrodes of diameter 40 mm used as a test capacitor.

Broadband dielectric spectroscopy (BDS) is a unique technique to determine the dielectric functions of a complex system over a range of frequencies. This technique reveals the electrical nature, especially dielectric, by assessing the molecular fluctuation and charge transport in the samples within the squat electric field. The value of complex impedance from the applied voltage and measured current can be calculated as,

$$Z^*(\omega) = \mathrm{Z}'(\omega) + \mathrm{jZ}''(\omega) = \frac{V^*(\omega)}{I^*(\omega)} \tag{18}$$

It evaluates the molecular and the collective response of the sample to the applied field and measures complex impedance function Z*(ω), where j the current density and ω is the angular frequency, from which the complex dielectric function (ε*(ω)) can be derived using the formula,

$$\varepsilon^*(\omega) = \varepsilon'(\omega) - i\varepsilon''(\omega) = \frac{1}{j\omega C_0 Z^*(\omega)} \tag{19}$$

where the imaginary part, ε″(ω), is proportional to the energy that is dissipated per period, and ε′(ω) is proportional to the energy that is

stored reversibly in the system per period. Consequently, a number of parameters can be derived from the complex dielectric function like conductivity $\sigma^*(\omega)$ by,

$$\sigma^*(\omega) = \sigma'(\omega) + j\sigma''(\omega) = j\omega\varepsilon_0\varepsilon^*(\omega) \quad (20)$$

Modulus $M^*(\omega)$ can also be derived.

$$M^*(\omega) = M'(\omega) + jM''(\omega) = \frac{1}{\varepsilon^*(\omega)} \quad (21)$$

Further, tan d can be calculated by,

$$\tan\delta = \varepsilon''(\omega)/\varepsilon'(\omega) \quad (22)$$

where $\varepsilon'(\omega)$ is the real part and $\varepsilon''(\omega)$ the imaginary part of the complex dielectric function (Poplavko, 2021). Table 3.4 shows the dielectric behavior of some of the reported polymer composites.

Taking all these literature into account and identifying the significance of the need to detailed study about materials involving chitosan and EVA, composites were developed and their behaviour was extensively evaluated.

Table 3.4: Literature on dielectric properties of polymer composites

Sl No	Material Type	Inference	Reference
1	EVA/ PANi	When compared to a composite with a higher filler loading, one with a lower PANi concentration tends to exhibit a relatively larger change in dielectric characteristics against applied pressure and time under compression. These lower loaded composites can be used as dielectric sensors.	(Rahaman, Chaki and Khastgir, 2013)
2	EVA/ ZnO nanocomposite	The conductivity increases with the increase of ZnO filler concentrations and resistivity increases with the increase of temperature.	(Sebastian *et al.*, 2015)
3	EVA composites filled with Carbon Nanotubes, Graphene Nanoplatelets and Iron Oxide Nanoparticles	Dielectric permeability decreases with the increase of frequency. Addition of 20 wt % of the fillers tend to impart slight betterment to the dielectric properties of the composite.	(Barkane *et al.*, 2019)
4	EVA/MWCNTs/hectorite	An enhancement on the dielectric properties such as dielectric constant and ac conductivity of EVA improved significantly with an	(Bhuyan, Srivastava and

		increase in filler addition up to 5 %.	Mittal, 2017)
5	PP-EVA-Organoclay	Organoclay-compatibilized nanocomposites exhibit increased dielectric losses compared to the non-compatibilized composites owing to the interfacial polarization processes, and increased conductivity.	(Shaw *et al.*, 2019)
6	EVA/cenosphere	The dielectric permittivity increases with the increase in filler loading and decreases with the increase in frequency due to the interaction of the cenosphere (a lightweight, inert, hollow sphere made largely of silica and alumina and filled with air or inert gas) with polymer matrix.	(Padhi, Priyadarsini and Nayak, 2020)
7	Polylactic Acid (PLA) Reinforced with TiO_2 decorated carbon nanotubes	The dielectric and thermal nature of introducing TiO_2 decorated carbon nanotubes were investigated. The decorated TiO_2 nanoparticles on the surface of MWCNTs can be used as insulating layers to suppress the dielectric loss compared to the pure PLA.	(Wu *et al.*, 2019)
8	Chitosan-zinc oxide nanoparticles (CS-	Chitosan matrix with ZnO NPs have dielectric constant higher than that of neat chitosan and	(Kaur *et al.*,

	ZnO NPs)	ZnO due to the formation of interfacial layer. The side groups of chitosan interacted strongly with ZnO NPs creating the layer between nanoparticles and matrix.	2021)
9	PA/Ethylene vinylacetate glycidyl methacrylate random terpolymer (EVA-GMA) blends with Hydroxylated $BaTiO_3$ (BT-OH) and multiwalled carbon nanotubes (MWCNTs	BT-OH acted as a high dielectric ceramic filler and nonconductive insulating barrier. However, MWCNTs served as a conductive filler by supporting the formation of more microcapacitors and inhibiting the conductive path.	(P. Wang et al., 2021)
10	Polyaniline-chitosan (PANi-CS) blends	In comparison with pure chitosan samples, the prepared PANi-CS samples have improved conductivity and dielectric properties. Moreover, the dielectric permittivity of the PANi-CS blends was influenced by dopants such as CH_3COOH and HCl.	(Ashley *et al.*, 2021)

Chapter 4
Degradation Kinetics of The Modified Chitosan Fillers

This chapter deals with the studies on chitosan grafted polymers (fillers). A detailed study on the degradation kinetics of chitosan grafted with polyaniline (PANi), methyl methacrylate (MMA), 2-hydroxy ethyl methacrylate (HEMA) were carried out by employing data obtained from thermogravimetric analysis. Model free methods such as Flynn-Wall-Ozawa (FWO), Kissinger-Akahira-Sunose (KAS), Starink, Tang, Friedman and Vyazovkin has been employed to calculate E_a of various α. In addition, thermodynamic parameters were also calculated for the said materials.

4.1. Chitosan grafted with polyaniline

4.1.1. Degradation Kinetics using TGA

The isoconversional analysis of the formed copolymers was carried out using four integral (FWO, KAS, Starink and Tang) and one differential method (Friedman). The study's findings will aid in understanding the pyrolytic attributes of the grafts. Figure 4.1 depicts the plots to determine activation energy (E_a) by utilizing FWO, KAS, Starink, Tang and Friedman methods at α ranging from 0.1 to 0.9. For each method the complexity of the values of E_a is by determining the slopes from the plots that are linearly fitted. The values obtained for E_a from the plots are mentioned in Table 4.1.

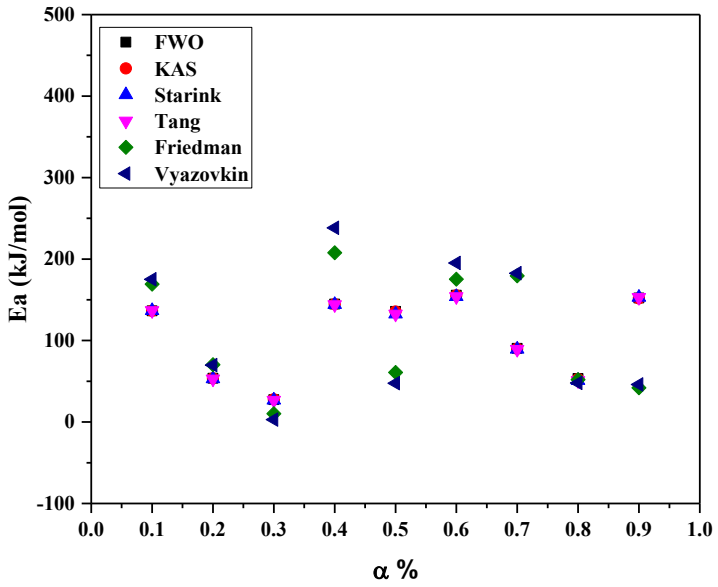

Figure 4.1: Activation energy (E_a) vs conversion (α) profiles of CPS using FWO, KAS, Starink, Tang, Friedman and Vyazovkin methods

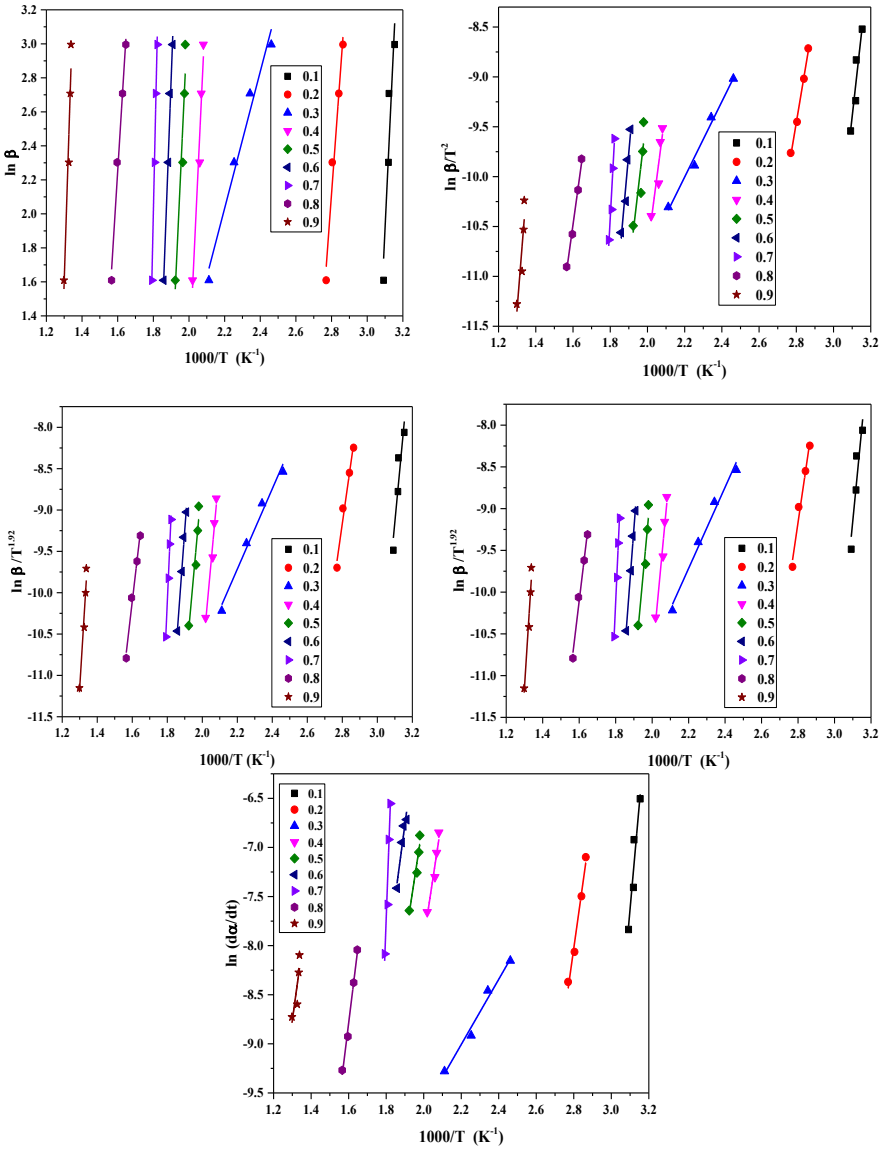

Figure 4.2: Typical linear regression lines of CPS using FWO, KAS, Starink, Tang and Friedman methods

Table 4.1: The energy of activation according to conversion degree for FWO, KAS, Starink, Tang, Friedman and Vyazovkin methods of CS & CPS

CS						
	FWO	**KAS**	**Starink**	**Tang**	**Friedman**	**Vyazovkin**
α	**E_a**					
0.1	47.91	47.18	54.47	54.55	38.09	26.64
0.2	208.10	208.03	221.58	221.70	214.90	214.20
0.3	217.2	217.13	217.65	217.77	227.09	226.89
0.4	226.03	225.96	226.41	226.53	242.25	240.27
0.5	237.68	237.62	237.87	237.99	264.40	265.70
0.6	266.27	266.21	265.73	265.85	324.34	328.01
0.7	356.43	356.38	357.63	357.75	395.120	391.84
0.8	433.56	433.52	432.50	432.64	449.86	449.02
0.9	758.77	758.73	741.77	741.92	832.69	816.70
Average	**305.77**	**305.64**	**306.18**	**306.30**	**332.08**	**328.81**

CPS						
	FWO	**KAS**	**Starink**	**Tang**	**Friedman**	**Vyazovkin**
α	**E_a**					
0.1	136.42	136.36	136.74	136.68	169.12	175.20
0.2	53.63	53.48	52.93	52.86	70.40	69.90
0.3	27.30	27.90	26.81	26.72	10.22	2.96
0.4	144.70	144.55	144.14	144.03	207.67	238.31
0.5	135.69	135.54	132.55	132.44	60.85	47.55
0.6	155.60	155.34	153.98	153.86	175.26	195.19
0.7	90.30	89.89	89.33	89.21	179.32	182.66
0.8	53.28	52.73	50.97	50.83	52.03	47.94
0.9	152.16	151.62	153.05	152.89	42.04	45.99
Average	**105.45**	**105.27**	**104.50**	**104.39**	**107.43**	**111.75**

*E_a is in kJ/mol

Based on the calculation and fitting curves, the average E_a for the polyaniline grafted chitosan was estimated within the range of 104-112 kJ/mol for the kinetic models**.** The values of E_a estimated between 304-332 kJ/mol for Chitosan. These values fall around the region reported in earlier works of chitosan degradation (Sonia and Priya Dasan, 2013). The E_a values obtained from the Friedman and Vyazovkin methods are greater than the E_a values produced using the other four models. A similar behaviour was also observed by Parthasarathy et al. (Parthasarathy *et al.*, 2022). This is due to the inclusion of the approximations and assumptions in the other four models (Stephy, Antony and Francis, 2021). The kinetic data revealed that with the increase in α, the E_a values changed through multiple steps rather than a single step due to the breakdown of the sample indicating the complex nature of the degradation process. Some of the earlier work report that the degradation in the pyrolytic process occurs in a series which is not apparent in the current study (Sonia and Priya Dasan, 2013). Each component present in the copolymer undergoes variable degradation leading to the non-linear behaviour.

4.1.2. Thermodynamic Properties

The thermodynamic parameter values ΔG, ΔH, and ΔS were determined using the E_a values that were obtained using the models. To reduce interaction effects, the Tp value was calculated based on the lowest heating rate (i.e., 5 °C/min) (Parthasarathy *et al.*, 2022)

Table 4.2: Pre-exponential factor and other thermodynamic parameters for CPS obtained by using activation energy deduced from FWO, KAS, Friedman and Vyazovkin methods.

	α	Pre-exponential factor, A (s^{-1})	Enthalpy, ΔH (kJ/mol)	Gibbs free energy, ΔG (kJ/mol)	Entropy, ΔS (J /mol)
FWO	**0.1**	4.74E-39	136.00	207.06	-1412.39
	0.2	1.23E-15	52.90	138.05	-968.82
	0.3	1.08E-08	25.63	194.58	-842.76
	0.4	6.89E-29	142.86	416.02	-1230.20
	0.5	6.76E-25	133.64	418.82	-1154.66
	0.6	1.86E-33	153.39	502.99	-1319.13
	0.7	7.35E-18	87.94	378.91	-1021.15
	0.8	4.95E-10	50.24	369.37	-873.34
	0.9	2.94E-21	148.03	690.23	-1090.83
	Average	**1.25E-09**	**103.40**	**368.45**	**-1101.48**
KAS	**0.1**	2.67E-36	136.36	204.36	-1359.75
	0.2	7.21E-15	53.48	136.61	-954.10
	0.3	4.71E-06	27.90	185.05	-792.20

	0.4	7.18E-33	144.55	432.79	-1306.43
	0.5	6.28E-16	135.54	376.26	-982.98
	0.6	4.89E-33	155.34	500.60	-1311.09
	0.7	1.17E-24	89.89	415.57	-1151.25
	0.8	1.35E-09	52.73	365.79	-865.04
	0.9	4.66E-13	151.62	611.67	-933.85
	Average	**5.23E-07**	**105.27**	**358.74**	**-1072.96**
Friedman	**0.1**	2.20E-31	168.70	232.37	-1265.62
	0.2	2.55E-14	69.67	152.60	-943.59
	0.3	2.00E-05	8.56	164.97	-780.20
	0.4	1.16E-25	205.82	465.26	-1168.42
	0.5	9.14E-10	58.80	272.44	-864.99
	0.6	1.75E-20	173.05	456.83	-1070.78
	0.7	3.25E-20	176.95	480.76	-1066.22
	0.8	4.11E-08	48.99	354.70	-836.61
	0.9	3.07E-06	37.91	437.20	-803.31
	Average	**2.56E-06**	**105.38**	**335.24**	**-977.75**
Vyazovkin	**0.1**	2.19E-32	174.78	239.42	-1284.80

	0.2	3.00E-14	69.17	151.99	-942.25
	0.3	1.93E-04	1.29	153.92	-761.32
	0.4	6.37E-29	236.46	509.77	-1230.85
	0.5	2.14E-08	45.50	252.66	-838.77
	0.6	2.06E-22	192.98	486.55	-1107.71
	0.7	1.66E-20	180.29	485.70	-1071.79
	0.8	9.25E-08	44.90	348.15	-829.87
	0.9	1.68E-06	41.87	443.64	-808.31
	Average	**2.17E-05**	**109.69**	**341.31**	**-986.18**

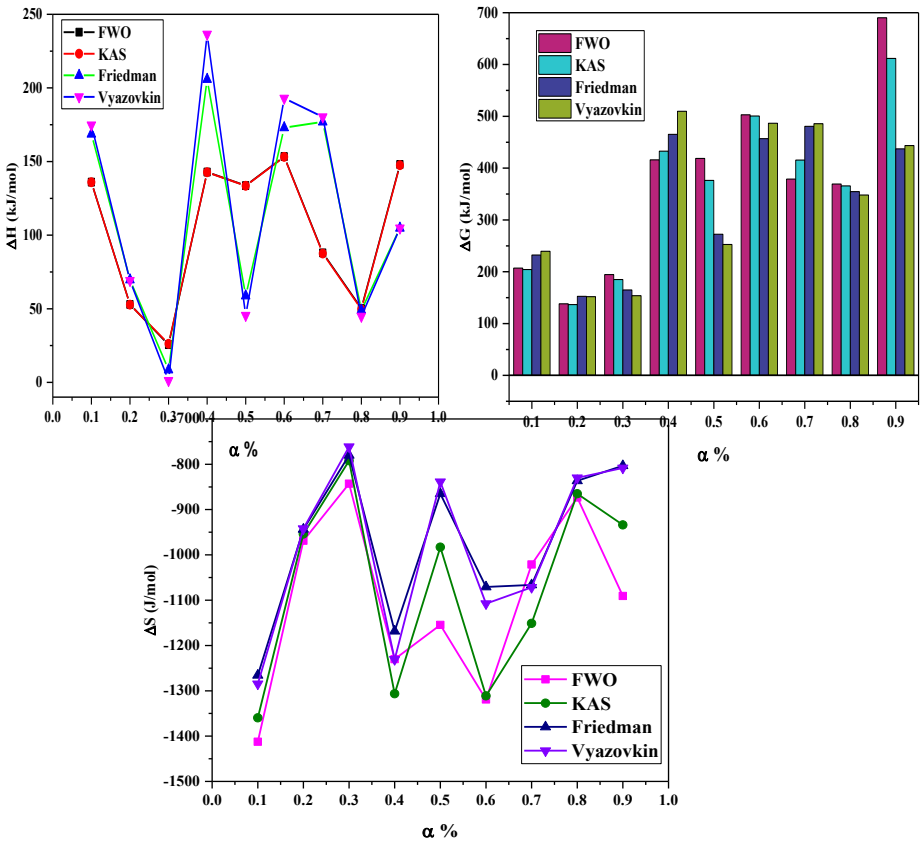

Figure 4.3: Change in enthalpy, change in Gibbs free energy and change in entropy with conversion profiles respectively of CPS

ΔH represents the energy required in converting reactants into an activated complex. The positive ΔH values throughout all α values lead us to believe that the pyrolysis of CPS is an endothermic process with average ΔH values as 103.40, 105.27, 105.38 and 109.69 kJ/mol for FWO, KAS, Friedman and Vyazovkin respectively.

The ΔG values delivers information about the available amount of energy for the pyrolysis process. The values of ΔG throughout the entire range of α was positive indicating a nonspontaneous pyrolysis

which requires an external heat input. The average ΔG values for FWO, KAS, Friedman and Vyazovkin were 368.45, 358.74, 335.24 and 341.31 kJ/mol respectively.

The negative ΔS values throughout the conversion fractions implies the creation of active complexes. The large ΔS values point towards the inclination to form biochar. Biochar is a key player in circular economy. Biochar is a marketable bio-material that can be utilised in application such as fertilisers and energy sector (Oni, Oziegbe and Olawole, 2019). Overall, these analyses indicated the endothermic nature of the process which necessitated energy input and progressed with the formation of activated complexes. Thus, knowing pyrolysis process kinetic parameters is critical for the design of pyrolizer, pyrolysis modelling, and pyrolysis process parameter optimization.

4.2. Chitosan grafted with MMA and HEMA

4.2.1. Thermal Degradation Kinetics

Kinetic information is obtained from dynamic measurements by various methods by utilizing data from thermogravimetric analysis. The degradation of polymers occurs as a result of the changes in the chemical structure and physical properties which can either be because of the external chemical and/or physical stress imparted by the scissions of the bond in the polymer backbone. Figures 4.4 and 4.5 represents the linear regression plots of CMM and CHM derived from FWO, KAS, Starink, Tang and Friedman (Arda, Bal and Acar, 2017).

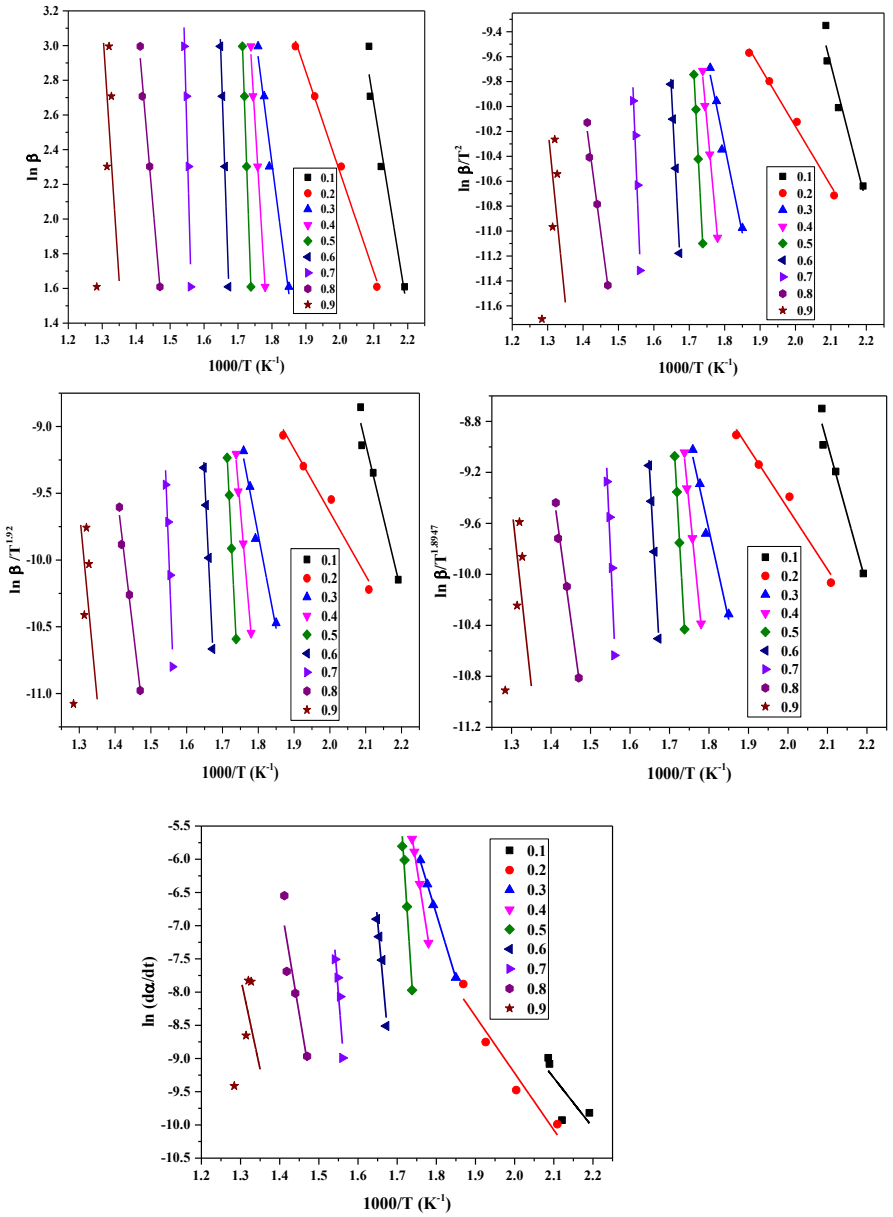

Figure 4.4: Typical linear regression lines of CMM using FWO, KAS, Starink, Tang and Friedman methods

Table 4.3: The energy of activation according to conversion degree for FWO, KAS, Starink, Tang, Friedman and Vyazovkin methods of CMM & CHM

CMM						
	FWO	**KAS**	**Starink**	**Tang**	**Friedman**	**Vyazovkin**
α	**E_a**					
0.1	11.30	7.75	17.37	17.47	57.51	58.51
0.2	87.46	87.16	30.52	30.63	142.31	141.23
0.3	127.04	126.90	116.02	116.14	162.13	161.72
0.4	155.52	155.42	263.40	263.52	179.84	175.52
0.5	177.58	177.50	444.02	444.14	226.57	231.01
0.6	265.35	265.28	463.90	464.03	317.10	312.38
0.7	564.37	564.34	588.56	588.69	581.57	600.72
0.8	149.36	148.93	160.89	161.03	233.39	319.48
0.9	-272.87	-272.79	-254.81	-254.65	-352.33	-342.27
Average	**140.57**	**140.06**	**131.98**	**132.10**	**172.01**	**184.26**

CHM						
	FWO	**KAS**	**Starink**	**Tang**	**Friedman**	**Vyazovkin**
α	**E_a**					
0.1	28.58	28.01	32.45	32.52	19.19	22.16
0.2	112.48	112.29	114.36	114.47	126.39	125.51
0.3	126.61	126.41	126.56	126.69	133.30	133.45
0.4	169.49	169.35	169.92	170.06	195.54	197.14
0.5	213.98	213.87	214.82	214.96	244.07	242.41
0.6	229.19	229.09	229.81	229.95	247.88	247.31
0.7	233.60	233.51	234.09	234.24	237.33	238.08
0.8	234.37	234.27	234.74	234.89	229.84	229.66
0.9	236.36	236.27	235.20	235.35	254.36	257.10
Average	**176.07**	**175.90**	**176.88**	**177.01**	**187.55**	**188.09**

*E_a is in kJ/mol

The results show that the average apparent activation energies were in the range 140-190 kJ/mol for CMM and 170-190 kJ/mol for CHM. The E_a values of CMM is in the range of PMMA composites involving clay (Nikolaidis and Achilias, 2018). Also, the r^2 values range from 0.94 to 0.99 throughout the whole range of E_a values indicating the feasibility of the methods used.

The change in activation energy with respect to conversion is shown in Figure 4.6.

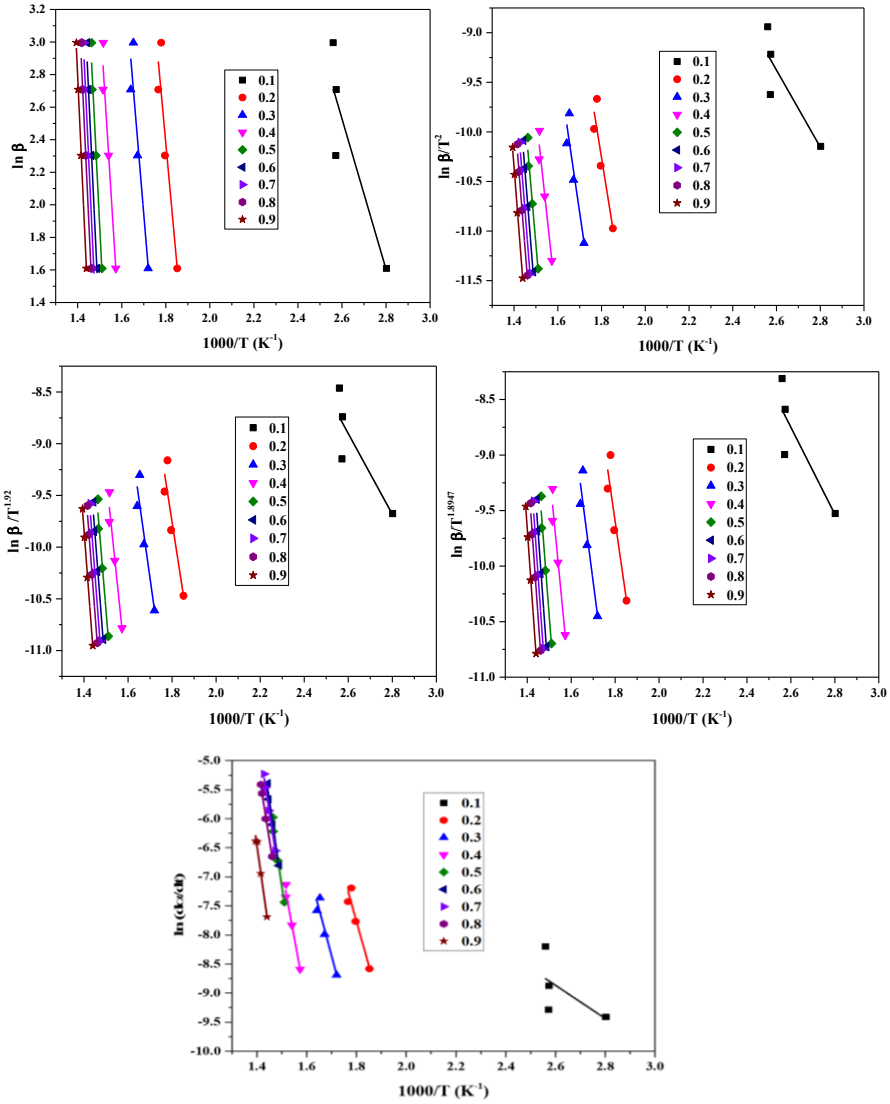

Figure 4.5: Typical linear regression lines of CHM using FWO, KAS, Starink, Tang and Friedman methods

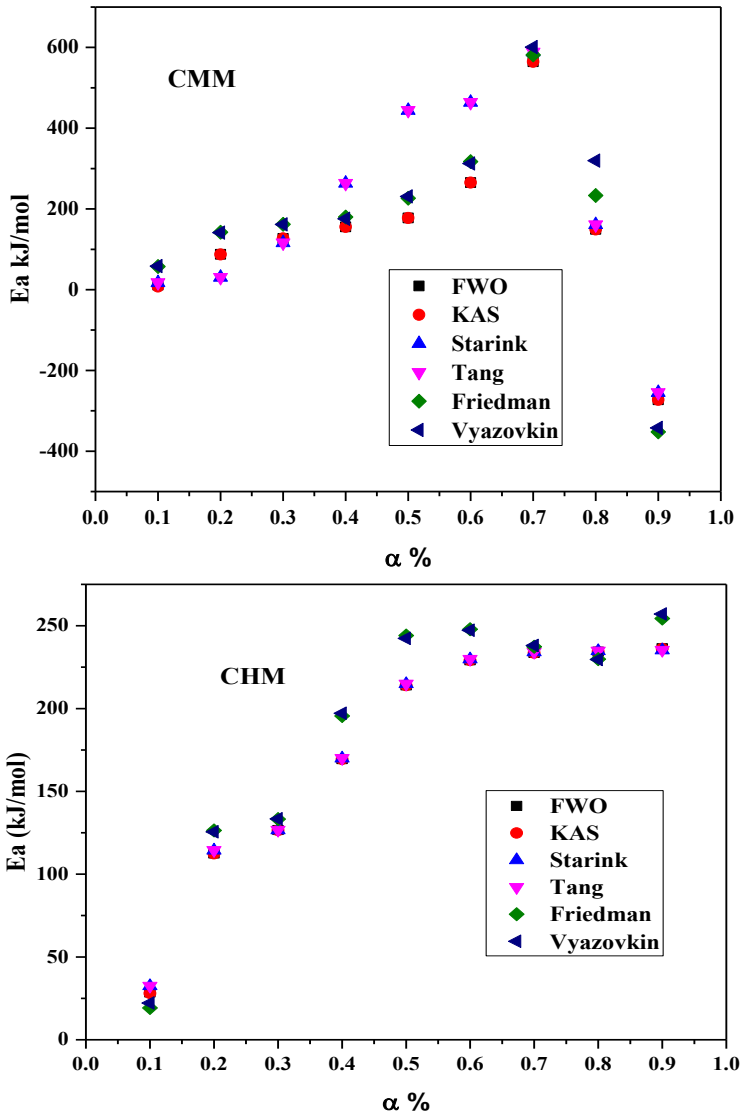

Figure 4.6: Activation energy (E_a) vs conversion (α) profiles of CMM & CHM using FWO, KAS, Starink, Tang, Friedman and Vyazovkin methods

Owing to the number of components present in the grafts and their interactions with each other leads the behaviour of activation energy with conversion. The nonlinear nature of the graph with each α show

the complex nature of the pyrolytic reaction indicating the involvement of several components in the material under inert atmosphere.

4.2.2. Thermodynamic Properties

Thermodynamic parameters play a significant role in better understanding of chemical bonding, structure, and reaction. The thermodynamic parameters obtained for the pyrolytic process of CMM and CHM are shown in Tables 4.4 and 4.5.

Table 4.4: Pre-exponential factor and other thermodynamic parameters for all CMM obtained by using activation energy deduced from FWO, KAS, Friedman and Vyazovkin methods.

	α	Pre-exponential factor, A (s^{-1})	Enthalpy, ΔH (kJ/mol)	Gibbs free energy, ΔG (kJ/mol)	Entropy, ΔS (J /mol)
FWO	**0.1**	1.66E+00	9.77	135.39	-685.28
	0.2	6.21E+05	85.78	202.29	-579.35
	0.3	2.82E+09	124.82	261.57	-511.68
	0.4	1.01E+12	153.11	286.95	-463.42
	0.5	8.07E+13	175.07	304.18	-427.40
	0.6	1.99E+21	262.65	355.71	-286.49
	0.7	7.93E+44	561.32	500.91	164.27
	0.8	2.99E+12	145.98	332.06	-457.27
	0.9	2.45E-11	-277.07	178.67	-901.05
	Average	**8.81E+43**	**137.94**	**284.19**	**-460.85**
KAS	**0.1**	2.38E+02	6.23	124.27	-643.97
	0.2	4.34E+05	85.49	202.60	-582.33
	0.3	2.81E+09	124.68	261.44	-511.72
	0.4	1.10E+12	153.02	286.66	-462.77
	0.5	8.95E+13	174.99	303.83	-426.54
	0.6	1.96E+21	262.58	355.69	-286.63
	0.7	1.95E+44	561.28	505.16	152.61
	0.8	3.03E+12	145.54	331.59	-457.17

	0.9	2.47E-11	-276.99	178.72	-900.97
	Average	**2.17E+43**	**137.42**	**283.33**	**-457.72**
Friedman	**0.1**	3.49E-07	55.98	205.02	-813.09
	0.2	1.49E+02	140.64	271.07	-648.63
	0.3	2.81E+12	159.91	281.33	-454.31
	0.4	1.11E+14	177.44	300.00	-424.40
	0.5	8.75E+17	224.06	329.83	-350.15
	0.6	6.34E+24	314.40	385.68	-219.43
	0.7	1.47E+44	578.51	523.25	150.25
	0.8	4.90E+14	230.00	398.84	-414.89
	0.9	8.85E-28	-356.54	258.41	-1215.81
	Average	**1.63E+43**	**169.38**	**328.16**	**-487.83**
Vyazovkin	**0.1**	6.75E-07	56.99	205.03	-807.61
	0.2	2.56E+02	139.55	269.09	-644.15
	0.3	2.69E+12	159.50	281.01	-454.67
	0.4	4.59E+13	173.12	297.80	-431.71
	0.5	2.19E+18	228.50	331.96	-342.51
	0.6	2.53E+24	309.68	383.44	-227.07
	0.7	5.08E+45	597.66	531.57	179.72
	0.8	1.87E+21	316.10	433.65	-288.86
	0.9	4.69E-27	-346.48	261.47	-1201.95
	Average	**5.65E+44**	**181.63**	**332.78**	**-468.76**

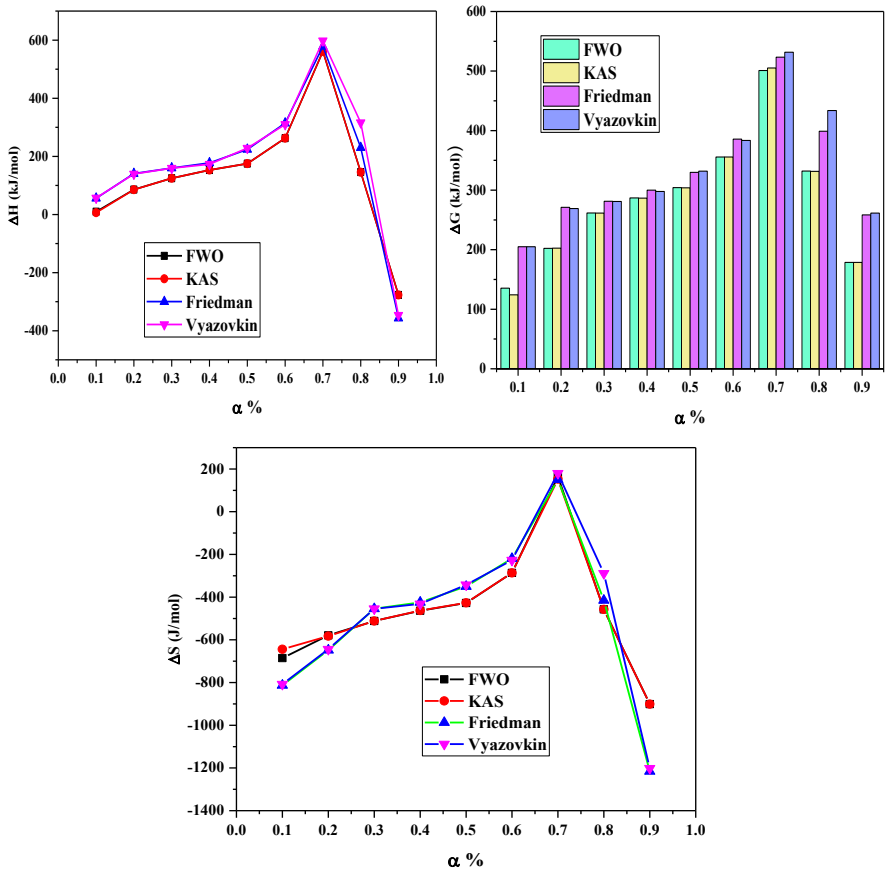

Figure 4.7: Change in enthalpy, change in Gibbs free energy and change in entropy with conversion profiles respectively of CMM

The complex composition of the sample and complex reactions that take place at the time of decomposition is indicated by the digression in pre-exponential values w.r.t conversion. The pre-exponential value ranges from 10^{-11} - 10^{45} for all the kinetic methods. In general, low pre-exponential factors ($<10^{9}$ s^{-1}) illustrates the closed complex. This is comparable to the values obtained for materials containing lignin, hemicellulose and cellulose (Kaur *et al.*, 2018; Santos *et al.*, 2020; Parthasarathy *et al.*, 2022).

Table 4.5: Pre-exponential factor and other thermodynamic parameters for CHM obtained by using activation energy deduced from FWO, KAS, Friedman and Vyazovkin methods.

	α	Pre-exponential factor, A (s^{-1})	Enthalpy, ΔH (kJ/mol)	Gibbs free energy, ΔG (kJ/mol)	Entropy, ΔS (J /mol)
FWO	**0.1**	1.81E+01	27.89	83.07	-658.90
	0.2	7.08E+07	110.26	254.99	-542.32
	0.3	3.24E+08	124.04	287.71	-530.87
	0.4	1.69E+11	166.47	340.63	-480.20
	0.5	2.30E+14	210.75	374.40	-420.81
	0.6	2.66E+15	225.87	385.74	-400.65
	0.7	5.19E+15	230.23	390.47	-395.23
	0.8	5.47E+15	230.95	393.40	-394.91
	0.9	5.98E+15	232.86	398.96	-394.36
	Average	**2.17E+15**	**173.26**	**323.26**	**-468.70**
KAS	**0.1**	2.79E+00	27.32	83.81	-674.43
	0.2	6.44E+07	110.07	255.01	-543.11
	0.3	3.05E+08	123.85	287.68	-531.38
	0.4	1.79E+11	166.33	340.32	-479.73
	0.5	2.55E+14	210.64	373.96	-419.95
	0.6	2.94E+15	225.77	385.30	-399.81
	0.7	5.74E+15	230.14	390.03	-394.39
	0.8	6.05E+15	230.85	392.96	-394.07

	0.9	6.61E+15	232.77	398.52	-393.54
	Average	**2.40E+15**	**173.08**	**323.06**	**-470.04**
Friedman	**0.1**	6.50E-02	18.49	77.60	-705.69
	0.2	4.06E+08	124.17	265.02	-527.81
	0.3	2.30E+08	130.73	295.29	-533.74
	0.4	3.72E+12	192.53	357.37	-454.51
	0.5	2.10E+16	240.84	389.89	-383.25
	0.6	5.04E+16	244.57	394.68	-376.21
	0.7	8.87E+15	233.96	392.38	-390.77
	0.8	2.22E+15	226.42	391.95	-402.40
	0.9	6.14E+16	250.86	408.81	-375.01
	Average	**1.60E+16**	**184.73**	**330.33**	**-461.04**
Vyazovkin	**0.1**	1.49E-01	21.47	80.00	-698.80
	0.2	3.59E+08	123.30	264.42	-528.82
	0.3	2.38E+08	130.89	295.36	-533.45
	0.4	5.19E+12	194.13	357.96	-451.74
	0.5	1.63E+16	239.18	389.06	-385.39
	0.6	4.69E+16	243.99	394.34	-376.80
	0.7	1.01E+16	234.71	392.68	-389.66
	0.8	2.11E+15	226.24	391.95	-402.84
	0.9	9.23E+16	253.60	410.12	-371.62
	Average	**1.86E+16**	**185.28**	**330.65**	**-459.90**

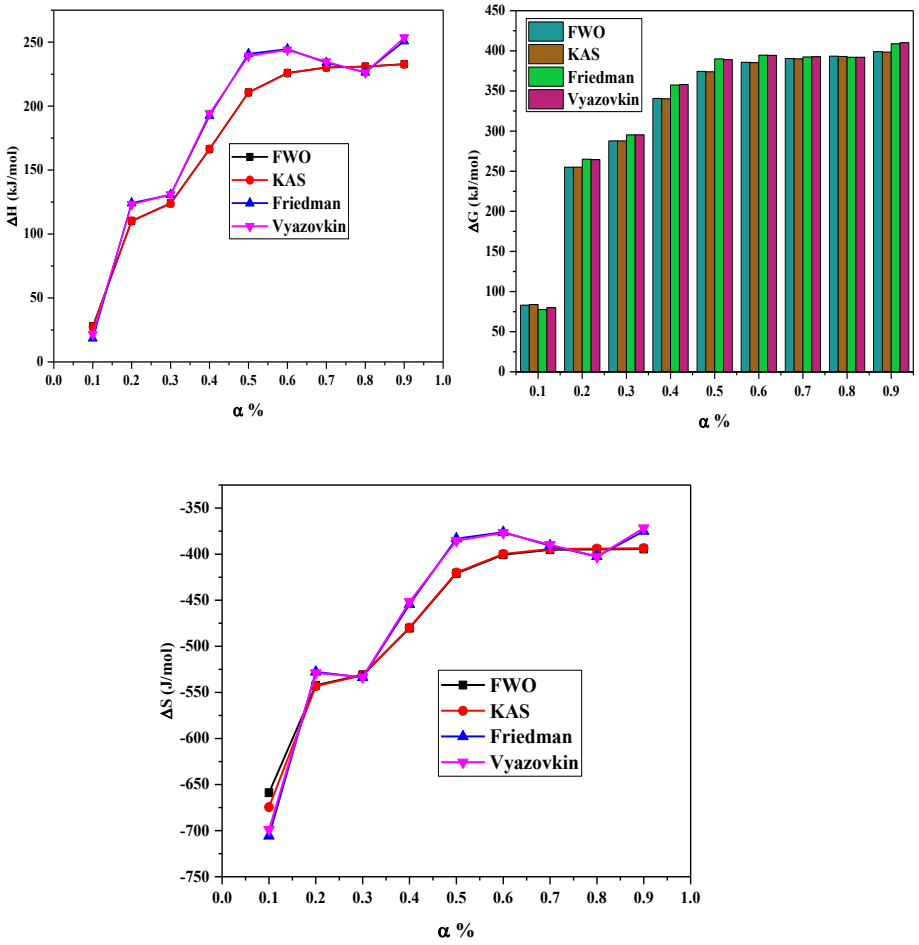

Figure 4.8: Change in enthalpy, change in Gibbs free energy and change in entropy with conversion profiles respectively of CHM

For both the copolymers, the thermodynamic parameters showed variation with increase of alpha which is in agreement with the E_a values that confirms the complexity of the degradation. The determination of enthalpy (ΔH) is fundamental to evaluate the total energy consumed in during the pyrolytic process. From tables 4.4 & 4.5 it is observed that there is a low energy barrier (around 3-5 kJ/mol) between the E_a and the ΔH values. This indicates that initiation of the

degradation process arises easily and favours complex formation. The trend of E_a proportional to ΔH is similar to that of the pyrolysis behaviour of lignocellulosic materials.

The total rise in the energy in order to form the activated complex denotes Gibbs free energy of the process. The positive values of ΔG implied a non-spontaneous nature suggesting the requirement of external heat to advance the pyrolysis reactions

It was observed that the values of ΔS were negative throughout the whole range of conversion. For the products, the extent of disorder through the bond dissociations are denoted by the negative values of ΔS.

4.3. Chitosan/Phytic acid Polyelectrolyte complex

4.3.1. Thermal Degradation Kinetics

This section focuses on evaluating the effect of β on the degradation characteristics and kinetic analysis of PEC using various non-isothermal methods. The energies of activation for different conversion are derived from these methods. In order to better explain the kinetic behaviour, model free methods are employed for the study (Stephy, Antony and Francis, 2023).

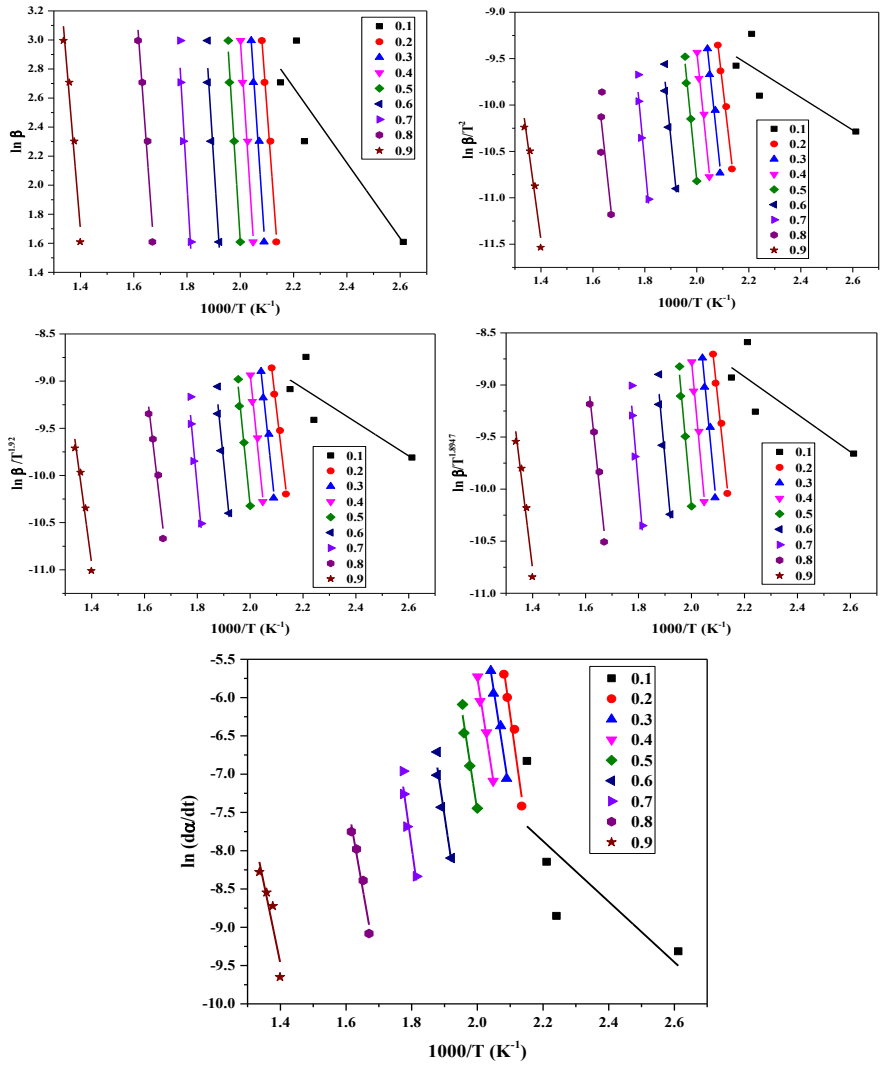

Figure 4.9: Typical linear regression lines of PEC using FWO, KAS, Starink, Tang and Friedman methods

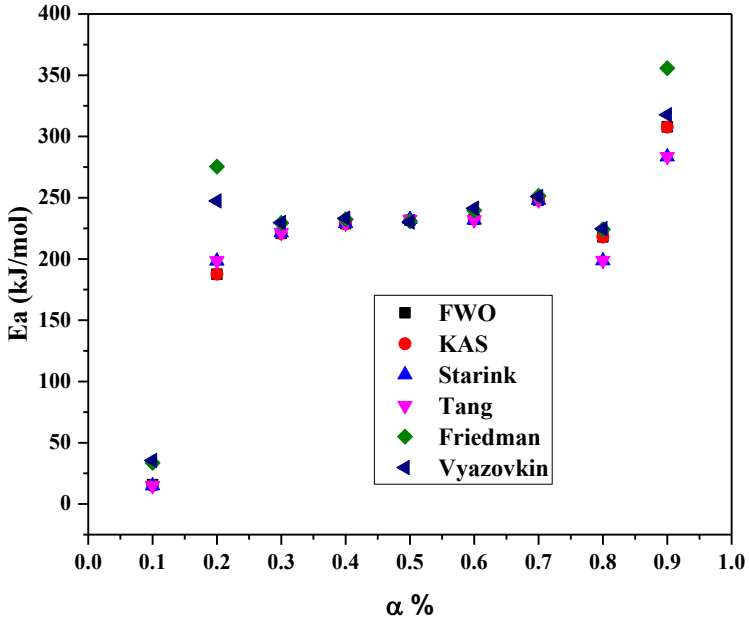

Figure 4.10: Activation energy (E_a) vs conversion (α) profiles of PEC using FWO, KAS, Starink, Tang, Friedman and Vyazovkin methods

Table 4.6: The energy of activation w.r.t. α for FWO, KAS, Starink, Tang, Friedman and Vyazovkin methods of PEC

	FWO	**KAS**	**Starink**	**Tang**	**Friedman**	**Vyazovkin**
α	**E_a**					
0.1	15.74	15.07	14.99	14.90	33.56	35.46
0.2	187.62	187.56	198.53	198.43	275.33	247.29
0.3	220.85	220.80	221.47	221.36	229.47	229.62
0.4	228.81	228.76	229.13	229.03	232.45	233.24
0.5	231.61	231.56	232.36	232.26	230.73	230.10
0.6	232.47	232.41	231.97	231.86	239.66	241.35
0.7	248.10	248.03	248.22	248.10	251.52	250.96
0.8	218.03	217.90	198.72	198.60	224.23	224.79
0.9	307.84	307.63	283.38	283.53	355.74	317.74
Average	**210.12**	**209.97**	**194.11**	**194.22**	**230.30**	**223.39**

*E_a is in kJ/mol

Ahmad *et al* stated that the pyrolysis of materials involving natural substances are heterogeneous reactions wherein activation energy plays a significant role. The apparent activation energies obtained from FWO, KAS, Starink and Tang are on par with the each other whereas Friedman and Vyazovkin showed comparatively higher values (Ahmad *et al.*, 2017).

4.3.2. Thermodynamic properties

The thermodynamic parameters, such as activation enthalpy (ΔH), Gibbs free energy (ΔG) and activation entropy (ΔS) are given in Table 4.7. From table, it is apparent that the values of activation energy and enthalpy are in accord with each other. During the pyrolysis of biochar, the degree of arrangement of carbon layers in biochar is depicted by ΔS. Also, the negative values of ΔS implies the formation of thermally more viable products from the reactants. The ΔG values signifies the rise in the amount of energy demanded to form an activated complex by the system.

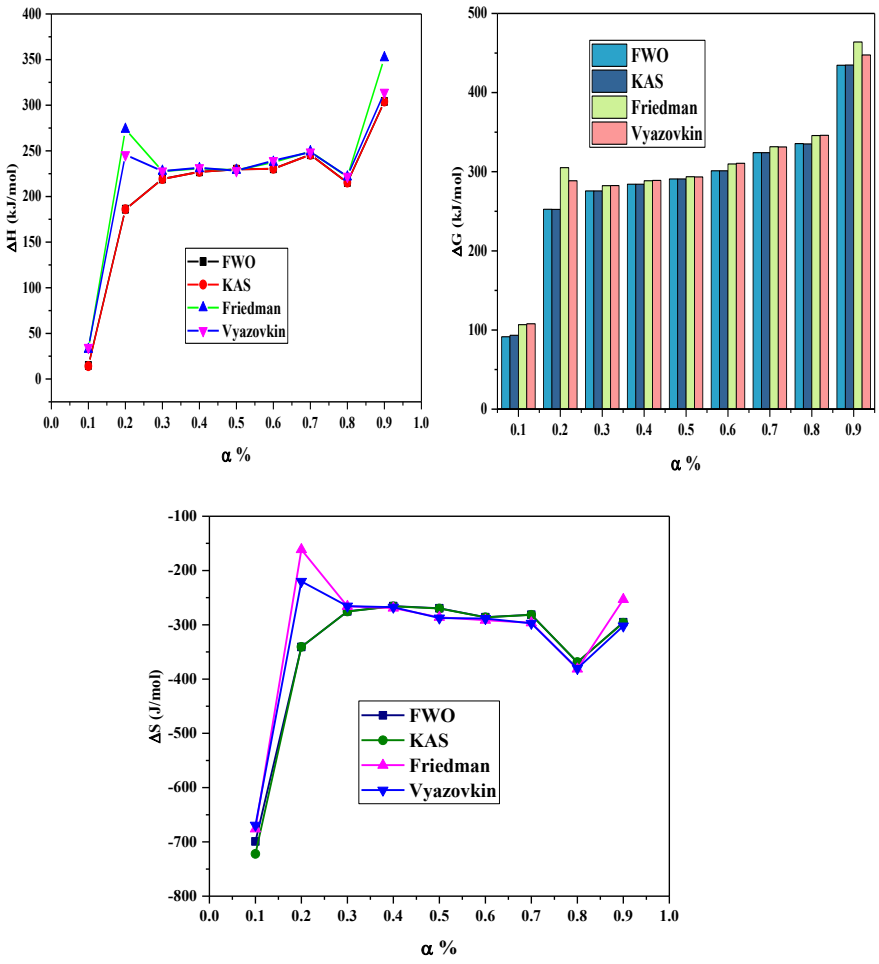

Figure 4.11: Change in enthalpy, change in Gibbs free energy and change in entropy with conversion profiles respectively of PEC

Table 4.7: Pre-exponential factor and other thermodynamic parameters for PEC obtained by using activation energy deduced from FWO, KAS, Friedman and Vyazovkin methods.

	α	Pre-exponential factor, A (s^{-1})	Enthalpy, ΔH (kJ/mol)	Gibbs free energy, ΔG (kJ/mol)	Entropy, ΔS (J /mol)
FWO	**0.1**	1.87E-01	14.82	91.48	-699.14
	0.2	1.71E+18	186.00	252.53	-340.93
	0.3	4.90E+21	219.14	275.71	-275.20
	0.4	1.64E+22	227.02	284.18	-265.55
	0.5	1.06E+22	229.72	290.88	-269.59
	0.6	1.60E+21	230.42	301.22	-286.05
	0.7	3.10E+21	245.79	324.06	-281.52
	0.8	9.42E+16	215.32	335.58	-369.31
	0.9	9.46E+20	304.17	434.60	-295.23
	Average	**4.17E+21**	**208.04**	**287.80**	**-342.50**

KAS	**0.1**	1.19E-02	14.15	93.33	-722.07
	0.2	1.75E+18	185.94	252.44	-340.74
	0.3	4.69E+21	219.09	275.73	-275.57
	0.4	1.55E+22	226.97	284.22	-266.01
	0.5	1.02E+22	229.67	290.90	-269.93
	0.6	1.59E+21	230.35	301.17	-286.11
	0.7	3.06E+21	245.72	324.03	-281.62
	0.8	1.04E+17	215.19	335.19	-368.51
	0.9	8.30E+20	303.96	434.87	-296.32
	Average	**3.98E+21**	**207.89**	**287.99**	**-345.21**
Friedman	**0.1**	3.04E+00	32.65	106.77	-675.96
	0.2	4.14E+27	273.71	305.19	-161.31
	0.3	1.49E+22	227.76	282.43	-265.94
	0.4	1.06E+22	230.67	288.59	-269.15
	0.5	1.45E+21	228.85	293.75	-286.15

	0.6	8.20E+20	237.60	309.78	-291.60
	0.7	5.30E+20	249.21	331.57	-296.21
	0.8	2.17E+16	221.52	345.76	-381.52
	0.9	1.45E+23	352.07	464.01	-253.38
	Average	**4.60E+26**	**228.23**	**303.09**	**-320.14**
Vyazovkin	**0.1**	6.76E+00	34.54	107.93	-669.31
	0.2	3.58E+24	245.67	288.59	-219.94
	0.3	1.56E+22	227.91	282.51	-265.59
	0.4	1.29E+22	231.46	289.03	-267.51
	0.5	1.22E+21	228.21	293.44	-287.55
	0.6	1.20E+21	239.29	310.69	-288.46
	0.7	4.70E+20	248.65	331.29	-297.20
	0.8	2.47E+16	222.08	345.96	-380.43
	0.9	4.09E+20	314.07	447.58	-302.20
	Average	**4.01E+23**	**221.32**	**299.67**	**-330.91**

In total, these analyses pointed towards the endothermic nature of the degradation process progressed by the formation of activated complexes by necessitating energy input.

Chapter 5
Development of Melt-mixed EVA/Chitosan and EVA/Chitosan-g-PANi Composites

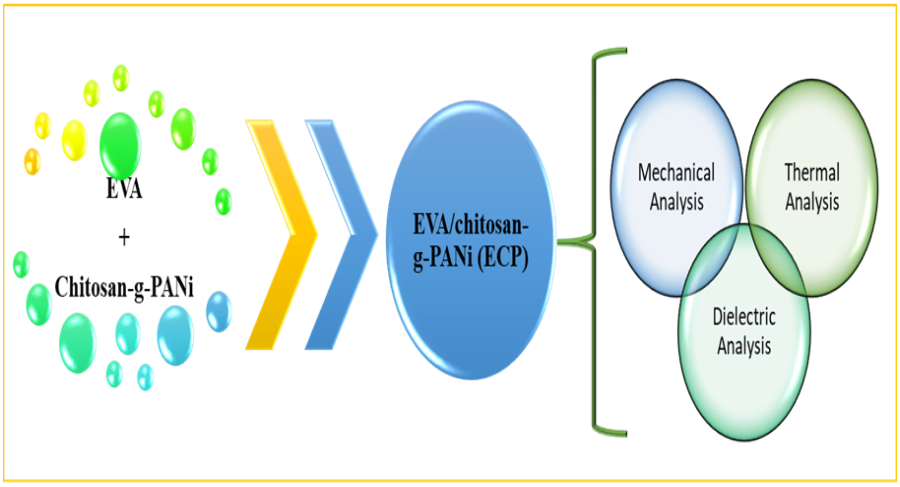

In this chapter composites of EVA with chitosan grafted polyaniline were fabricated. The materials were characterized using infra-red spectral analysis and thermogravimetric analysis. Detailed kinetic studies on the thermal degradation of the composites were carried out by utilizing FWO, KAS, Starink, Tang, Friedman and Vyazovkin methods. Activation energy values obtained from the same were used to calculate the thermodynamic parameters of the formed composites. Mechanical (using UTM) and dielectric (using Broadband dielectric spectroscopy) properties also were analysed for the said composites.

Composites are those materials which comprises of a matrix and filler. Owing to the ease of availability, broad range of applications and notable physical properties natural fibers are a solid contender in composites as reinforcements (Subramanian, 2019). These composites are made by maintaining ecology–economy–technology balance and reinforcing two or more biofibers to enhance their properties (Luo et al., 2020). As a result of the recyclability and degradability the utilization of natural fillers to manufacture polymer composites is well established and has obtained significance (George, Bhadra and Bhowmick, 2010; P. Wang et al., 2021). The use of such materials in composites has increased due to their inexpensiveness, recycling capacity and for the fact that during composite production, they can compete well w.r.t. the strength per weight of material involved (Berthet et al., 2015).

Being an outstanding biomaterial with properties such as non-toxicity, biocompatibility and biodegradability, chitosan the deacetylated product of chitin shows a great potential as a biofiller (Stephy, Antony and Francis, 2021). However, the high brittleness and poor mechanical strength calls for the modification of the material. Chemical modification methods like graft polymerization may seem like a breakthrough to tune the nature of chitosan according to one's requirement. Graft polymerization is introduction of an existing polymer by introducing a new group or polymer on to the existing polymer's backbone. This method is employed to improve the properties of the parent polymer and to tune it according to the requirements of the composite (Taylor et al., 2014).

Polyaniline, one of the most used conducting polymers is a viable candidate to be used in grafting due to its various properties like better environment stability, ease of doping, less energy requirement, good dispersion and abundant of amino groups on the polymer chain. Grafting it onto chitosan can better the conducting ability and the mechanical strength of the biofiller. Moreover, polyaniline-grafted biodegradable materials show outstanding applications in various fields like treatment water, biomedical applications and tissue engineering together with modified electrode and microbial fuel cell etc. (Shahadat *et al.*, 2017).

In this study, chitosan grafted with polyaniline through oxidative-radical copolymerization using ammonium persulfate as initiator is used as a modified biofiller to fabricate a biocomposite with ethylene-co-vinyl acetate (EVA) as the matrix. The composite is expected to show improved mechanical and thermal properties than that of the individual matrix and filler. The formulation used is given below.

Table 5.1: Formulation for ECP series (chitosan-g-PANi as filler)

Sample Name	Composition	
	EVA (g)	**Chitosan-g-PANi (wt %)**
ECP1	30	2.5
ECP2	30	5
ECP3	30	7.5
ECP4	30	10

5.1. Infrared Characterization

The absorbance bands at ~2920, ~2850 and 720 cm^{-1} are of ethylene groups on EVA. The overtone band due to the double frequency of carbonyl group of vinyl acetate units is at 3400 cm^{-1} (Stephy, Antony and Francis, 2021). The characteristic absorbance bands for EVA/ chitosan-g-PANi composites are found to be same with the characteristic peaks of neat EVA (Makhetha, Mpitso and Luyt, 2017). The only difference is in their absorbance value which is found to be less for EVA/ chitosan-g-PANi composite compared to neat EVA and also the reappearance of the carbonyl band in the prepared composite (Stephy, Antony and Francis, 2021). The interference created by the high absorbance value of EVA masks the peaks of chitosan-g-polyaniline (Figure 5.1).

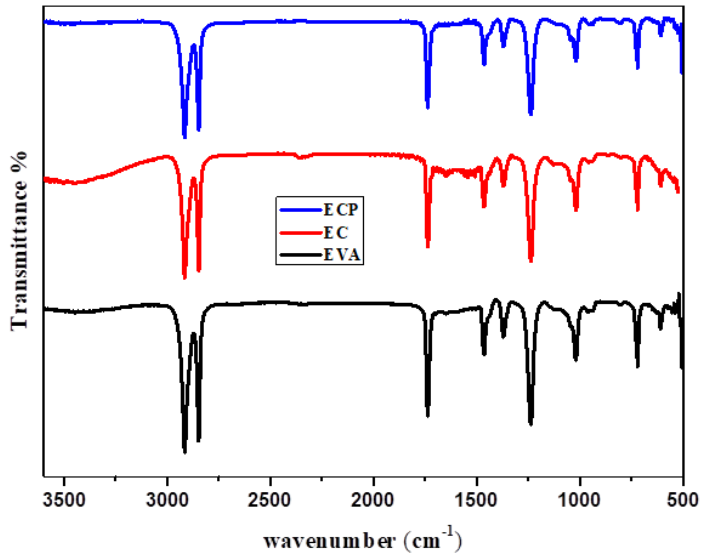

Figure 5.1: Infrared spectra of EVA, EVA/chitosan (EC) and EVA/chitosan-g-PANi (ECP)

5.2. Thermal characterization

The thermal characterization of the filler and the composite was carried out using thermogravimetric analysis. It is observed that typically EVA shows two significant stages of degradation (Stephy, Antony and Francis, 2021). The first degradation (Stage I) corresponds to the decomposition of vinyl acetate, which starts at about 280 ^{o}C. The second degradation (Stage II) occurs over the temperature range of 410–500 ^{o}C, which corresponds to the degradation of poly(ethylene) backbone (Berthet et al., 2015) (Table 5.2).

Table 5.2: **Degradation temperatures of the materials**

	Stage I (^{o}C)	**Stage II (^{o}C)**
EVA	342	463
EC3	341	465
ECP3	352	477

The degradation of the prepared EVA/chitosan-g-PANi composites starts at a higher temperature than chitosan-g-PANi and EVA owing to the improved thermal stability of the composites. From the figure it can be seen that the temperature of degradation of EVA/ chitosan-g-PANi composites has been shifted to a higher temperature as the filler content varies between 2.5–10 wt %. This can be attributed to the interaction between chitosan-g-PANi and vinyl acetate part of EVA (Stephy, Antony and Francis, 2021).

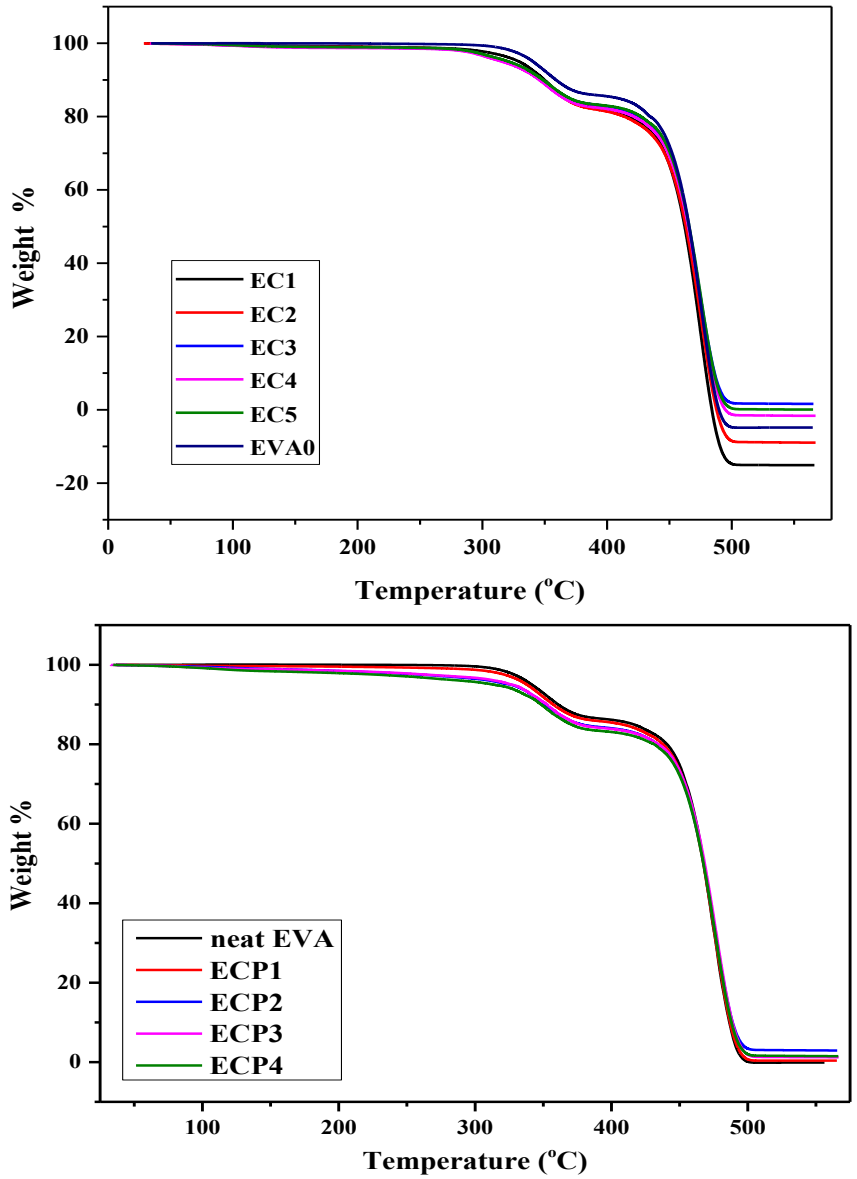

Figure 5.2: TGA thermograms of the prepared EVA/ chitosan (EC) and EVA/chitosan-g-PANi (ECP) composites

5.3. Kinetic analysis of Thermal Degradation

Over a period of decades, the prediction of reaction mechanism and kinetic parameters have become imperative for the sustenance and disposal of materials of polymer decent. This is in view to interpret the physical as well as chemical processes that lead to the degradation and combustion aspects. One of the effective factors that is closely associated with energy needed for the dissociation of bonds in the polymeric chain during degradation is the energy of activation (E_a). Thomas *et al* stated that the tendency of the individual cleavage of the bonds will be a reflection of the values obtained when the material is heated gradually (Thomas *et al.*, 2020). This, in turn, helps to comprehend the condensed-phase activity of the material while undergoing thermal degradation, and thereby its susceptibility to form combustible volatiles.

The deduction of kinetic parameters such as the Arrhenius pre-exponential factor, A and the energy of activation, E_a can be done using the thermal profiles under different heating rate. Hence, the right chemical modification(s) of the polymer material to change it in a way that enhances its thermal stability stems from having adequate information about the thermolytic profile of a material.

The non-isothermal solid-state reaction kinetic data can be generally divided into model-fitting and isoconversional methods. The Kinetics Committee of the International Confederation for Thermal Analysis and Calorimetry (ICTAC) does not endorse the use of model-fitting methods due to its innate uncertainty in the determination of kinetic parameters (Farrell *et al.*, 2021). The basic assumption of each degree

of conversion as a single-step process and the applicability of the Arrhenius equation to the specific region related to this conversion makes isoconversional methods more appropriate to evaluate effective activation energies of a solid-state reaction without hypothesising a reaction model (Haile *et al.*, 2015; Tirrell, 2018).

The classification of isoconversional methods is further done into integral and differential methods. Among them the most used integral methods are FWO and KAS due to the utilization of the simplified temperature integral (Stephy, Antony and Francis, 2021). Friedman isoconversional method comes under the umbrella of differential methods and is considered to be more accurate than the integral ones. The simultaneous use of the conversion and conversion rate data obtained by numerical differentiation causes an increase in the noise level of the data obtained.

The kinetic plots of the EVA/chitosan composites (EC) for different models are given in Figure 5.3.

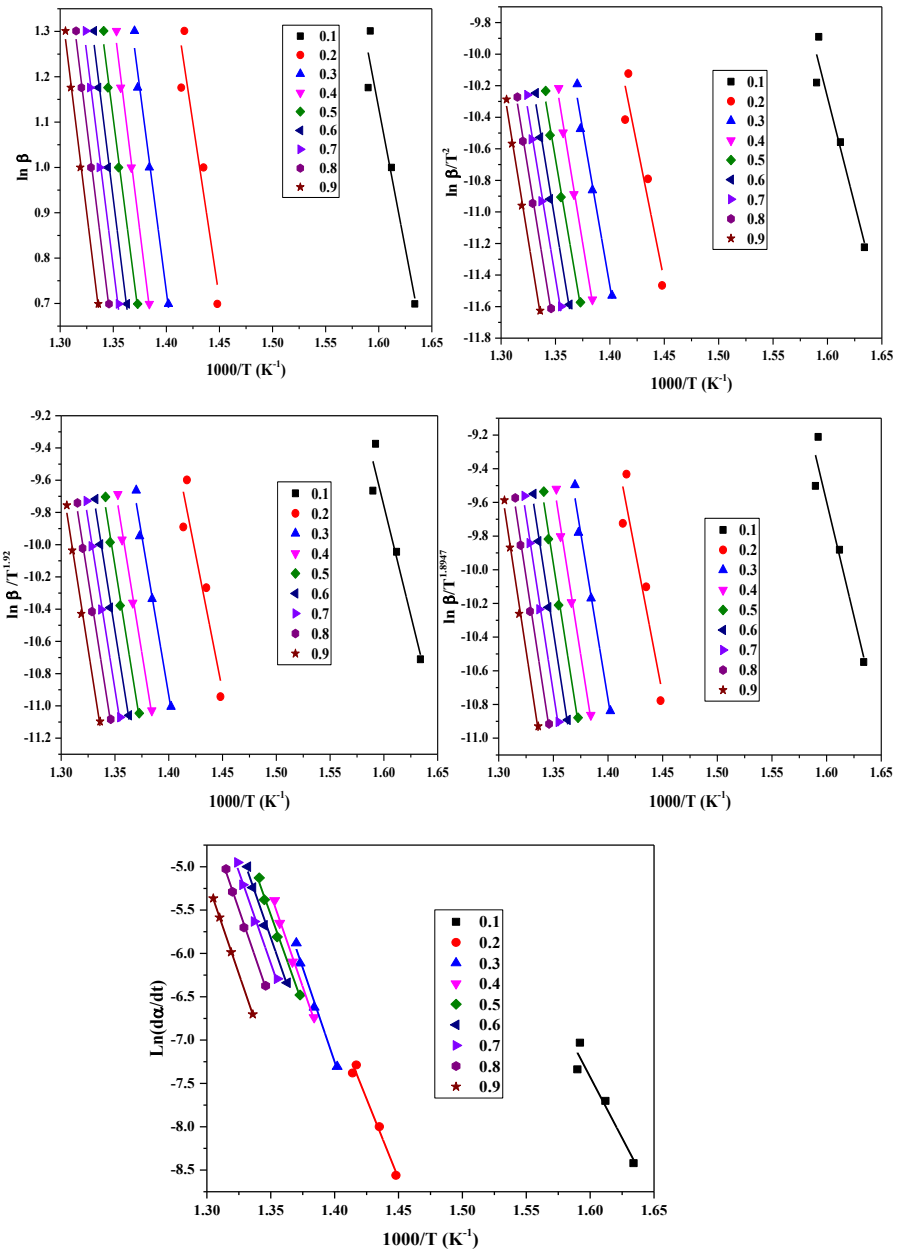

Figure 5.3: Typical linear regression lines of EVA/chitosan (EC) using FWO, KAS, Starink, Tang and Friedman methods

Table 5.3: The energy of activation according to conversion degree for FWO, KAS, Starink, Tang, Friedman and Vyazovkin methods of neat EVA and EC composites

EVA						
	FWO	**KAS**	**Starink**	**Tang**	**Friedman**	**Vyazovkin**
α	**E_a**					
0.1	221.20	221.12	223.60	223.74	216.65	218.53
0.2	252.02	251.93	249.12	249.27	273.47	276.09
0.3	295.85	295.77	296.52	296.67	316.59	317.23
0.4	306.89	306.81	307.43	307.59	323.16	322.08
0.5	314.68	314.60	315.24	315.40	330.31	331.96
0.6	319.56	319.48	320.02	320.17	334.89	340.15
0.7	324.09	324.02	324.97	325.13	328.87	327.35
0.8	323.40	323.32	324.01	324.17	321.05	319.68
0.9	324.60	324.52	325.43	325.59	328.28	325.86
Average	**298.03**	**297.95**	**298.48**	**298.64**	**308.14**	**308.77**

EC						
	FWO	**KAS**	**Starink**	**Tang**	**Friedman**	**Vyazovkin**
α	**E_a**					
0.1	224.90	224.79	225.85	225.98	225.15	227.20
0.2	265.95	265.80	281.96	282.10	287.85	280.04
0.3	328.16	328.08	328.18	328.34	354.68	359.71
0.4	341.95	341.88	342.05	342.20	351.82	355.33
0.5	345.70	345.63	346.15	346.31	351.70	354.46
0.6	348.38	348.31	349.03	349.19	353.35	354.92
0.7	349.89	349.82	350.31	350.47	353.81	355.89
0.8	353.26	353.19	353.79	353.94	357.60	350.51
0.9	354.78	354.71	355.18	355.34	358.77	357.18
Average	**323.66**	**323.58**	**325.83**	**325.99**	**332.75**	**332.80**

*E_a is in kJ/mol

The obtained E_a values were calculated over the conversion range of 0.1–0.9 with a step interval of 0.1. The r^2 values range from 0.96 to 0.99 throughout the whole range of E_a values indicating the viability of the methods used. It should be noted that the E_a values derived from the models are similar, denoting these outcomes to be comparable (Stephy, Antony and Francis, 2021, 2023).

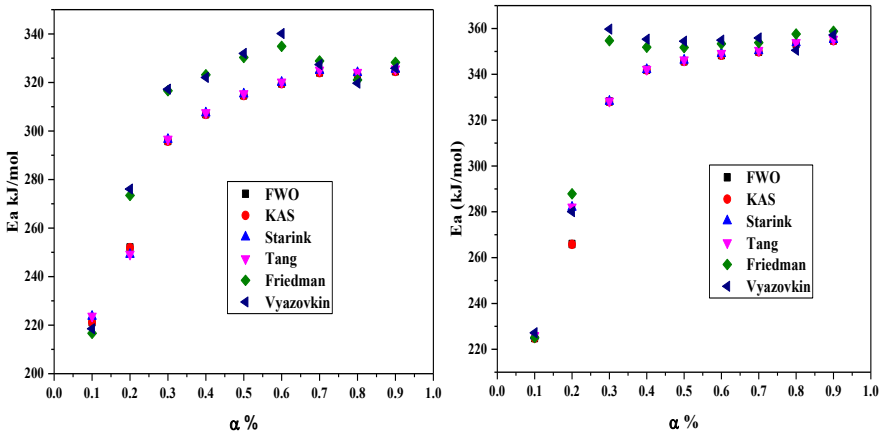

Figure 5.4: Activation energy (E_a) vs conversion (α) profiles of neat EVA and EVA/chitosan (EC) using FWO, KAS, Starink, Tang, Friedman and Vyazovkin methods

It can be clearly seen from Table 5.3 that E_a values of the composites showed significant variation with the increase in filler content compared to the E_a values of neat EVA. The estimated values of activation energies from different models at multiple heating rates of 5, 10, 15 and 20 °C/min are in close agreement with each other. The values for activation energy for conversion rates from 0.2 to 0.4 increased owing to faster degradation of the chitosan part. This observation is similar to that of the systems involving EVA with cellulose as filler where the cellulose part degrades faster due to the

evolution of acetic acid at the first stage of the EVA degradation (Stephy, Antony and Francis, 2021).

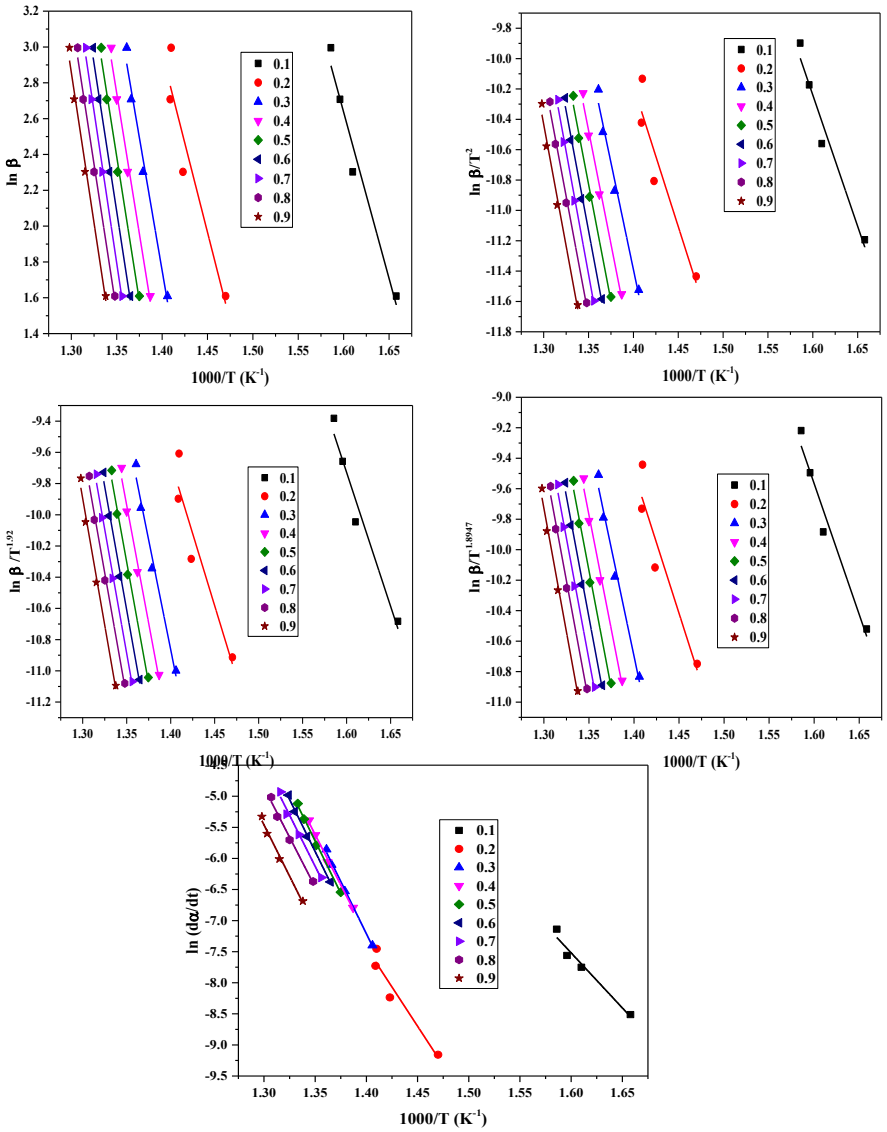

Figure 5.5: Typical linear regression lines of EVA/chitosan-g-PANi (ECP) using FWO, KAS, Starink, Tang and Friedman methods

Table 5.4: The energy of activation according to conversion degree for FWO, KAS, Starink, Tang, Friedman and Vyazovkin methods of ECP composites

	FWO	**KAS**	**Starink**	**Tang**	**Friedman**	**Vyazovkin**
α	**E_a**					
0.1	138.63	138.51	142.62	142.75	150.66	142.73
0.2	142.21	142.01	153.59	153.74	195.26	193.42
0.3	232.16	232.06	233.19	233.34	277.15	273.71
0.4	250.88	250.79	251.37	251.52	272.22	269.08
0.5	258.27	258.18	258.68	258.84	280.24	283.82
0.6	262.64	262.55	263.15	263.30	277.40	280.00
0.7	264.40	264.30	264.79	264.95	268.07	273.18
0.8	265.22	265.13	265.71	265.87	269.59	263.49
0.9	268.80	268.70	269.44	269.60	277.50	275.10
Average	**231.47**	**231.36**	**233.62**	**233.77**	**252.01**	**250.50**

*E_a is in kJ/mol

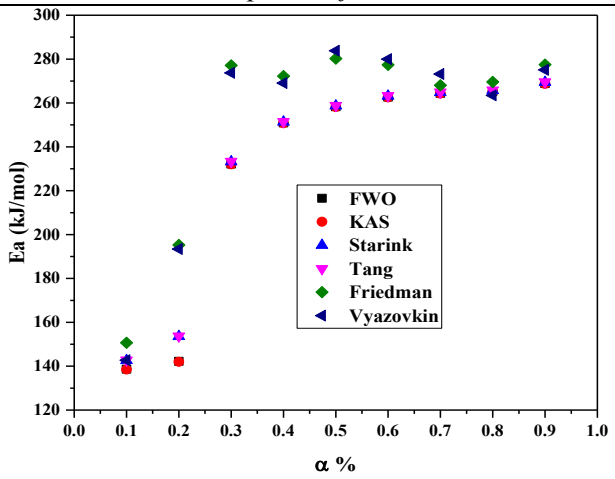

Figure 5.6: Activation energy (E_a) vs conversion (α) profiles of EVA/chitosan-g-PANi (ECP) using FWO, KAS, Starink, Tang, Friedman and Vyazovkin method

It should be noted that the E_a values derived using the FWO, KAS, Starink, Tang and Vyazovkin models are similar, denoting these outcomes to be comparable. The absence of approximation makes the values from Friedman method slightly different from the other models. Similar observations are made by some of the earlier research (Parthasarathy *et al.*, 2022; Patil, Ku and Vasudev, 2023).

5.4. Thermodynamic Properties

Thermodynamic parameters of a process are essential to determine the viability of thermal and energy processes. These values of parameters such as energy requirement, energy barrier and thermodynamic equilibrium can be acquired from kinetics and thermodynamic investigation**.**

The Pre-exponential factor, change in enthalpy, Gibbs free energy, and entropy corresponding to the value of a were computed respectively for FWO, KAS, Friedman and Vyazovkin methods, and the obtained results from the analysis are presented in Table 5.5 and 5.6 for neat EVA and EC composites respectively.

Table 5.5: Pre-exponential factor and other thermodynamic parameters for neat EVA obtained by using activation energy deduced from FWO, KAS, Friedman and Vyazovkin methods.

	α	Pre-exponential factor, A (s^{-1})	Enthalpy, ΔH (kJ/mol)	Gibbs free energy, ΔG (kJ/mol)	Entropy, ΔS (J /mol)
FWO	**0.1**	1.96E+15	218.30	358.41	-402.05
	0.2	8.09E+15	248.50	414.48	-391.90
	0.3	8.39E+18	292.19	439.68	-334.50
	0.4	4.45E+19	303.16	447.22	-320.79
	0.5	1.49E+20	310.90	452.28	-310.85
	0.6	3.15E+20	315.74	455.78	-304.71
	0.7	6.41E+20	320.24	458.90	-298.87
	0.8	5.52E+20	319.51	460.09	-300.20
	0.9	6.58E+20	320.66	462.15	-298.83
	Average	**2.63E+20**	**294.35**	**438.78**	**-329.19**
KAS	**0.1**	2.17E+15	218.22	358.04	-401.23
	0.2	8.89E+15	248.41	414.06	-391.12
	0.3	8.75E+18	292.10	439.45	-334.15
	0.4	4.57E+19	303.08	447.03	-320.56
	0.5	1.51E+20	310.82	452.14	-310.71

	0.6	3.18E+20	315.66	455.66	-304.62
	0.7	6.44E+20	320.16	458.81	-298.84
	0.8	5.57E+20	319.43	459.97	-300.12
	0.9	6.65E+20	320.58	462.03	-298.74
	Average	**2.66E+20**	**294.27**	**438.58**	**-328.90**
Friedman	**0.1**	3.37E+14	213.75	358.97	-416.70
	0.2	1.13E+17	269.95	426.64	-369.96
	0.3	1.66E+20	312.92	449.49	-309.71
	0.4	4.88E+20	319.43	454.54	-300.88
	0.5	1.61E+21	326.52	458.91	-291.07
	0.6	3.38E+21	331.07	462.04	-284.97
	0.7	1.29E+21	325.01	460.99	-293.09
	0.8	3.7E+20	317.15	459.29	-303.53
	0.9	1.23E+21	324.34	463.37	-293.63
	Average	**9.47E+20**	**304.46**	**443.80**	**-318.17**
Vyazovkin	**0.1**	3.72E+14	215.63	360.56	-415.87
	0.2	1.25E+17	272.57	428.91	-369.14
	0.3	1.83E+20	313.56	449.77	-308.88
	0.4	5.38E+20	318.34	453.09	-300.06

	0.5	1.77E+21	328.18	460.19	-290.25
	0.6	3.73E+21	336.33	466.93	-284.15
	0.7	1.42E+21	323.49	459.10	-292.27
	0.8	4.08E+20	315.79	457.54	-302.70
	0.9	1.36E+21	321.92	460.55	-292.80
	Average	**1.05E+21**	**305.09**	**444.07**	**-317.35**

To reduce interaction effects, the Tp value was calculated based on the lowest heating rate. The reason is that increasing heating rates results in more interaction between sample components. The E_a values obtained from all of the chosen models were used to calculate the values of ΔH, ΔG, and ΔS.

Table 5.6: Pre-exponential factor and other thermodynamic parameters for all EVA/chitosan samples obtained by using activation energy deduced from FWO, KAS, Friedman and Vyazovkin methods.

	α	Pre-exponential factor, A (s^{-1})	Enthalpy, ΔH (kJ/mol)	Gibbs free energy, ΔG (kJ/mol)	Entropy, ΔS (J /mol)
FWO	**0.1**	9.44E+15	222.09	353.81	-388.76
	0.2	1.83E+17	262.48	415.18	-365.84
	0.3	2.60E+21	324.50	450.71	-286.80
	0.4	1.88E+22	338.22	459.74	-270.50
	0.5	2.91E+22	341.91	463.51	-267.00
	0.6	4.02E+22	344.55	466.30	-264.41
	0.7	4.70E+22	346.03	468.42	-263.19
	0.8	7.55E+22	349.35	471.17	-259.33
	0.9	8.91E+22	350.83	473.46	-258.05
	Average	**3.36E+22**	**319.99**	**446.92**	**-291.54**
KAS	**0.1**	1.03E+16	221.98	353.46	-388.04
	0.2	1.91E+17	262.33	414.88	-365.48
	0.3	2.51E+21	324.42	450.77	-287.10
	0.4	1.77E+22	338.14	459.89	-271.00
	0.5	2.74E+22	341.84	463.67	-267.52
	0.6	3.77E+22	344.49	466.48	-264.95
	0.7	4.42E+22	345.96	468.59	-263.71
	0.8	7.08E+22	349.28	471.35	-259.87

	0.9	8.38E+22	350.76	473.64	-258.57
	Average	**3.16E+22**	**319.91**	**446.97**	**-291.80**
Friedman	**0.1**	4.23E+15	147.85	281.84	-395.45
	0.2	1.53E+18	191.79	337.13	-348.19
	0.3	9.14E+22	273.49	386.67	-257.20
	0.4	5.35E+22	268.49	386.12	-261.83
	0.5	5.05E+22	276.46	395.97	-262.42
	0.6	6.38E+22	273.57	393.55	-260.56
	0.7	6.70E+22	264.21	385.23	-260.24
	0.8	1.19E+23	265.69	385.71	-255.52
	0.9	1.38E+23	273.55	394.46	-254.43
	Average	**6.48E+22**	**248.34**	**371.85**	**-283.98**
Vyazovkin	**0.1**	6.62E+15	139.91	272.64	-391.71
	0.2	4.47E+17	189.95	339.56	-358.43
	0.3	2.18E+23	270.05	380.06	-249.98
	0.4	9.66E+22	265.35	380.77	-256.91
	0.5	8.02E+22	280.04	397.80	-258.58
	0.6	8.20E+22	276.17	395.19	-258.48
	0.7	9.29E+22	269.32	389.07	-257.52
	0.8	3.91E+22	259.59	383.97	-264.81
	0.9	1.03E+23	271.15	393.21	-256.82
	Average	**7.91E+22**	**246.84**	**370.25**	**-283.69**

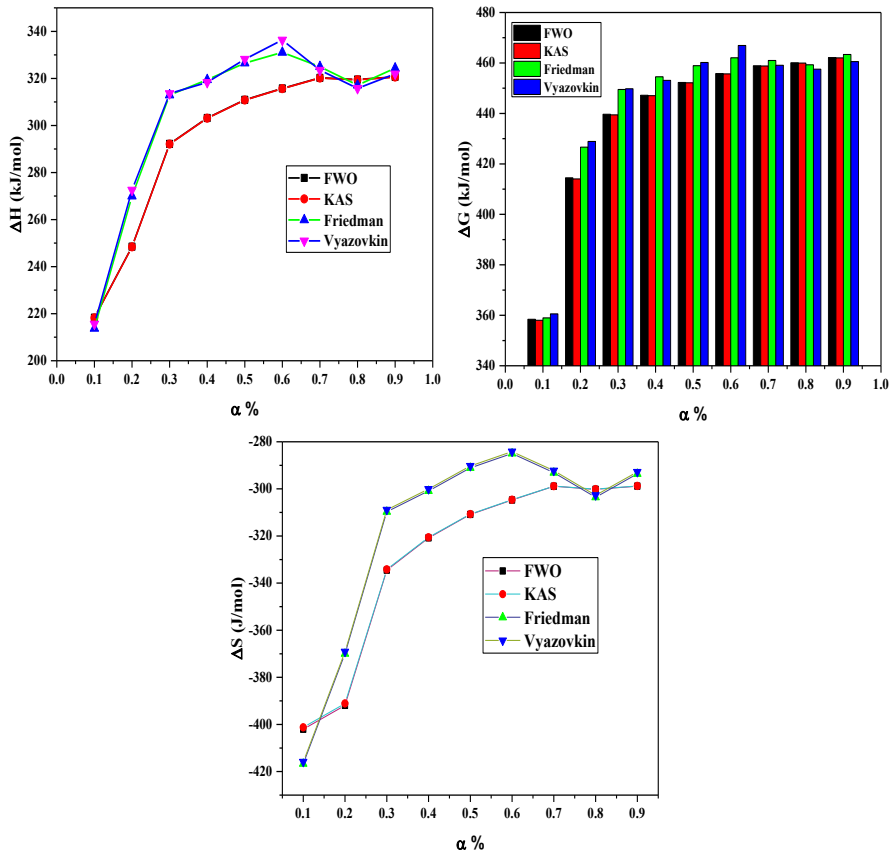

Figure 5.7: Change in enthalpy, change in Gibbs free energy and change in entropy with conversion profiles respectively of neat EVA

The fact that all α values ΔH is positive supports the idea that pyrolysis of the samples is an endothermic process with heat energy requirement to proceed. Thus, implying the utilization of external energy during pyrolysis.

The ΔG values for all conversion fractions in the table are positive. As indicated by the positive ΔG values, the pyrolysis process requires a driving force completion. A steady energy output throughout the degradation is indicated by the values of ΔG.

Negative ΔS values were found in a few conversion fractions, indicating the creation of active complexes. It is significant to mention that the low entropy values indicated degradation process approaching thermodynamic equilibrium.

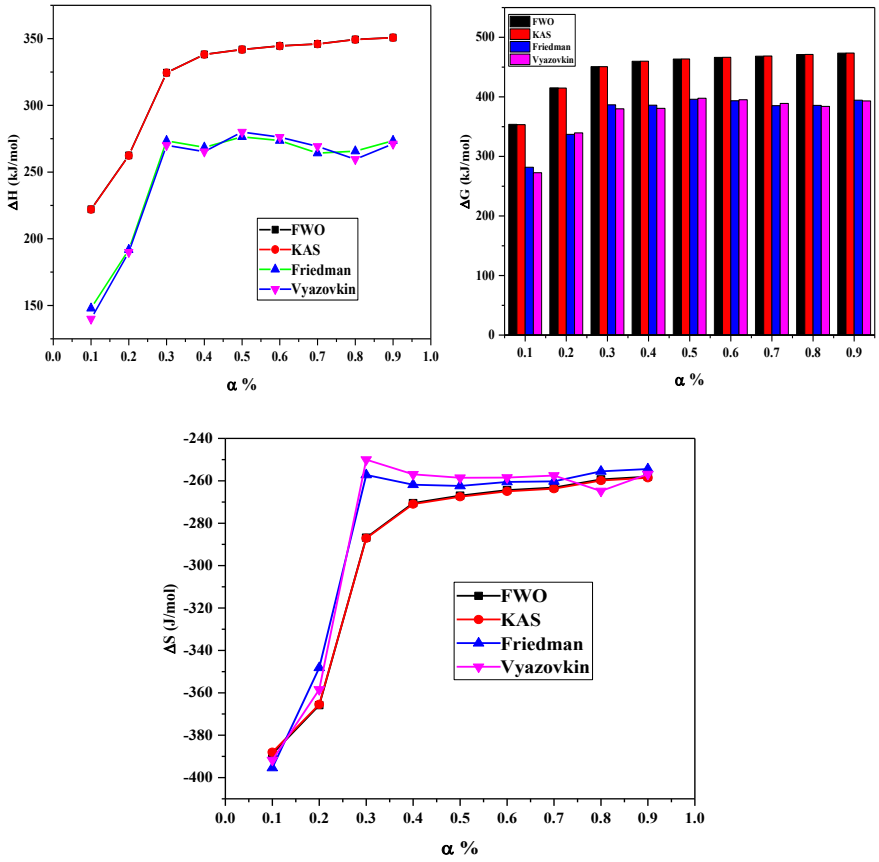

Figure 5.8: Change in enthalpy, change in Gibbs free energy and change in entropy with conversion profiles respectively of EVA/chitosan composite

It should be noted that the thermodynamic parameters show lower values for neat EVA. This indicated that the developed EVA/chitosan composite has better thermal degradation kinetics compared to that of neat EVA

Table 5.7: Pre-exponential factor and other thermodynamic parameters for all EVA/chitosan-g-PANi samples obtained by using activation energy deduced from FWO, KAS, Friedman and Vyazovkin methods.

	α	Pre-exponential factor, A (s^{-1})	Enthalpy, ΔH (kJ/mol)	Gibbs free energy, ΔG (kJ/mol)	Entropy, ΔS (J /mol)
FWO	**0.1**	4.04E+08	135.89	310.57	-529.61
	0.2	6.52E+07	138.83	361.27	-546.52
	0.3	1.62E+14	228.52	414.55	-424.69
	0.4	3.27E+15	247.16	426.26	-399.89
	0.5	1.06E+16	254.50	431.80	-390.25
	0.6	2.13E+16	258.82	435.52	-384.52
	0.7	2.84E+16	260.54	437.94	-382.23
	0.8	3.28E+16	261.33	439.97	-381.11
	0.9	6.03E+16	264.86	443.31	-376.15
	Average	**1.74E+16**	**227.83**	**411.24**	**-423.88**
KAS	**0.1**	3.94E+08	135.77	310.51	-529.80
	0.2	5.64E+07	138.63	361.57	-547.73
	0.3	1.79E+14	228.42	414.08	-423.85
	0.4	3.61E+15	247.06	425.81	-399.09
	0.5	1.16E+16	254.41	431.35	-389.46
	0.6	2.34E+16	258.73	435.07	-383.75
	0.7	3.12E+16	260.45	437.48	-381.44
	0.8	3.61E+16	261.23	439.50	-380.32

	0.9	6.62E+16	264.76	442.85	-375.37
	Average	**1.91E+16**	**227.72**	**410.91**	**-423.42**
Friedman	**0.1**	2.40E+09	147.92	317.72	-514.79
	0.2	1.33E+11	191.88	388.53	-483.15
	0.3	2.00E+17	273.50	433.61	-365.50
	0.4	9.82E+16	268.50	434.94	-371.61
	0.5	3.85E+17	276.47	440.19	-360.36
	0.6	2.57E+17	273.58	440.77	-363.83
	0.7	6.01E+16	264.21	438.72	-375.99
	0.8	8.17E+16	265.70	440.78	-373.52
	0.9	3.05E+17	273.55	445.62	-362.67
	Average	**1.54E+17**	**248.37**	**420.10**	**-396.83**
Vyazovkin	**0.1**	5.30E+08	139.99	313.92	-527.35
	0.2	1.18E+11	190.03	387.09	-484.13
	0.3	1.17E+17	270.07	432.12	-369.96
	0.4	5.90E+16	265.36	433.69	-375.85
	0.5	6.98E+17	280.04	441.53	-355.42
	0.6	3.91E+17	276.18	441.77	-360.34
	0.7	1.36E+17	269.32	440.68	-369.21
	0.8	3.11E+16	259.60	438.44	-381.55
	0.9	2.03E+17	271.16	444.82	-366.04
	Average	**1.82E+17**	**246.86**	**419.34**	**-398.87**

EVA/chitosan-g-PANi composites show similar trend as to the EVA/chitosan samples. A gradual increase in both enthalpy and free energy values show that the thermal decomposition of EVA/chitosan-g-PANi is an endothermic, endergonic process.

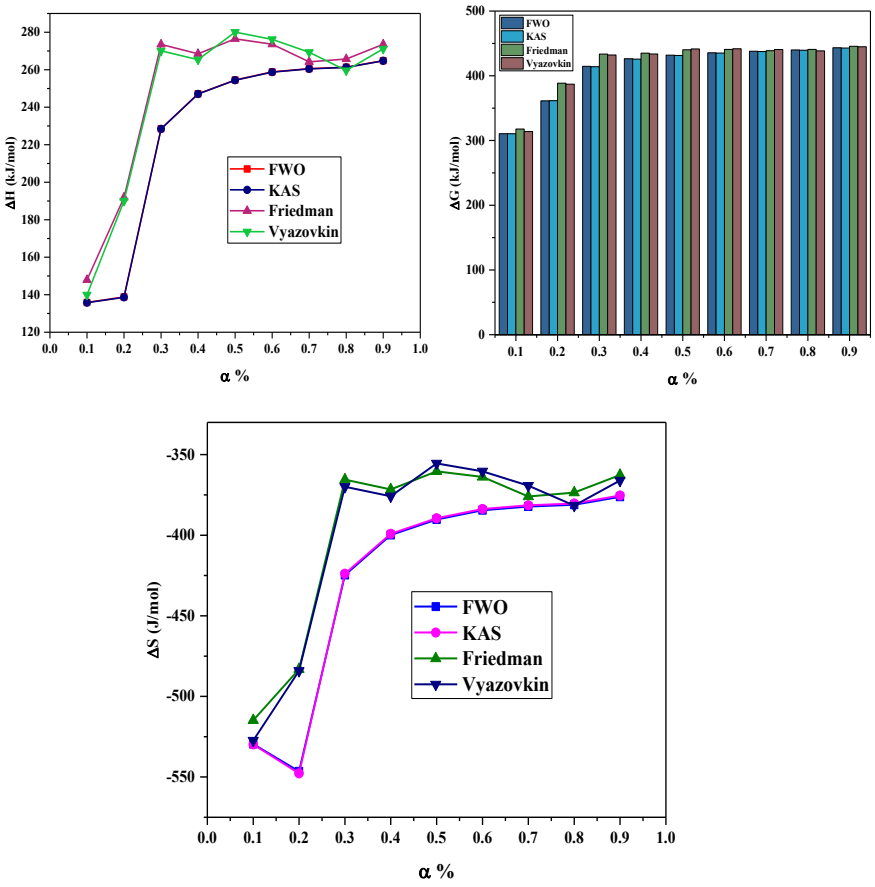

Figure 5.9: Change in enthalpy, change in Gibbs free energy and change in entropy with conversion profiles respectively of EVA/chitosan-g-PANi

5.5. Mechanical properties

The mechanical properties of EVA vary according to the VA content in it. The higher the content lesser the crystallinity of the polymer. The

lower crystalline nature indicates the improvement in the flexibility of the chain owing to the better orientation and ease of alignment in the direction of applied stress. Neat EVA does not show any specific yield point and also no neck formation which agrees with previous studies (Sefadi and Luyt, 2012).

Different mechanical properties like tensile strength, elongation at break, and Young's modulus of the developed composites are calculated from stress–strain plots (Figure 5.10 & 5.11). The composites with both chitosan and PANi grafts showed lesser tensile strength than the raw EVA. Raw EVA has a tensile strength of ~27 MPa. The chitosan loaded composites initially show an increase of the mechanical properties. Further, a decrease in the values is observed after 6 % addition of the filler to the matrix. This may be attributed to the inadequate interaction between the matrix and filler at higher filler concentration. The values of the tensile properties are denoted in Table 5.8. Another reason for the decline in tensile values may be the agglomeration of the filler at higher loading that in turn makes the composite less mechanically viable. A similar trend was observed by Sonia *et al* for composites of EVA with cellulose (Sonia and Priya Dasan, 2013).

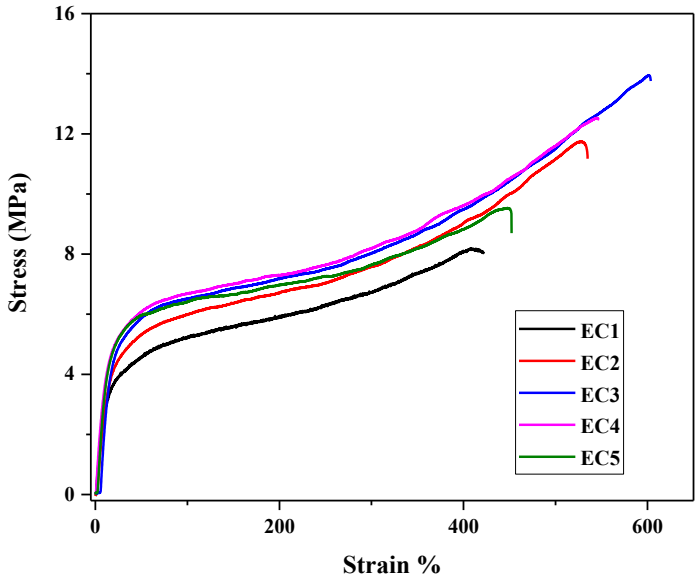

Figure 5.10: Stress-strain behavior of EVA/chitosan composites

Table 5.8: Tensile strength, elongation at break, and Young's modulus of EVA/chitosan (EC) composites

Composite	TS at break (MPa)	Elongation at break %	Young's Modulus (MPa)
EC1	8.19 ± 0.6	408 ± 8.4	25.08 ± 5.84
EC2	11.75 ± 0.49	527 ± 8.1	22.31 ± 8.74
EC3	13.95 ± 0.48	602 ± 9.9	28.40 ± 3.27
EC4	12.53 ± 0.51	545 ± 8.7	27.04 ± 9.83
EC5	9.24 ± 0.21	398 ± 13.4	20.39 ± 13.7

It was observed that with progressive increase in concentration of the filler, all mechanical properties like tensile strength (TS) at break, tensile modulus (TM) and elongation at break (EB) as percentage (%) under consideration increases for the prepared composite systems.

The prepared EVA/chitosan-g-PANi composites show tensile strength up to 16.57 MPa with the increase in the filler addition (Table 5.9). The composites with modified filler, chitosan-g-PANi, has shown improved strength considerably due to the interactions between the filler and matrix indicating better mixing leading to the formation of interfacial area (Saïed and Aïder, 2014). This can further lead to the effective distribution of stress across the composite. The elongation at break and the Young's modulus calculated from the initial linear region of the stress-strain plot also show an increase with the filler. This too suggests better miscibility of the matrix and the filler and the formation of a strong interface between the matrix and the filler.

Table 5.9: **Tensile strength, elongation at break, and Young's modulus of EVA/chitosan-g-PANi (ECP) composites**

Composite	TS at break (MPa)	Elongation at break %	Young's Modulus (MPa)
ECP1	8.87 ± 0.45	413 ± 6.3	13.36 ± 1.46
ECP2	12.19 ± 0.46	537 ± 5.1	18.63 ± 1.74
ECP3	14.47 ± 0.54	653 ± 5.5	22.17 ± 4.66
ECP4	16.57 ± 0.89	723 ± 4.4	25.26 ± 6.21
EVA0	27.22	-	-

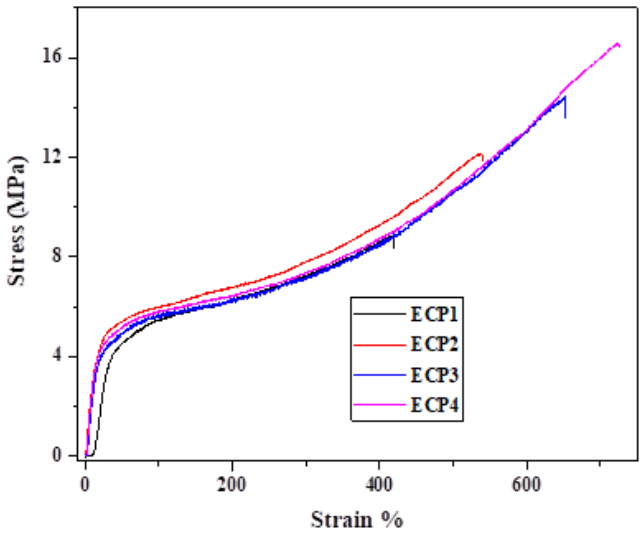

Figure 5.11: Stress-strain behavior of EVA/chitosan-g-PANi (ECP) composites

5.6. Dielectric Properties

Ethylene-co-vinyl acetate (EVA) based composites display interesting dielectric properties that make them appropriate for diverse electrical and electronic applications. The dielectric properties of EVA-based composites are influenced by a variety of factors, such as the matrix properties, the type and concentration of fillers or additives, and the processing techniques utilised. These can be tuned according to the formulation, processing conditions and the application envisioned for the developed composite. The analysis of physical effects occurring in polymer composites, such as molecular mobility, polarization, conductivity, interfacial phenomena, phase changes, polymerization, crystallization, etc. can be carried out using Broadband dielectric spectroscopy. It is to be noted that the results presented are aimed only at room temperature measurements.

The dielectric constant ε', or permittivity, is a measure of the energy stored in a sample during a cyclic electric excitation. The energy stored is usually in the form of a non-uniform dipole distribution or ionic charge layers. With increased addition of fillers, dielectric constant is increased at any measured frequency. There is an observed decrease in the dielectric constant value for the maximum concentration of filler which is attributed to the agglomeration of the filler at higher concentration. For neat EVA or any composite, dielectric constant is found to decreased with the increase of frequency (Sebastian *et al.*, 2015; Padhi, Priyadarsini and Nayak, 2020). Due to the presence of EVA, some charge carriers present in fillers get confined and is not able to freely discharge at the electrodes which results in space charges accumulating at the interface of conducting filler and insulating matrix combined with microscopic distortion of applied electric field. This phenomenon is termed as Maxwell-Wagner-Sillers (MWS) interfacial polarization. This effect is observed for composites that contain EVA as matrix in the literature (Wang *et al.*, 2021).

The tan δ of all composites remained at low values and showed no drastic variation over the entire frequency range indicative of the low leakage current and energy loss in the composites.

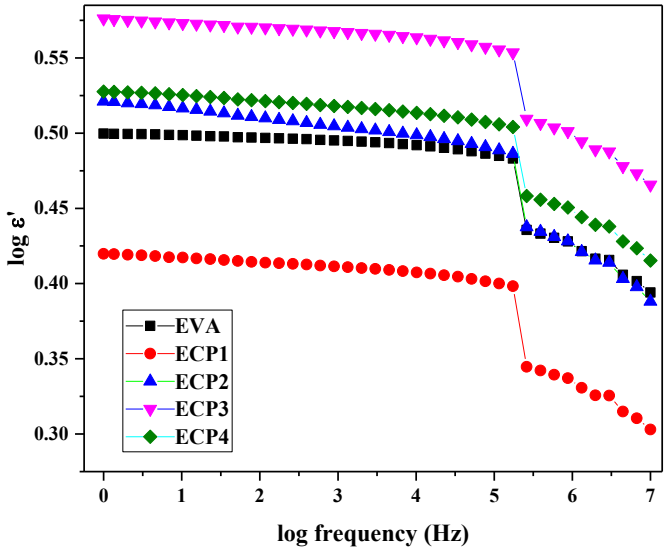

Figure 5.12: Frequency dependence of ε′ of EVA/chitosan-g-PANi (ECP) composites.

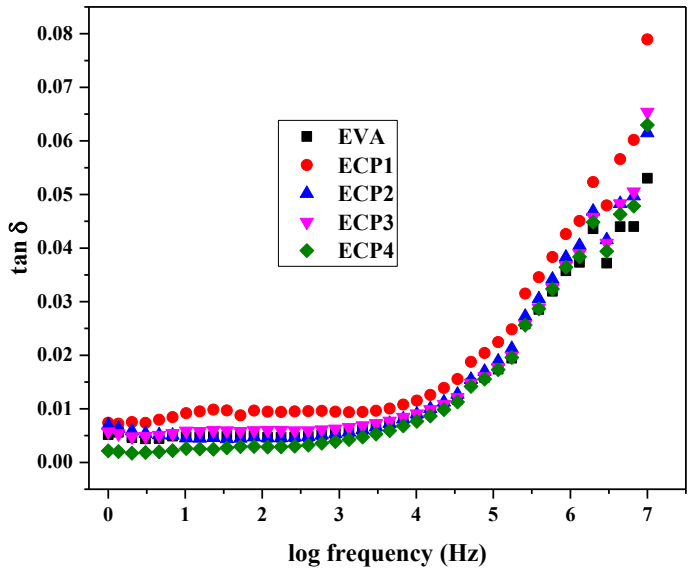

Figure 5.13: Frequency dependence of tan δ (dielectric loss) of EVA/chitosan-g-PANi (ECP) composites.

Chapter 6
Development of Ethylene-co-vinyl acetate (EVA)/vinyl grafted chitosan composites

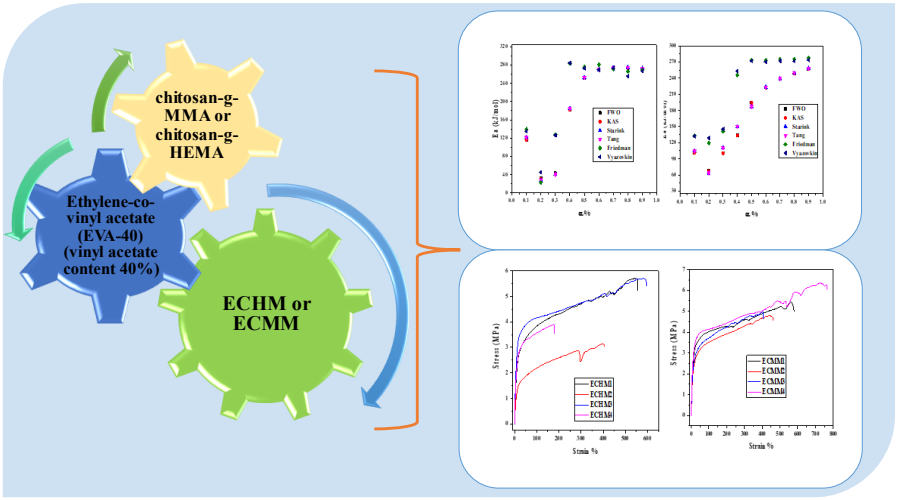

This chapter explicates the development of composites of EVA with vinyl grafted chitosan as fillers. A brief note on the relevance of the study is given with the introduction. The samples were characterized via infrared spectra and thermogravimetric analysis. The kinetic degradation parameters and thermodynamic parameters were elucidated with the assistance of model free

methods. Mechanical data obtained from Universal testing Machine is also elaborated in the course of the study.

EVA, a copolymer of ethylene and vinyl acetate can be a sensible option as a matrix for grafted composites owing to its inexpensiveness, good processability, excellent mechanical properties & long shelf life. Depending on the applications intended the composite formulation can be tuned. Though EVA with VA content ranging from of 2–70 % can be obtained in the market, the most used EVA grades range from 9 to 40 % VA content. This is because these EVAs can be used in an extensive array of applications such as hot melt adhesives, shoe soles, high clarity packaging and agricultural mulch films (Esmizadeh, Tzoganakis and Mekonnen, 2020),

One of the promising directions in materials science is related to the creation of "hybrids" based on natural and synthetic polymers. Being a unique material with multiple applications, ethylene-co-vinyl acetate (EVA) is a feasible matrix for composite fabrication (Stephy, Antony and Francis, 2021). A large number of materials can be used as fillers in these composites in order to tackle the growing demand for materials with improved performance characteristics. The potential of composites derived from polysaccharides like chitosan and cellulose as fillers have been explored (Sadeghifar *et al.*, 2017; Aragão Melo *et al.*, 2018b; Luo *et al.*, 2020). These polysaccharidic materials imparts a crystalline nature to the otherwise amorphous EVA.

One of the main disadvantages of materials involving chitosan is its low mechanical property and high moisture intake. In order to overcome the inadequacies of raw chitosan as filler, chemical modification by introducing synthetic monomers via grafting can be carried out. There is a wide range of options to choose from the

methods of grafting. One of it is by promoting grafting with the help of redox initiator such as ceric ammonium nitrate (CAN). Being prominent resources owing to the antimicrobial, thermal stability and better mechanical properties vinyl monomers namely, Hydroxy ethyl methacrylate (HEMA) and methyl methacrylate (MMA) plays an important place among them.

Narasagoudr 2021 investigated the thermal degradation of ethyl vanillin crosslinked chitosan/poly(vinyl alcohol) blend films and found that the improved thermal stability of the films could be attributed to the formation of Schiff base and intermolecular hydrogen bonding (Narasagoudr *et al.*, 2021). Keeping this idea in mind, development of enhanced materials with chitosan grafts as fillers are developed and a detailed study on the thermal degradation and mechanical properties was carried out. Even though in a pragmatic view, kinetics is just a means to provide the liaison between the time, temperature and conversion of a reaction, the knowledge of the kinetics of pyrolytic decomposition of these materials can be beneficial towards the quantitative analyses of phenomena that occurs during thermal decomposition(Gharsallah *et al.*, 2021). It may also help us to better understand and plan their industrial processing. In the literature, there is no enough information on kinetic parameters of pyrolysis of such materials makes it a relevant topic to further evaluate on (Naqvi *et al.*, 2018; Yousef *et al.*, 2020, 2023).

Table 6.1. represents the formulations used in this chapter for the studies carried out.

Table 6.1. Formulations for the prepared composite

Series Prepared	Sample Name	Composition	
		EVA (g)	**Chitosan-g-PANi (wt %)**
ECMM series (chitosan-g-MMA as filler)	ECMM1	30	2.5
	ECMM2	30	5
	ECMM3	30	7.5
	ECMM4	30	10
		EVA (g)	**Chitosan-g-HEMA (wt %)**
ECHM series (chitosan-g-HEMA as filler)	ECHM1	30	2.5
	ECHM2	30	5
	ECHM3	30	7.5
	ECHM4	30	10

6.1. Infrared Characterization

The spectrum of EVA with the chitosan grafts shows almost all the characteristic peaks of both EVA and the fillers. The absorbances of the composites shows a lower value than that of neat EVA owing to the interference of high absorbance values of EVA that masks effect of the fillers in the composite. Also, the slight shift of the peaks towards lower wavenumbers agrees with the interaction between the fillers and the matrix especially carbonyl peak. Both these behaviours are similar throughout the composites developed (ECMM 2 and ECHM 2).

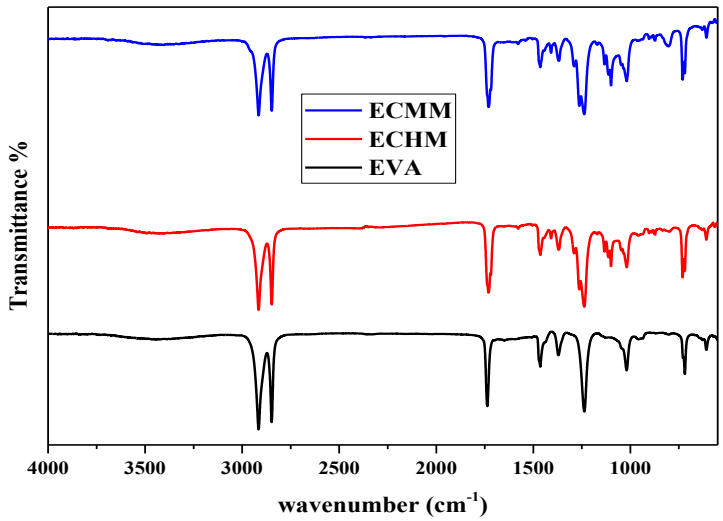

Figure 6.1: Infrared spectra of EVA, EVA/ chitosan-g-HEMA (ECHM) and EVA/ chitosan-g-MMA (ECMM)

6.2. Thermal characterization

Thermal decomposition denotes degradation of a substance by inducing heat which results in the formation of products with varied composition from that of the reactant (Vyazovkin *et al.*, 2014; Koga *et al.*, 2023). The TG curves of composites containing different amount of chitosan grafts as fillers are shown in figure

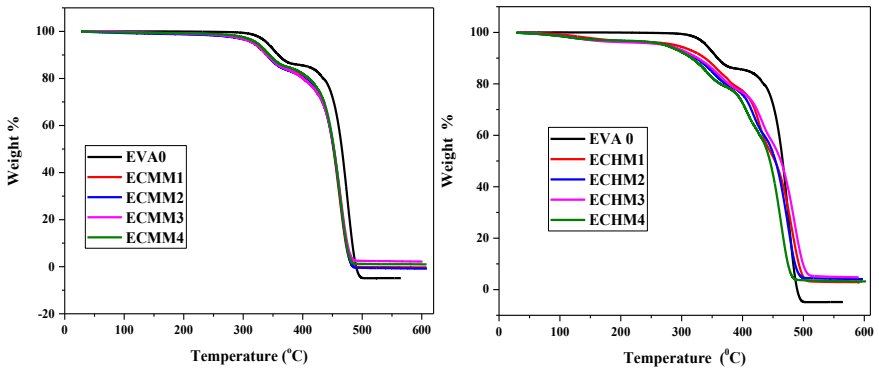

Figure 6.2: Thermograms of ECMM and ECHM composite

The thermograms of composites with CMM as fillers show the typical two step degradation as that of EVA whereas composites with CHM as filler shows a three-step degradation. The initial stage of the decomposition is attributed to the deacetylation of EVA chains, i.e. the decomposition of the acetate groups of the polymer side chain, which is common to the reported EVA composites (Moradkhani *et al.*, 2020).

For ECMM composites the trend is similar to that of the other composites like ECP and ECPE. However, from the thermograms it can be observed that ECHM composites undergo a slightly complicated decomposition. This additional curve can be attributed towards the degradation of the HEMA in the chitosan graft present in the composite. A similar observation was made by Yang et al when HEMA was grafted with silk fabric (Patwa *et al.*, 2019).

Table 6.2: **Degradation temperatures of the materials**

	Stage I (ºC)	**Stage II (ºC)**	**Stage III (ºC)**
EVA	342	463	-
ECMMS3	331	451	-
ECHMC3	335	413	464

6.3. Kinetic Analysis of Thermal Degradation

Figure depict the linear fitted plots of ECMM and ECHM for different model free methods within the conversion range of 0.1 to 0.9. The corresponding activation energy values are given in Table 6.3. Model free methods are employed to evaluate the degradation kinetics in this study. These approaches let the estimation of activation energy independent of reaction mechanism which is considered to be apt for

the investigation of composites where there is no comprehension about the reaction mechanism (Vyazovkin and Sbirrazzuoli, 2006; Shirdel, Omrani and Ehsani, 2017; Yousef *et al.*, 2021).

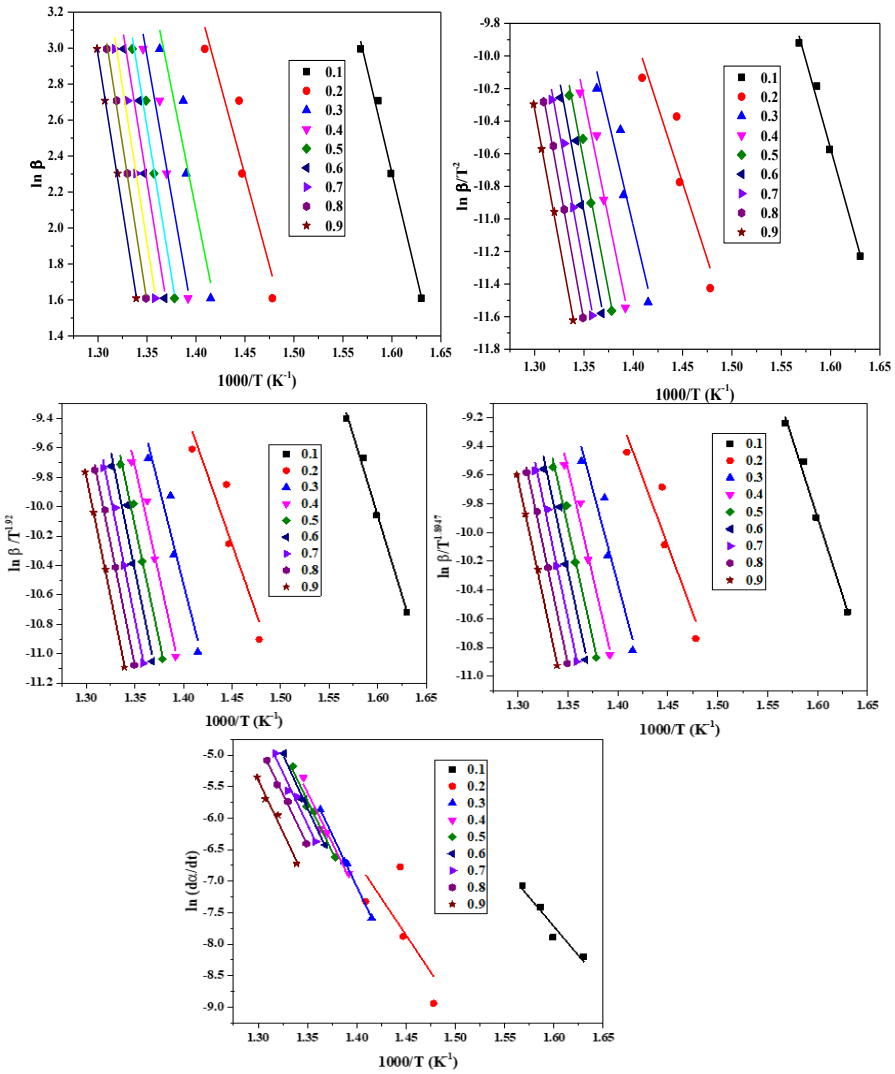

Figure 6.3: Typical linear regression lines of ECMM using FWO, KAS, Starink, Tang and Friedman methods

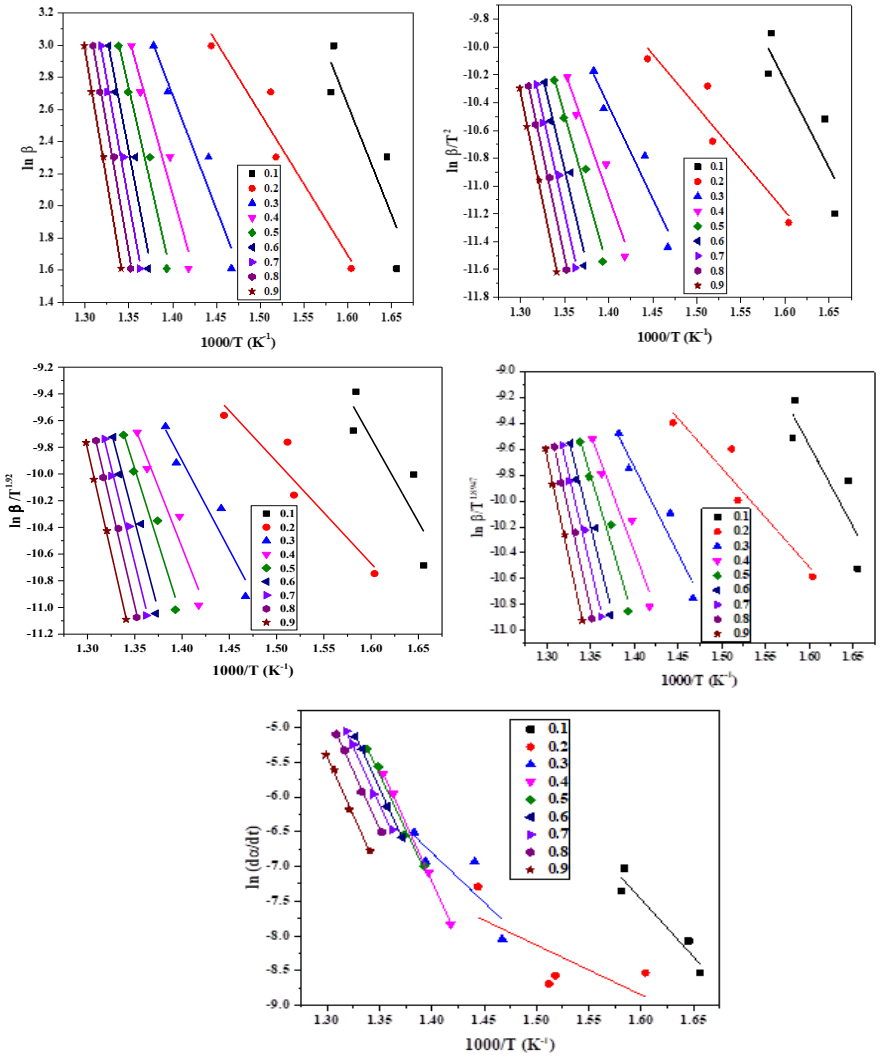

Figure 6.4: Typical linear regression lines of ECHM using FWO, KAS, Starink, Tang and Friedman methods

With the exception of certain conversions, the activation energies showed linear relationships with conversion. This is similar throughout every composite that was under our study. The variation in the activation energy w.r.t. conversion implies that the degradation follows a complex mechanism.

Table 6.3: The energy of activation according to conversion degree for FWO, KAS, Starink, Tang, Friedman and Vyazovkin methods of ECMM and ECHM composites

ECMM						
	FWO	**KAS**	**Starink**	**Tang**	**Friedman**	**Vyazovkin**
α	**E_a**					
0.1	116.30	116.02	121.43	121.56	139.22	134.84
0.2	31.69	30.36	27.84	27.98	22.62	45.05
0.3	42.82	41.69	40.37	40.52	127.94	126.21
0.4	182.15	181.94	184.39	184.55	283.12	284.48
0.5	251.89	251.79	252.53	252.68	275.79	272.78
0.6	269.14	269.05	269.81	269.97	280.96	269.58
0.7	273.59	273.51	274.16	274.32	271.73	273.17
0.8	273.69	273.60	274.61	274.76	265.89	255.32
0.9	271.50	271.40	272.43	272.59	268.84	266.78
Average	**190.31**	**189.93**	**190.84**	**190.99**	**215.12**	**214.25**

ECHM						
	FWO	**KAS**	**Starink**	**Tang**	**Friedman**	**Vyazovkin**
α	**E_a**					
0.1	101.49	101.20	104.58	104.71	132.86	131.92
0.2	67.78	67.13	63.44	63.58	119.30	128.79
0.3	100.70	100.31	110.75	110.90	140.88	145.32
0.4	133.66	133.37	149.93	150.08	245.71	253.08
0.5	194.14	193.97	186.88	187.03	273.32	271.85
0.6	222.73	222.60	223.34	223.49	273.24	270.20
0.7	238.47	238.36	239.08	239.24	274.81	272.03
0.8	248.96	248.85	249.55	249.70	275.17	271.55
0.9	257.26	257.16	258.05	258.20	277.27	273.51
Average	**173.91**	**173.66**	**176.18**	**176.33**	**223.62**	**224.25**

*E_a is in kJ/mol

This variation of E_a signifies that the pyrolysis does not follow a single step reaction mechanism. Compared with the other models Friedman method exhibited a slightly higher value for E_a which is due to the lack of approximations included in the calculation for these methods (Zhang, 2021).

The activation energies for FWO, KAS, Starink, Tang, Friedman and Vyazovkin averaged as 190.31, 189.93, 190.84, 190.99, 215.12 and 214.25 kJ/mol respectively for ECMM and 173.92, 173.66, 176.18, 176.33, 223.612 and 224.25 kJ/mol respectively for ECHM. These values suggest the reliability of these methods used for E_a calculation.

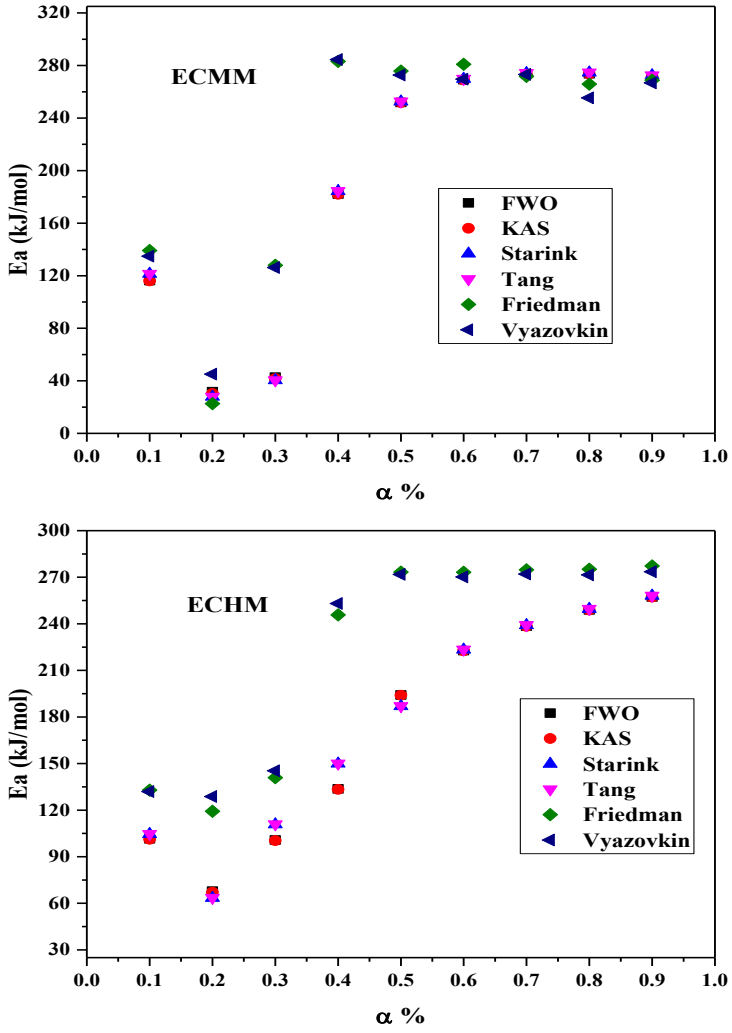

Figure 6.5: Activation energy (E_a) vs conversion (α) profiles of ECMM and ECHM using FWO, KAS, Starink, Tang, Friedman and Vyazovkin method.

6.4. Thermodynamic Properties

Thermodynamic parameters such as ΔH, ΔG, and ΔS for EVA based composites with chitosan grafts as fillers are listed in the table 6.4 and 6.5.

Table 6.4: Pre-exponential factor and other thermodynamic parameters for ECMM obtained by using activation energy deduced from FWO, KAS, Friedman and Vyazovkin methods

	α	Pre-exponential factor, A (s^{-1})	Enthalpy, ΔH (kJ/mol)	Gibbs free energy, ΔG (kJ/mol)	Entropy, ΔS (J /mol)
FWO	**0.1**	4.41E+06	113.47	306.63	-567.43
	0.2	6.76E-01	28.34	310.46	-699.29
	0.3	4.50E+00	39.21	335.89	-684.14
	0.4	4.32E+10	178.45	398.09	-493.26
	0.5	4.68E+15	248.13	427.71	-397.00
	0.6	7.60E+16	265.33	436.59	-373.93
	0.7	1.51E+17	269.74	440.27	-368.33
	0.8	1.49E+17	269.80	442.24	-368.53
	0.9	1.04E+17	267.56	443.55	-371.64
	Average	**5.37E+16**	**186.67**	**393.49**	**-480.39**
KAS	**0.1**	3.51E+06	113.19	306.99	-569.33
	0.2	6.71E-02	27.00	316.87	-718.49
	0.3	7.28E-01	38.08	341.33	-699.28
	0.4	4.36E+10	178.24	397.84	-493.19
	0.5	5.11E+15	248.03	427.28	-396.28
	0.6	8.24E+16	265.24	436.20	-373.26
	0.7	1.63E+17	269.66	439.88	-367.66
	0.8	1.61E+17	269.71	441.83	-367.84

	0.9	1.13E+17	267.47	443.13	-370.93
	Average	**5.83E+16**	**186.29**	**394.59**	**-484.03**
Friedman	**0.1**	2.40E+08	136.39	318.23	-534.18
	0.2	2.54E-02	19.27	312.41	-726.59
	0.3	3.75E+06	124.33	371.86	-570.79
	0.4	6.34E+17	279.41	437.96	-356.06
	0.5	1.95E+17	272.03	437.59	-366.01
	0.6	4.79E+17	277.15	441.41	-358.63
	0.7	1.12E+17	267.88	439.54	-370.78
	0.8	4.71E+16	262.00	438.91	-378.09
	0.9	8.26E+16	264.90	441.79	-373.51
	Average	**1.72E+17**	**211.48**	**404.41**	**-448.29**
Vyazovkin	**0.1**	1.06E+08	132.01	316.18	-541.01
	0.2	1.53E+00	41.70	321.09	-692.51
	0.3	3.49E+06	122.60	370.39	-571.38
	0.4	8.18E+17	280.78	438.38	-353.93
	0.5	1.16E+17	269.02	436.52	-370.30
	0.6	7.87E+16	265.77	436.91	-373.64
	0.7	1.39E+17	269.32	440.15	-368.98
	0.8	8.69E+15	251.43	434.92	-392.14
	0.9	5.73E+16	262.85	441.17	-376.56
	Average	**1.35E+17**	**210.61**	**403.97**	**-448.94**

ΔH is a state function indicating the energy difference between the reactants and the products, ΔG represents the amount of available energy within the material and ΔS indicate the chaos in the system. Generally, ΔH goes on par with the E_a trend. About <5 kJ/mol difference between the values of E_a and ΔH is observed for all methods which reflect the occurrence of pyrolysis reaction indicating the easier product formation. This is common for both sets of composites.

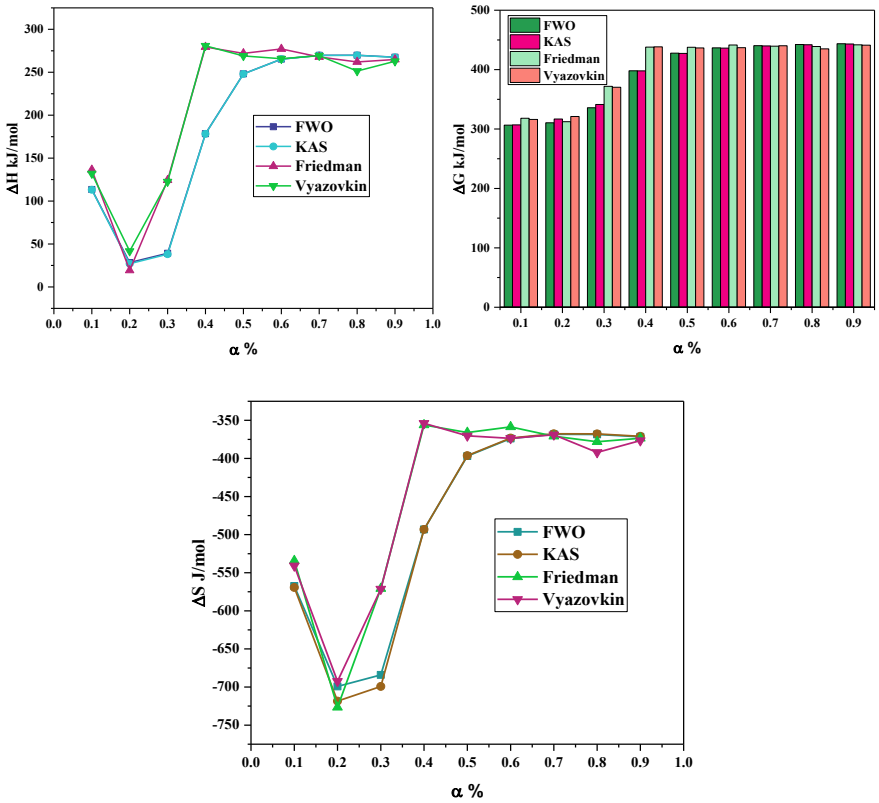

Figure 6.6: Change in enthalpy, change in Gibbs free energy and change in entropy with conversion profiles respectively of ECMM

Table 6.5: Pre-exponential factor and other thermodynamic parameters for ECHM obtained by using activation energy deduced from FWO, KAS, Friedman and Vyazovkin method.

	α	Pre-exponential factor, A (s^{-1})	Enthalpy, ΔH (kJ/mol)	Gibbs free energy, ΔG (kJ/mol)	Entropy, ΔS (J /mol)
FWO	**0.1**	2.94E+05	98.73	293.85	-589.69
	0.2	2.78E+02	64.54	317.72	-648.97
	0.3	6.12E+04	97.20	351.73	-604.75
	0.4	1.43E+07	130.01	376.13	-559.80
	0.5	3.21E+11	190.41	404.39	-476.66
	0.6	3.56E+13	218.94	418.29	-437.63
	0.7	4.70E+14	234.64	426.59	-416.27
	0.8	2.62E+15	245.08	432.65	-402.09
	0.9	1.03E+16	253.33	438.06	-390.84
	Average	**1.49E+15**	**170.32**	**384.38**	**-502.96**
KAS	**0.1**	2.15E+05	98.45	294.43	-592.31
	0.2	1.04E+02	63.89	320.26	-657.12
	0.3	3.81E+04	96.81	353.00	-608.69
	0.4	1.17E+07	129.72	376.56	-561.42
	0.5	3.38E+11	190.24	404.02	-476.22
	0.6	3.89E+13	218.81	417.82	-436.88
	0.7	5.18E+14	234.52	426.10	-415.47
	0.8	2.89E+15	244.98	432.16	-401.26

	0.9	1.13E+16	253.23	437.58	-390.04
	Average	**1.64E+15**	**170.07**	**384.66**	**-504.38**
Friedman	**0.1**	7.93E+07	130.11	309.82	-543.17
	0.2	6.14E+05	116.05	344.26	-584.95
	0.3	3.38E+07	137.38	369.81	-552.25
	0.4	1.34E+15	242.05	421.08	-407.18
	0.5	1.29E+17	269.59	435.40	-369.36
	0.6	1.34E+17	269.46	437.63	-369.19
	0.7	1.82E+17	270.97	440.08	-366.73
	0.8	2.04E+17	271.29	441.96	-365.87
	0.9	3.03E+17	273.34	444.78	-362.70
	Average	**1.06E+17**	**220.03**	**404.98**	**-435.71**
Vyazovkin	**0.1**	6.98E+07	129.17	309.24	-544.22
	0.2	3.80E+06	125.54	347.84	-569.79
	0.3	7.93E+07	141.82	371.28	-545.17
	0.4	4.56E+15	249.42	423.96	-396.98
	0.5	1.05E+17	268.12	434.71	-371.08
	0.6	8.15E+16	266.42	436.46	-373.31
	0.7	1.17E+17	268.20	438.98	-370.36
	0.8	1.14E+17	267.67	440.61	-370.73
	0.9	1.60E+17	269.58	443.52	-368.00
	Average	**6.47E+16**	**220.66**	**405.18**	**-434.40**

The average ΔH of Friedman method is slightly higher for ECMM composites. The principles used to calculate the parameters are evaluated to comprehend the differences between the values of the four models. It was deduced that these differences are due to the assumptions and approximations used in the other models than the Friedman.

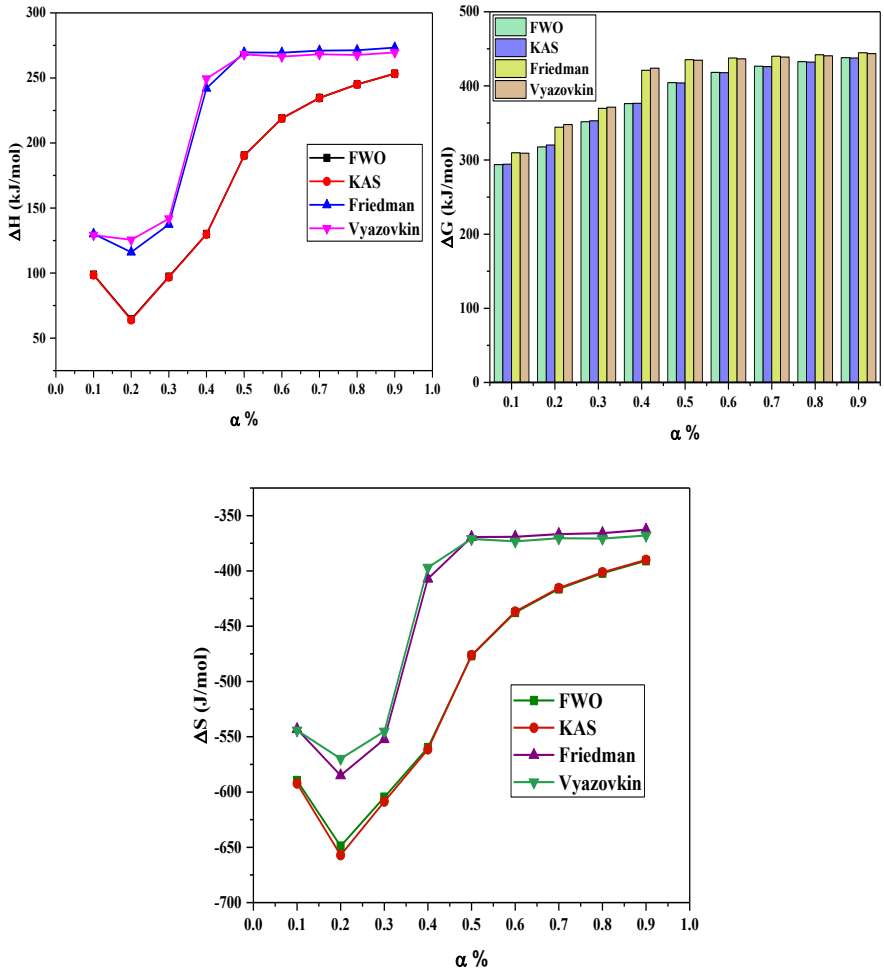

Figure 6.7: Change in enthalpy, change in Gibbs free energy and change in entropy with conversion profiles respectively of ECHM.

The thermodynamic parameters were averaged in the ranges 186-2120 kJ/mol (ΔH), 393-405 kJ/mol (ΔG), and (-448) – (-484) J/mol K (ΔS) at 5 ° C/min for ECMM while these parameters were averaged in the ranges of 170–221 kJ/mol (ΔH), 384–406 kJ/mol (ΔG), and (- 434) – (-505) J/mol K (ΔS) for ECHM. As observed for other composites the ΔH values are positive denoting endothermic nature of the process.

The values and trend of the thermodynamic parameters reveal that the process is non-spontaneous and endothermic at all temperatures for both sets of composites (Monika, Mulchandani and Katiyar, 2019; Singh *et al.*, 2019).

6.5. Mechanical Properties

Different mechanical properties like tensile strength, elongation at break, and Young's modulus of both ECHM and ECMM composites are calculated from stress–strain plots are given in the figure 6.8 and their values in table 6.6**.**

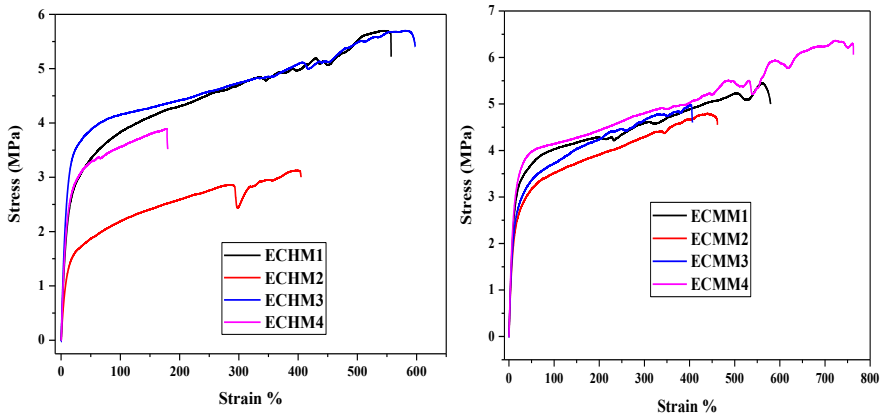

Figure 6.8: Stress-strain behavior of ECHM and ECMM composites

Table 6.6: **Tensile strength, elongation at break, and Young's modulus of ECHM and ECMM composites**

Composite		TS at break (MPa)	Elongation at break %	Young's Modulus (MPa)
ECHM	**1**	5.70 ± 0.59	544 ± 8.6	19.93 ± 10.83
	2	2.44 ± 0.58	399 ± 13.2	13.57 ± 15.90
	3	5.70 ± 0.50	581 ± 11.5	22.86 ± 5.74
	4	3.89 ± 0.17	214 ± 4.5	17.22 ± 14.90
ECMM	**1**	10.53 ± 1.35	665 ± 9.8	59.41 ± 3.17
	2	4.79 ± 6.50	540 ± 7.1	12.66 ± 14.54
	3	5.60 ± 0.45	460 ± 8.1	19.05 ± 8.73
	4	13.13 ± 2.47	723 ± 19.5	69.58 ± 7.49
EVA0		27.22		-

The composites with both the grafts showed lesser tensile strength than the raw EVA, ~27 MPa. Neat EVA does not show a particular yield point and also no neck formation, a behaviour that has been reported in the previous studies (Sefadi and Luyt, 2012). The tensile strength for ECHM composites shows a wavy nature due to the agglomeration of the filler also due to the increase in crystallinity imparted by the grafts onto the matrix. However, the tensile properties of composites with varying concentration of CMM showed the traditional nature of increase with increase in filler content. The slight increase in the values for the composite with 2.5 % of fillers is because of the domination of the matrix quantity in it and also it shows the elongation as that of neat EVA as reported in literature. The nature of elongation of the composites with low filler concentration goes in accordance with neat EVA from literature (Shelenkov, Pantyukhov and Popov, 2020).

Chapter 7
Development of Ethylene-co-vinyl acetate (EVA)/ Polyelectrolyte (PEC) composites

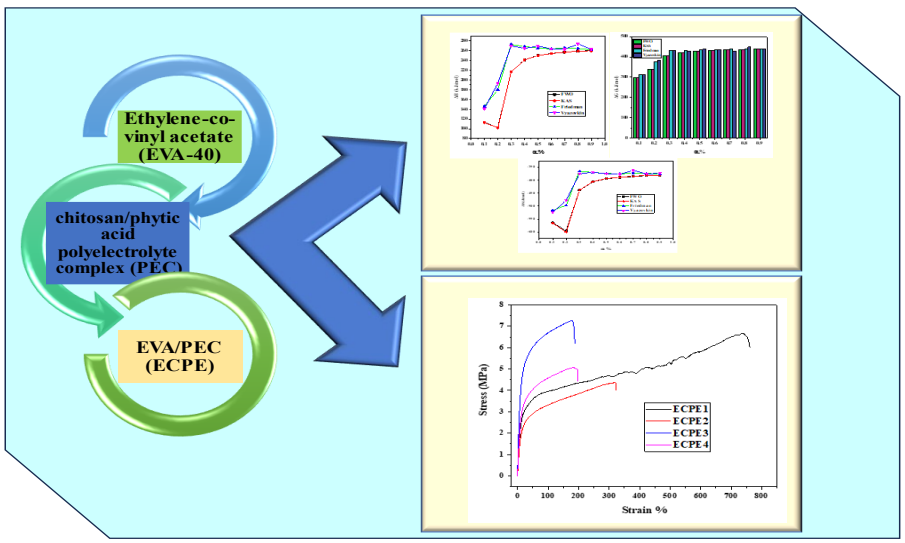

This chapter details the formation of composites by varying the amount of chitosan/phytic acid polyelectrolyte as filler. The IR characterization and thermal analysis of the formed composites were carried out. Since the details on the pyrolytic degradation of these materials as not known, an evaluation on the degradation kinetics and the thermodynamic parameters in accordance with the process was executed. The influence of PEC on the tensile properties of the composites was studied with the help of data obtained from UTM.

Polyelectrolytes are polymeric materials that contain ionic or ionizable groups. They can be categorized into polyanions, polycations, or polyampholytes depending on the charges carried by the chains *viz*.; negative, positive charges or both. Even though hydrogen bonding, hydrophobic effect, or van der Waals forces play a role in the formation of polyelectrolytes, electrostatic contribution generally dominates the interaction between the complexation. A complex formed between chitosan and an oppositely charged molecule, polyelectrolyte, leads to the formation of polyelectrolyte complex of chitosan. The properties such as stability, solubility and mechanical strength of chitosan can be altered by the formation of the polyelectrolyte complex. The enhancement of stability is via crosslinking and shielding of chitosan during the complex formation.

Phytic acid (PA), also known as myo-inositol hexaphosphate (IP6), is a naturally occurring compound found mainly in grains, legumes, and seeds. It acts as the primary storage form of phosphorus in plants (Zhang *et al.*, 2014, 2020). This innocuous polyprotic acid is highly charged with six phosphate groups that extends from the core of the myo-inositol ring. The multiplicity nature makes PA a unique molecule which can complex with both bi or trivalent cations present in a phosphate group itself, either between phosphate groups of the same molecule or between phosphate groups of different molecules.

An electrostatic interaction is formed between the amino groups (cationic) present in chitosan and the negatively (anionic) charged groups of the polyelectrolyte. In the case of chitosan/phytic acid polyelectrolyte complex (PEC), the phosphate groups are the anionic

charge providing entity. This results in creating a 3-D network of bridges between the two entities advancing the mechanical stress, deformation, and degradation of the complex. These kinds of complexes can also be called a polyelectrolytic complex or a polyelectrolyte multilayer. The complex formed can be of gel-like or insoluble particles by tuning the fraction of phytic acid to chitosan (Cheng *et al.*, 2019; Zhang *et al.*, 2020).

The negatively charged phytic acid molecules act as a hindrance and blocks direct exposure of chitosan with degrading agents such as presence of enzymes and external conditions. This shielding effect can better the stability and extend the lifespan of chitosan-based materials, making them more suitable for applications that require long-term functionality. The complexation between phytic acid and chitosan can transform the properties of chitosan which imparts new functionalities to the resulting complex. The research on formation of phytic acid-chitosan polyelectrolyte complexes are currently on going and utilized in various applications, such as drug delivery systems, wound healing materials, and food packaging.

PEC can be mixed with various other materials in order to further tweak its characteristic according to the specific requirement. Lu *et al* developed a PEC nanofiltration membrane for with transformable hydrophilicity/hydrophobicity (Lu *et al.*, 2020). EVA can be an apt polymer that can be used to modify the properties and lead to unique applications. PEC can act as a reinforcement which brings in more rigidity to the EVA matrix leading to improved interaction capability, barrier properties, adhesion and sustainability. Thus, the formed

composite material can be utilized for a variety of applications such as packaging, biomedical engineering, coatings, and functional materials (Sukhishvili, Kharlampieva and Izumrudov, 2006; Hamman, 2010; Meka *et al.*, 2017; Rumyantsev, Jackson and Pablo, 2021)

Table 7.1: Formulation for the prepared EVA/PEC composite

Sample Name	**Composition**	
	EVA (g)	**PEC (wt %)**
ECPE1	30	2.5
ECPE2	30	5
ECPE3	30	7.5
ECPE4	30	10

7.1. Infrared Characterization

Figure represents the infrared spectrum of pristine EVA and EVA with PEC as filler. The typical bands of ethylene groups of EVA at ~2920, ~2850 and 720 cm^{-1} can be seen in the composite as well. The bands at ~ 1630 and ~1180 cm^{-1} indicated the interaction from the PEC filler to the matrix. The bands towards the lower wavelengths at ~1070 cm^{-1} also can be attributed to the presence phosphate group from the filler.

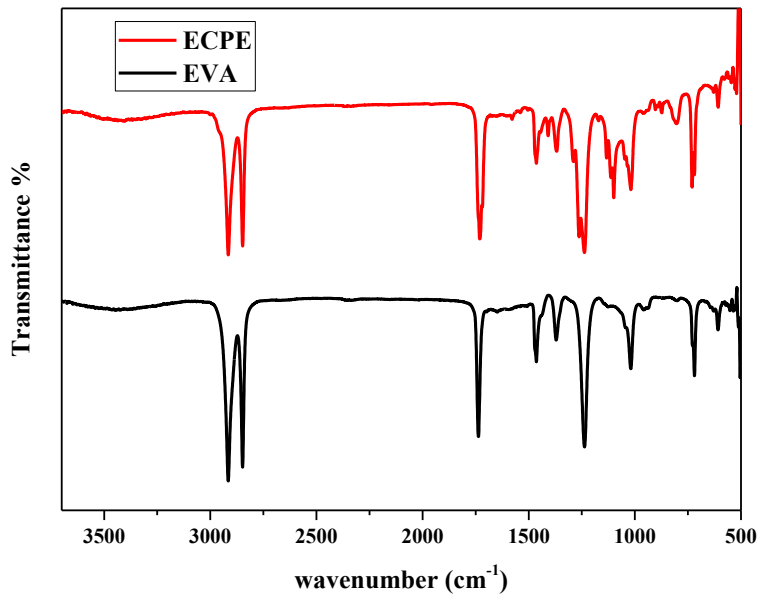

Figure 7.1: Infrared spectra of EVA and EVA/PEC composite (ECPE)

7.2. Thermal characterization

The typical two stage degradation of EVA was observed in the current composite also indicating that EVA has retained its characteristic nature throughout. For the composites containing PEC as filler the degradation tends to begin earlier than raw EVA. This can be attributed to the phosphorus-, nitrogen- and carbon-containing derivative group present in the filler encouraging the faster degradation of the acetate chain of EVA. As the amount of filler increases the rate of weight loss increases at the first stage which gradually decreases at higher temperatures. Subsequently, the residues increase with the increase of PEC content and this indicates the better stability achieved by the composite in the later stages. These results imply the initial degradation induced by PEC accelerates the formation of protective

char layer which further restrain the weight loss suggesting the enhancement of thermal stability.

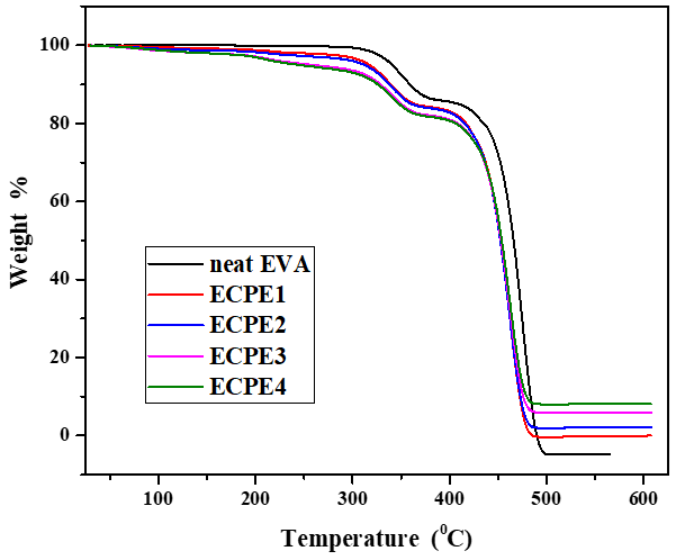

Figure 7.2: TGA thermograms of the prepared EVA/PEC (ECPE) composites

7.3. Kinetic analysis of thermal degradation

The thermogravimetric data plays a crucial role during the investigation of pyrolysis of any material. The data obtained leads to the calculation of kinetic parameters used to predict the dynamic characteristics of pyrolysis degradation. For the entire degradation temperature range and varied heating rates, the relationship between, α, A and E_a illustrates the pyrolysis process.

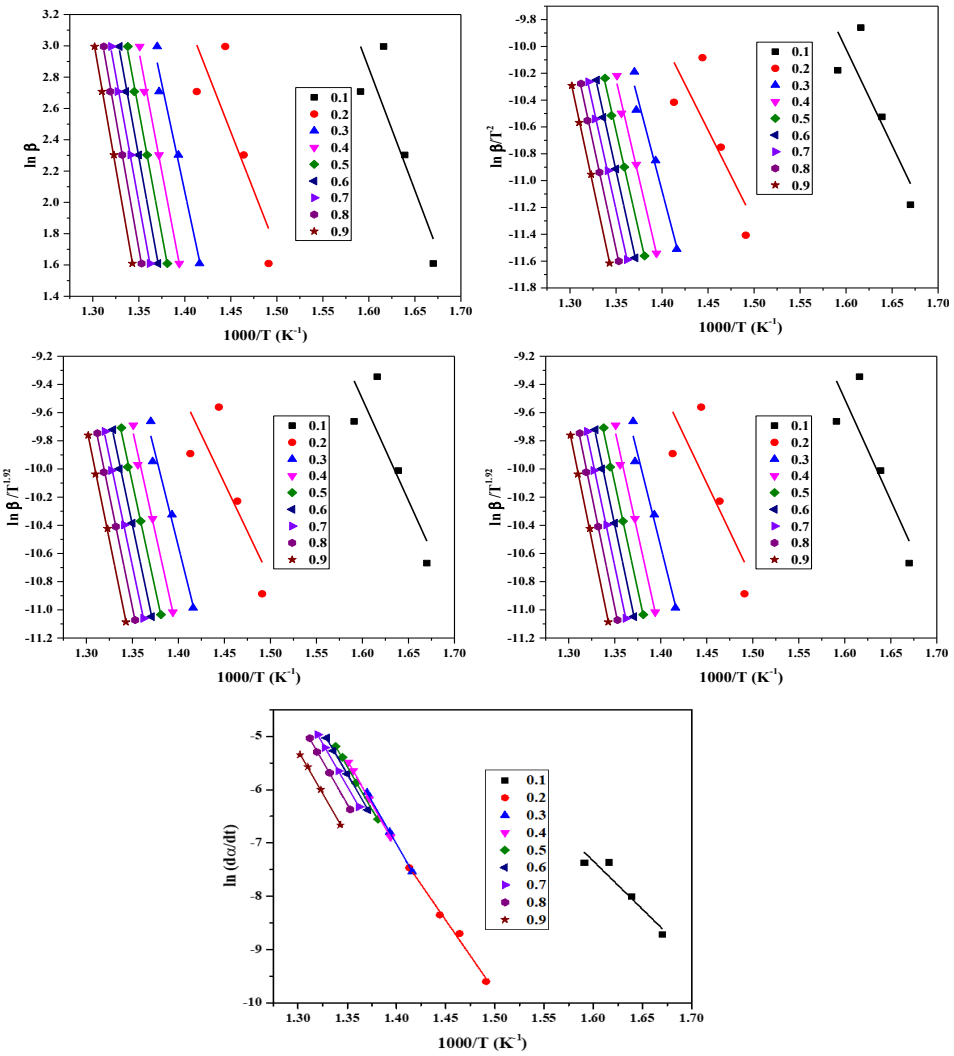

Figure 7.3: Typical linear regression lines of EVA/PEC (ECPE) using FWO, KAS, Starink, Tang and Friedman methods

Table 7.2: The energy of activation according to conversion degree for FWO, KAS, Starink, Tang, Friedman and Vyazovkin methods of ECPE composites

	FWO	KAS	Starink	Tang	Friedman	Vyazovkin
α	**E_a**					
0.1	116.12	115.80	120.35	120.48	148.87	143.89
0.2	105.68	105.11	112.87	113.01	183.27	196.35
0.3	220.50	220.38	222.30	222.45	276.31	273.36
0.4	244.96	244.86	245.48	245.63	272.34	268.45
0.5	253.91	253.81	254.52	254.68	269.17	272.94
0.6	258.03	257.94	258.61	258.76	267.43	267.89
0.7	260.81	260.72	261.28	261.44	269.69	266.66
0.8	263.12	263.02	263.64	263.80	268.36	277.55
0.9	263.88	263.79	264.34	264.50	265.76	266.98
Average	**220.78**	**220.60**	**222.60**	**222.75**	**246.80**	**248.23**

*E_a is in kJ/mol

The E_a values that result from FWO, KAS, Starink and Tang models are similar which indicates that these outcomes are comparable. However, the E_a values obtained from the Friedman method are greater than the E_a values produced using the FWO, KAS, and Starink models. This can be attributed to the absence of the assumptions while doing the calculations for Friedman method.

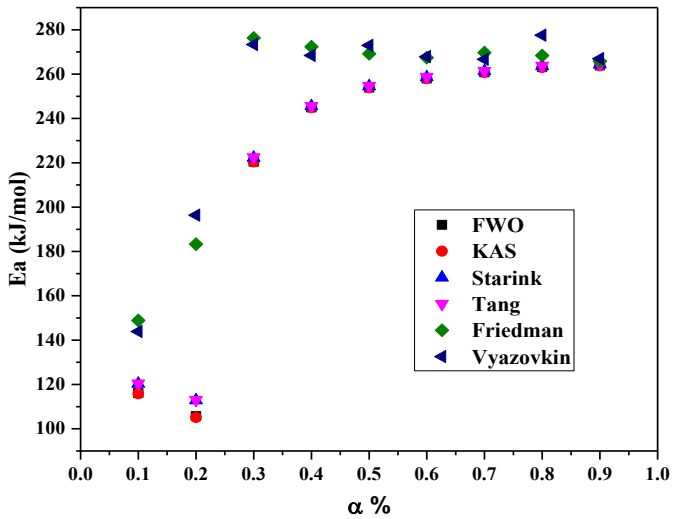

Figure 7.4: Activation energy (E_a) vs conversion (α) profiles of EVA/PEC (ECPE) using FWO, KAS, Starink, Tang, Friedman and Vyazovkin method

Throughout the whole range of conversion, the kinetic data exhibited a rise in the E_a values with the progression of α indicating the degradation to pass through multiple steps rather than a single step.

7.4. Thermodynamic Properties

The thermodynamic parameter values ΔG, ΔH, and ΔS were determined using the E_a values that were obtained using the kinetic models. These values indicate towards the feasibility of the degradation reaction.

Table 7.3: Pre-exponential factor and other thermodynamic parameters for all EVA/PEC samples obtained by using activation energy deduced from FWO, KAS, Friedman and Vyazovkin methods.

	α	Pre-exponential factor, A (s^{-1})	Enthalpy, ΔH (kJ/mol)	Gibbs free energy, ΔG (kJ/mol)	Entropy, ΔS (J /mol)
FWO	**0.1**	6.08E+06	113.42	297.18	-564.38
	0.2	1.64E+05	102.38	339.26	-596.06
	0.3	2.94E+13	216.90	407.02	-438.80
	0.4	1.52E+15	241.27	421.73	-406.20
	0.5	6.30E+15	250.16	428.15	-394.51
	0.6	1.21E+16	254.24	431.89	-389.17
	0.7	1.90E+16	256.98	434.77	-385.51
	0.8	2.81E+16	259.24	437.38	-382.34
	0.9	3.29E+16	259.96	439.62	-381.13
	Average	**1.11E+16**	**217.17**	**404.11**	**-437.57**
KAS	**0.1**	5.11E+06	113.09	297.32	-565.84
	0.2	9.46E+04	101.80	340.51	-600.65
	0.3	3.24E+13	216.78	406.55	-438.00
	0.4	1.68E+15	241.17	421.26	-405.37
	0.5	6.92E+15	250.06	427.70	-393.73
	0.6	1.33E+16	254.14	431.43	-388.39
	0.7	2.09E+16	256.88	434.32	-384.72
	0.8	3.08E+16	259.15	436.93	-381.57

	0.9	3.61E+16	259.87	439.16	-380.35
	Average	**1.22E+16**	**216.99**	**403.91**	**-437.62**
Friedman	**0.1**	2.00E+09	146.16	314.23	-516.18
	0.2	2.32E+10	179.97	377.67	-497.49
	0.3	2.06E+17	272.71	430.93	-365.17
	0.4	1.17E+17	268.65	433.07	-370.09
	0.5	7.50E+16	265.42	434.12	-373.92
	0.6	6.04E+16	263.64	435.19	-375.81
	0.7	9.31E+16	265.85	437.56	-372.30
	0.8	8.09E+16	264.48	438.52	-373.55
	0.9	5.81E+16	261.84	439.27	-376.40
	Average	**7.67E+16**	**243.19**	**415.62**	**-402.32**
Vyazovkin	**0.1**	8.15E+08	141.18	311.68	-523.66
	0.2	2.50E+11	193.04	382.89	-477.71
	0.3	5.82E+16	269.76	432.54	-375.68
	0.4	1.33E+17	264.75	428.71	-369.04
	0.5	6.17E+16	269.19	438.63	-375.54
	0.6	5.40E+16	264.10	436.08	-376.75
	0.7	3.26E+17	262.83	429.73	-361.88
	0.8	6.41E+16	273.68	448.62	-375.48
	0.9	8.53E+16	263.06	438.98	-373.21
	Average	**8.69E+16**	**244.62**	**416.43**	**-401.00**

The A values for all of the models were between 10^4 and 10^{17} s^{-1}. The wide range between these values signify that the pyrolysis of the composite is a complicated process.

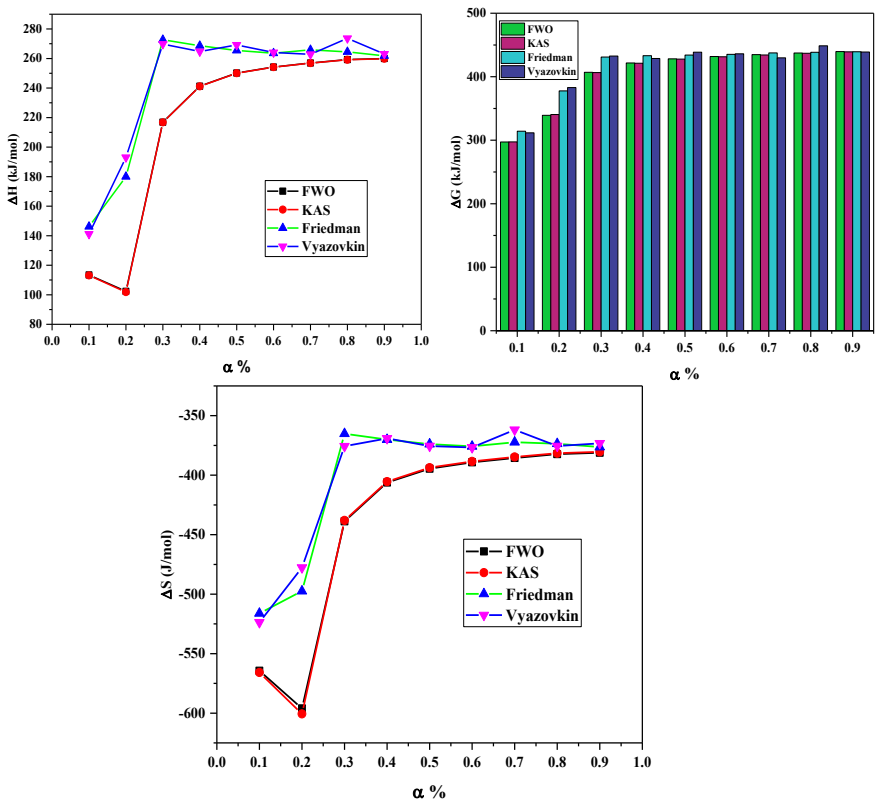

Figure 7.5: Change in enthalpy, change in Gibbs free energy and change in entropy with conversion profiles respectively of EVA/PEC

The ΔH values range from 100 kJ/mol to 275 kJ/mol for the developed ECPE composites. The fact that all α have positive enthalpy values supports the idea that pyrolysis is an endothermic process that requires heat energy to proceed. Further, the change in Gibbs free energy ranges between 290 kJ/mol and 450 kJ/mol from all the isoconversional methods. Also, the positive ΔG values indicates that

the pyrolysis is an endothermic reaction which entails a driving force to complete the process. The ΔS values range between -360 J/mol to -600 J/mol. The negative ΔS values of the process means the formation if active complexes.

The calculated thermodynamic parameters implies that pyrolysis of the composites is extremely feasible and is a complex process.

7.5. Mechanical Properties

The mechanical properties of the composites are analysed by the tensile studies on them using the universal testing machine (UTM). As with the other composites, the tensile strength is lesser than neat EVA. However, the EVA/PEC composites show a parabolic nature.ie, there is a subsequent increase and then decrease with the amount of the filler.

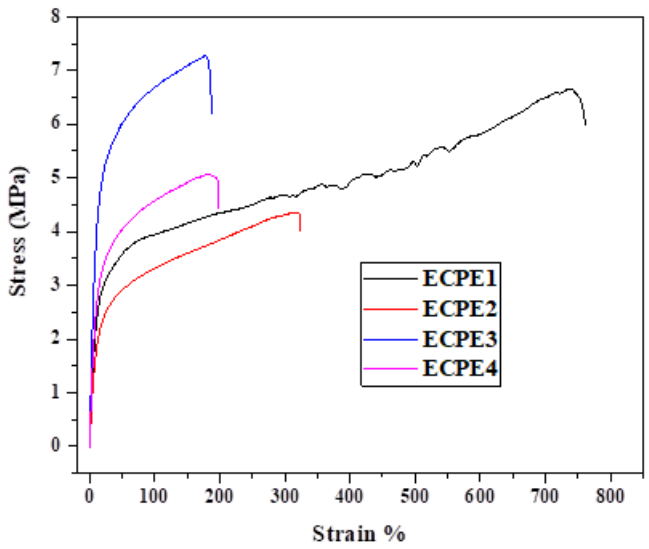

Figure 7.6: Stress-strain behavior of EVA/PEC composites

Table 7.4: Tensile strength, elongation at break, and Young's modulus of EVA/PEC (ECPE) composites

Composite	TS at break (MPa)	Elongation at break %	Young's Modulus (MPa)
ECPE1	6.66 ± 0.35	698 ± 5.3	33.28 ± 1.36
ECPE2	4.36 ± 0.36	319 ± 4.1	25.93 ± 1.64
ECPE3	7.27 ± 0.44	267 ± 5.3	51.92 ± 4.56
ECPE4	5.07 ± 0.81	243 ± 4.1	37.10 ± 6.11
EVA0	27.22	-	-

The drop in the tensile strength and Young's modulus for the highest filler content can be attributed to the agglomeration of the filler. The decrease in the elongation at break for higher filler contents indicates that addition of PEC imparts a stiffer nature to the composite. This trend is similar to those composites with cellulosic fillers which tend to reduce the amorphous nature of the EVA matrix (Aragão Melo *et al.*, 2018; Shelenkov, Pantyukhov and Popov, 2020) .

Chapter 8
Conclusions

Polymer composites have become an integral part from house hold materials to instruments used for space technology applications. Detailed investigation of such ubiquitous materials is the need of the hour. This section summarizes the overall behaviour of the developed EVA based composites presented throughout the thesis.

The development of EVA with modified chitosan and studying the thermal degradation and mechanical properties is the main objective of the present study. The work evolves from synthesizing the grafts, analysing their degradation kinetics, using the said grafts as fillers in the EVA composites and finishing off by studying the mechanical, thermal degradation kinetics, thermodynamic parameters of the thus developed composites.

8.1. Thermal degradation kinetics of the EVA composites

Thermal degradation measurements of the composites were carried out using thermogravimetric analyzer in nitrogen atmosphere. The samples were heated from ambient temperature to 600 °C at four heating rates (β) of 5, 10, 15 and 20°C/min. Four heating rates were used for the analysis so that the values obtained can be reliable. To assess the kinetic parameters six "model free" multiple heating rate methods viz, FWO, KAS, Starink, Tang, FR and Vyazovkin. The table shows the E_a values w.r.t a for the differential FWO and integral Friedman methods.

It can be noted that the E_a values from FR is slightly on the higher side which is due to the lack of approximations and also due to the presence of experimental noise during the calculation of E_a with FR method.

During the course of the thesis, all the composites underwent a multi-step degradation mechanism which is evident from the E_a values and also from the graphs obtained by plotting the same vs conversion (α). Thus, the assumption of multiple single - step kinetics, each of which is associated with a certain extent of conversion aka iso-conversion can be concluded as a better method to determine the thermal degradation/pyrolysis of complex systems.

The overall degradation process goes through similar thermodynamics. The large part of the ΔH values is positive indicating the requirement of heat energy to proceed which insinuates the process to be endothermic. The positive values of ΔG implies that the degradation process to be an endergonic reaction entailing a driving force to complete the process. Further, the negative ΔS values of the process means the formation of active complexes during the thermal degradation.

Table 8.1 shows the values of kinetic and thermodynamic parameters of degradation at α= 0.5. It can be observed that at 50 % conversion, the composites show high activation energy values along with the thermodynamic parameters. Among the developed composites those with chitosan-g-HEMA (ECHM) shows lower values of kinetic and thermodynamic parameters making them the least thermally stable composites of the lot. Also, ECP has better thermal stability and higher values of E_a, ΔH, ΔG and ΔS.

Table 8.1: Kinetic and thermodynamic parameters for α = 0.5 as derived from FWO and Friedman methods

Composite Name	FWO				Friedman			
	Activation energy, E_a (kJ/mol)	Enthalpy, ΔH (kJ/mol)	Gibbs free energy, ΔG (kJ/mol)	Entropy, ΔS (J /mol)	Activation energy, E_a (kJ/mol)	Enthalpy, ΔH (kJ/mol)	Gibbs free energy, ΔG (kJ/mol)	Entropy, ΔS (J /mol)
EVA	314.68	310.90	452.28	-310.85	330.31	326.52	458.91	-291.07
EC3	345.70	341.91	463.51	-267.00	351.70	276.46	395.97	-262.42
ECP4	258.27	254.50	431.80	-390.25	280.24	276.47	440.19	-360.36
ECMM4	251.89	248.13	427.71	-397.00	275.79	272.03	437.59	-366.01
ECHM3	194.14	190.41	404.39	-476.66	273.32	269.59	435.40	-369.36
ECPE3	253.91	250.16	428.15	-394.51	269.17	265.42	434.12	-373.92

8.2. Mechanical Properties

The values of the tensile properties of the formed composites depended mainly on the concentration and the nature of the fillers. The general trend observed was that the properties increased with the increase of the filler quantity. The elongation values though mainly indicated the influence of the nature of EVA matrix. Overall, the composites showed a good mechanical stability wherein these composites can be used for various applications. Table 8.2 depicts the values of tensile strength and Young's modulus of the best candidates among the developed composites.

Table 8.2: Tensile strength and Young's modulus values of developed composites

Composite Name	Tensile strength (MPa)	Young's modulus (MPa)
EVA	27.22	-
EC3	13.95 ± 0.48	28.40 ± 3.27
ECP4	16.57 ± 0.89	25.26 ± 6.21
ECMM4	13.13 ± 2.47	69.58 ± 7.49
ECHM3	5.70 ± 0.50	22.86 ± 5.74
ECPE3	7.27 ± 0.44	51.92 ± 4.56

8.3. Dielectric Properties of ECPS composites

The composites with polyaniline grafted chitosan as fillers were investigated in particular for their dielectric properties. A decrease in dielectric constant with increase in frequency can be observed. Also, the presence of EVA confines the free discharge of charge carriers indicating the lower dielectric behaviour of the composites.

In short, the impact of the present work is significant not only in finding kinetic data of different EVA composites, but also, it is very much relevant to design methods for alternate management of plastic waste by approaching them with ample inferences for waste management and energy production.

With the combination of experimental and mathematical advances the accuracy and intricacy of the results obtained allows for the developing, analysing, and application of pyrolysis kinetic models. The studies of this work further help in reducing the waste disposal (land-filling) by providing an alternative end-of-life route.

Chapter 9

Recommendations

The present research work opens a broad arena for future researchers to explore other aspects of EVA/Chitosan based composite materials.

- The kinetic information of the thermal behaviour and degradation would be very helpful in developing cost effective industrial applications and also to get basic insight into the different parameters that helps in developing materials with better thermal characteristics.

- The developed composites in can be explored more towards an alternate waste management process.

- Additionally, the composites developed can be investigated towards their application in flame retardancy and food packaging.

- It has been reported that the composite with chitosan/ modified chitosan as filler show biological activity. Hence the developed composites can be evaluated for their anti-microbial and cytotoxic nature. Also, composites with Polyelectrolyte complexes as fillers can be used towards drug delivery applications

- Furthermore, composite with a compatibiliser such as ethyl acrylic acid (EAA) can be developed and investigated for their EMI shielding properties.

References

References

Abbasian, M. *et al.* (2017) 'Grafting of aniline derivatives onto chitosan and their applications for removal of reactive dyes from industrial effluents', *International Journal of Biological Macromolecules*, 95, pp. 393–403. Available at: https://doi.org/10.1016 /j.ijbiomac .2016.11.075.

Aboughaly, M. *et al.* (2023) 'Enhancing the Potential of Polymer Composites Using Biochar as a Filler: A Review', *Polymers*, 15(19). doi:10.3390/polym15193981.

Agarwal Professor, R., Chaudhary Associate Professor, M. and Singh, J. (2015) 'Waste Management Initiatives in India for Human Well Being', *European Scientific Journal, ESJ*, 7881(June), pp. 1857–7881. Available at: https://eujournal.org/index.php/ esj/article/ view/5715.

Ahmad, M.S. *et al.* (2017) 'Kinetic analyses and pyrolytic behavior of Para grass (Urochloa mutica) for its bioenergy potential', *Bioresource Technology*, 224, pp. 708–713. doi:10.1016/j.biortech.2016.10.090.

Ahn, J.S., Choi, H.K. and Cho, C.S. (2001) 'A novel mucoadhesive polymer prepared by template polymerization of acrylic acid in the presence of chitosan', *Biomaterials*, 22(9), pp. 923–928. doi:10.1016/S0142-9612(00)00256-8.

Al-Allaq, E.S., Al-Lami, H.S. and Al-Mowali, A.H. (2019) 'Synthesis and Thermal Stability with Microstructure Study of some Chitosan-Dicarboxylic Acids Grafted Copolymers', *Iraqi Journal of Polymers*, 23(1), pp. 1–15.

Aragão Melo, A.R. *et al.* (2018) 'The effect of modified cellulose particles on morphology and properties ethylene vinyl acetate copolymer', *Polymer Testing*, 68, pp. 333–339. Available at: https://doi.org/10.1016/j.polymertesting.2018.04.012.

Arda, B., Bal, A. and Acar, I. (2017) 'Characterization of the thermal oxidative degradation kinetics of thermoplastics', *Instrumentation Science and Technology*, 45(5), pp. 558–576. Available at: https://doi.org/10.1080/10739149.2017.1278705.

Ashley, N. *et al.* (2021) 'Effect of polyaniline on the structural, conductivity, and dielectric properties of chitosan', *Carbohydrate Polymer Technologies and Applications*, 2, p. 100129. Available at: https://doi.org/10.1016/j.carpta.2021.100129.

Azizi, S. *et al.* (2018) 'Electrical and thermal conductivity of ethylene vinyl acetate composite with graphene and carbon black filler', *Polymer Testing*, 72, pp. 24–31. Available at: https://doi.org/10.1016/j.polymertesting. 2018.09.031.

Bakar, N.A. *et al.* (2015) 'Thermal and dynamic mechanical properties of grafted kenaf filled poly (vinyl chloride)/ethylene vinyl acetate composites', *Materials and Design*, 65, pp. 204–211. Available at: https://doi.org/10.1016/j.matdes.2014.09.027.

Bari, S.S. and Mishra, S. (2017) 'Effect of calcium sulphate nanorods on mechanical properties of chitosan-hydroxyethyl methacrylate (HEMA) copolymer nanocomposites', *Carbohydrate Polymers*, 157, pp. 409–418. doi:10.1016/j.carbpol.2016.09.083.

Barkane, A. *et al.* (2019) 'Dielectric Properties of Ethylene Vinyl Acetate Copolymer Composites Filled with Carbon Nanotubes , Graphene Nanoplatelets and Iron Oxide Nanoparticles', 800, pp. 195–199. Available at: https://doi.org/10.4028/www.scientific.net/KEM.800.195.

Bee, S. *et al.* (2013) 'Nuclear Instruments and Methods in Physics Research B Investigation of nano-size montmorillonite on electron beam irradiated flame retardant polyethylene and ethylene vinyl acetate blends', *Nuclear Inst. and Methods in Physics Research, B*, 299, pp. 42–50. Available at: https://doi.org/10.1016/j.nimb.2013.01.040.

Berthet, M.A. *et al.* (2015) 'Sustainable food packaging: Valorising wheat straw fibres for tuning PHBV-based composites properties', *Composites Part A: Applied Science and Manufacturing*, 72, pp. 139–147. Available at: https://doi.org/10.1016/j.compositesa. 2015.02.006.

Bhagabati, P. (2020) *Biopolymers and biocomposites-mediated sustainable high-performance materials for automobile applications*, *Sustainable Nanocellulose and Nanohydrogels from Natural Sources*. INC. Available at: https://doi.org/10.1016/B978-0-12-816789-2.00009-2.

Bhuyan, B., Srivastava, S.K. and Mittal, V. (2017) 'Ethylene-co-Vinyl Acetate/MWCNTs/Hectorite Elastomeric Nanocomposites: Characterization and Electrical Properties', *Journal of Nanoscience and Nanotechnology*, 18(6), pp. 4057–4064. doi:10.1166/jnn.2018. 15029.

Bonilla, J., Salazar, R.P. and Mayorga, M. (2019) 'Kinetic triplet of Colombian sawmill wastes using thermogravimetric analysis', *Heliyon*, 5(10), p. e02723. Available at: https://doi.org/10.1016/j.heliyon. 2019.e02723.

Cai, W. *et al.* (2020) 'Experimental and numerical simulation of phase change process for paraffin/expanded graphite/ethylene-vinyl acetate ternary composite', *Applied Thermal Engineering*, 169, p. 114896. Available at: https://doi.org/10.1016/j.applthermaleng.2019.114896.

Carmona, A.R. and Colorado Lopera, H.A. (2022) 'A new composite made from Luffa Cylindrica and ethylene vinyl acetate (EVA): Mechanical and structural characterization for its use as Mouthguard (MG)', *Journal of the Mechanical Behavior of Biomedical Materials*, 126. Available at: https://doi.org/10.1016/j.jmbbm.2021.105064.

Çepelioğullar, Ö. *et al.* (2018) 'Activation energy prediction of biomass wastes based on different neural network topologies', *Fuel*, 220(February), pp. 535–545. Available at: https://doi.org/10.1016/j.fuel.2018.02.045.

Chaudhuri, S. and Chakraborty, R. (2013) 'Optimization of biodegradation of natural fiber (Chorchorus capsularis): HDPE composite using response surface methodology', pp. 865–875. Available at: https://doi.org/10.1007/s13726-013-0185-8.

Chen, G. *et al.* (2017) 'Comparison of kinetic analysis methods in thermal decomposition of cattle manure by themogravimetric analysis', *Bioresource Technology*, 243, pp. 69–77. Available at: https://doi.org/10.1016/j.biortech.2017.06.007.

Chen, J. *et al.* (2022) 'Facile Preparation of Chitosan-Based Composite Film with Good Mechanical Strength and Flame Retardancy', pp. 1–12.

Chen, Z. *et al.* (2019) 'Investigations on Cunninghamia Lanceolate Cedar Wood Pyrolysis by Thermogravimetric-Fourier Transform Infrared Analysis and a Modified Discrete Distributed Activation Energy Model Kinetic Method', *Energy and Fuels*, 33(12), pp. 12499–12507. Available at: https://doi.org/10.1021/acs. energyfuels. 9b03059.

Cheng, X.W. *et al.* (2019) 'A bio-resourced phytic acid/chitosan polyelectrolyte complex for the flame retardant treatment of wool fabric', *Journal of Cleaner Production*, 223, pp. 342–349. Available at: https://doi.org/10.1016/j.jclepro.2019.03.157.

Dehouche, N., Kaci, M. and Kaid, N. (2019) 'Thermo-mechanical recycling effects on morphology and properties of ethylene vinyl acetate copolymer/olive husk flour composites', *International Journal of Plastics Technology*, 23(2), pp. 246–252. Available at: https://doi.org/10.1007/s12588-019-09256-1.

Esmizadeh, E., Tzoganakis, C. and Mekonnen, T.H. (2020) 'Degradation behavior of polypropylene during reprocessing and its biocomposites: Thermal and oxidative degradation kinetics', *Polymers*, 12(8). Available at: https://doi.org/10.3390/POLYM12081627.

Farrell, C. *et al.* (2021) 'Pyrolysis Kinetic Modeling of a Poly(ethylene-co-vinyl acetate) Encapsulant Found in Waste Photovoltaic Modules', *Industrial and Engineering Chemistry Research*, 60(37), pp. 13492–13504. doi:10.1021/acs.iecr.1c01989.

Formela, K. *et al.* (2018) 'Reactive extrusion of bio-based polymer blends and composites–current trends and future developments', *Express Polymer Letters*, 12(1), pp. 24–57. Available at: https://doi.org/10.3144/expresspolymlett.2018.4.

George, J.J., Bhadra, S. and Bhowmick, A.K. (2010) 'Influence of Carbon-Based Nanofillers on the Electrical and Dielectric Properties of Ethylene Vinyl Acetate Nanocomposites'. Available at: https://doi.org/10.1002/pc.

Gharsallah, A. *et al.* (2021) 'Thermal degradation kinetics of Opuntia Ficus Indica flour and talc-filled poly (lactic acid) hybrid biocomposites by TGA analysis', *Journal of Composite Materials*, 55(22), pp. 3099–3118. Available at: https://doi.org/10.1177/00219983211008202.

Guo-hui, W. *et al.* (2019) 'Enhancement of flame retardancy and radiation shielding properties of ethylene vinyl acetate based radiation shielding composites by EB irradiation', *Progress in Nuclear Energy*, 112(July 2018), pp. 225–232. Available at: https://doi.org/10.1016/j.pnucene.2019.01.001.

Haile, M. *et al.* (2015) 'SC', *Polymer Degradation and Stability* [Preprint]. Available at: https://doi.org/10.1016/j.polymdegradstab.2015.01.022.

Hamadache, H. *et al.* (2019) 'Different compatibility approaches to improve the thermal and mechanical properties of EVA/starch composites', *Polymer Composites*, 40(8), pp. 3242–3253. Available at: https://doi.org/10.1002/pc.25179.

Hamid, Y., Svoboda, P. and Svobodova, D. (2020) 'Influence of Electron Beam Irradiation on High-Temperature Mechanical Properties of Ethylene Vinyl Acetate/Carbon Fibers Composites', *Journal of Vinyl and Additive Technology*, 26(3), pp. 325–335. Available at: https://doi.org/10.1002/vnl.21747.

Hamman, J.H. (2010) 'Chitosan based polyelectrolyte complexes as potential carrier materials in drug delivery systems', *Marine Drugs*, 8(4), pp. 1305–1322. Available at: https://doi.org/10.3390/md8041305.

Han, H. *et al.* (2022) 'Flexible Ethylene-vinyl Acetate Copolymer/Fluorographene Composite Films with Excellent Thermal Conductive and Electrical Insulation Properties for Thermal Management', *ES Materials and Manufacturing*, 15, pp. 53–64. Available at: https://doi.org/10.30919/esmm5f523.

Hanif, M.P.M. *et al.* (2017) 'Effect of oxidation agent on wood biomass in ethylene vinyl acetate conductive polymer: Tensile properties, tensile fracture surface and electrical properties', *Journal of Physics: Conference Series*, 908(1). Available at: https://doi.org/10.1088/1742-6596/908/1/012008.

Hemalatha, R. *et al.* (2011) 'Synthesizing and characterization of chitosan graft co polymer: adsorption studies for Cu (II) and Cr (VI)', *International Journal of Environmental Sciences*, 2(2), pp. 805–828. doi:10.6088/ijes.00202020041.

Heydari, M., Rahman, M. and Gupta, R. (2015) 'Kinetic study and thermal decomposition behavior of lignite coal', *International Journal of Chemical Engineering*, 2015. Available at: https://doi.org/ 10.1155/2015/481739.

Hobson, J. *et al.* (2022) 'Synergistic Effect of Cerium Oxide for Improving the Fire-Retardant, Mechanical and Ultraviolet-Blocking Properties of EVA/Magnesium Hydroxide Composites', *Materials*, 15(17). Available at: https://doi.org/10.3390/ma15175867.

Hosseini, S.H., Simiari, J. and Farhadpour, B. (2009) 'Chemical and Electrochemical Grafting of Polyaniline onto Chitosan', 18(1), pp. 3–13.

Jena, D.P. *et al.* (2021) 'Structural, thermal and dielectric behavior of two-dimensional layered Ti3C2Tx(MXene) filled ethylene–vinyl acetate (EVA) nanocomposites', *Journal of Materials Science: Materials in*

Electronics, 32(6), pp. 8081–8091. Available at: https://doi.org/ 10.1007 /s10854-021-05531-3.

Jeraal, M.I. *et al.* (2019) 'Assessment of the Thermal Degradation of Sodium Lauroyl Isethionate Using Predictive Isoconversional Kinetics and a Temperature-Resolved Analysis of Evolved Gases', *Industrial and Engineering Chemistry Research*, 58(19), pp. 8112–8122. Available at: https://doi.org/10.1021/acs.iecr.9b00797.

Kaur, D. *et al.* (2021) 'Dielectric Properties of ZnO-Based Nanocomposites and Their Potential Applications', *International Journal of Optics*, 2021. Available at: https://doi.org/10.1155/2021/9950202.

Kaur, R. *et al.* (2018) 'Pyrolysis kinetics and thermodynamic parameters of castor (Ricinus communis) residue using thermogravimetric analysis', *Bioresource Technology*, 250, pp. 422–428. Available at: https://doi.org/10.1016/j.biortech.2017.11.077.

Khairkar, S.R. and Raut, A.R. (2014) 'Synthesis of Chitosan-graft-Polyaniline-Based Composites', *American Journal of Materials Science and Engineering*, 2(4), pp. 62–67. doi:10.12691/ajmse-2-4-3.

Koga, N. *et al.* (2023) 'ICTAC Kinetics Committee recommendations for analysis of thermal decomposition kinetics', *Thermochimica Acta*, 719(October 2022). Available at: https://doi.org/10.1016/ j.tca.2022.179384.

Laoutid, F. *et al.* (2019) 'Synergistic flame-retardant effect between lignin and magnesium hydroxide in poly(ethylene-co-vinyl acetate)', *Flame Retardancy and Thermal Stability of Materials*, 2(1), pp. 9–18. Available at: https://doi.org/10.1515/flret-2019-0002.

Laoutid, F. *et al.* (2021) 'Calcium carbonate and ammonium polyphosphate flame retardant additives formulated to protect ethylene vinyl acetate copolymer against fire: Hydrated or carbonated calcium?', *Journal of Vinyl and Additive Technology*, 27(2), pp. 264–274. Available at: https://doi.org/10.1002/vnl.21800.

Lazzari, L.K. *et al.* (2022) 'Thermal Degradation Kinetics and Lifetime Prediction of Cellulose Biomass Cryogels Reinforced by its Pyrolysis Waste', *Materials Research*, 25, pp. 11–13. Available at: https://doi.org/10.1590/1980-5373-MR-2021-0455.

Lebreton, L.C.M. *et al.* (2017) 'River plastic emissions to the world ' s oceans', *Nature Communications*, 8, pp. 1–10. Available at: https://doi.org/10.1038/ncomms15611.

Lestari, U.R., Priambodo, G. and Nurhajati, D.W. (2021) 'EVA/starch/POE composite for footwear material: How the chemical composition affects its properties compared to standards', *Majalah Kulit, Karet, dan Plastik*, 37(2), p. 115. Available at: https://doi.org/ 10.20543/mkkp.v37i2.7449.

Lu, Y. *et al.* (2020) 'Chinese Journal of Chemical Engineering TiO 2 - incorporated polyelectrolyte composite membrane with transformable hydrophilicity / hydrophobicity for nano fi ltration separation', 28, pp. 2533–2541.

Luo, L. *et al.* (2020) 'Insight into Pyrolysis Kinetics of Lignocellulosic Biomass: Isoconversional Kinetic Analysis by the Modified Friedman Method', *Energy and Fuels*, 34(4), pp. 4874–4881. Available at: https://doi.org/10.1021/acs.energyfuels.0c00275.

Ma, D.X. *et al.* (2022) 'ZIF-67 In Situ Grown on Attapulgite: A Flame Retardant Synergist for Ethylene Vinyl Acetate/Magnesium Hydroxide Composites', *Polymers*, 14(20). Available at: https://doi.org/10.3390/polym14204408.

Makhetha, T.A., Mpitso, K. and Luyt, A.S. (2017) 'Preparation and characterization of EVA/PLA/sugarcane bagasse composites for water purification', *Journal of Composite Materials*, 51(9), pp. 1169–1186. Available at: https://doi.org/10.1177/ 002199 8316675399.

Manoj, M. *et al.* (2021) 'Composites based on poly(ethylene-co-vinyl acetate) and silver-calcined scallop shell powder: Mechanical, thermal, photocatalytic, and antibacterial properties', *Journal of Elastomers and Plastics*, 53(7), pp. 902–921. Available at: https://doi.org/10.1177/0095244321996396.

Di Maro, M. *et al.* (2020) 'Influence of chitosan on the mechanical and biological properties of HDPE for biomedical applications', *Polymer Testing*, 91, p. 106610. Available at: https://doi.org/10.1016/ j.polymertesting.2020.106610.

Matta, S. *et al.* (2021) 'Investigation of different types of biochar on the thermal stability and fire retardance of ethylene-vinyl acetate

copolymers', *Polymers*, 13(8). Available at: https://doi.org/10.3390/polym13081256.

Meka, V.S. *et al.* (2017) 'A comprehensive review on polyelectrolyte complexes', *Drug Discovery Today*, 22(11), pp. 1697–1706. Available at: https://doi.org/10.1016/j.drudis.2017.06.008.

Mishra, G., Kumar, J. and Bhaskar, T. (2015) 'Kinetic studies on the pyrolysis of pinewood', *Bioresource Technology*, 182, pp. 282–288. Available at: https://doi.org/10.1016/j.biortech.2015.01.087.

Monika, Mulchandani, N. and Katiyar, V. (2019) 'Generalized kinetics for thermal degradation and melt rheology for poly (lactic acid)/poly (butylene succinate)/functionalized chitosan based reactive nanobiocomposite', *International Journal of Biological Macromolecules*, 141, pp. 831–842. doi:10.1016/j.ijbiomac.2019.09.058

Moradkhani, G. *et al.* (2020) 'Phosphorization of exfoliated graphite for developing flame retardant ethylene vinyl acetate', *Integrative Medicine Research*, 9(4), pp. 7341–7353. Available at: https://doi.org/10.1016/j.jmrt.2020.04.085.

Naqvi, S.R. *et al.* (2018) 'Pyrolysis of high-ash sewage sludge: Thermo-kinetic study using TGA and artificial neural networks', *Fuel*, 233(February), pp. 529–538. Available at: https://doi.org/10.1016/j.fuel.2018.06.089.

Narasagoudr, S.S. *et al.* (2021) 'Thermal degradation kinetics of ethyl vanillin crosslinked chitosan/poly(vinyl alcohol) blend films for food packaging applications', *Chemical Data Collections*, 34(May), p. 100739. Available at: https://doi.org/10.1016/j.cdc.2021.100739.

Navare, K. *et al.* (2021) 'Circular economy monitoring – How to make it apt for biological cycles?', *Resources, Conservation and Recycling*, 170(February), p. 105563. Available at: https://doi.org/10.1016/j.resconrec.2021.105563.

Nikolaidis, A.K. and Achilias, D.S. (2018) 'Thermal degradation kinetics and viscoelastic behavior of poly(methyl methacrylate)/ organomodified montmorillonite nanocomposites prepared via in situ bulk radical polymerization', *Polymers*, 10(5). doi:10.3390/polym10050491.

Omastová, M., Číková, E. and Mičušík, M. (2019) 'Electrospinning of ethylene vinyl acetate/carbon nanotube nanocomposite fibers',

Polymers, 11(3). Available at: https://doi.org/10.3390/ polym1 1030550.

Oni, B.A., Oziegbe, O. and Olawole, O.O. (2019) 'Significance of biochar application to the environment and economy', Annals of Agricultural Sciences, 64(2), pp. 222–236. doi:10.1016/j.aoas.2019.12.006.

Oyatogun, G.M. *et al.* (2020) *Chitin, chitosan, marine to market*, *Handbook of Chitin and Chitosan: Volume 1: Preparation and Properties*. doi:10.1016/B978-0-12-817970-3.00011-0.

P, S.H.K. *et al.* (2019) 'B : Fluid Interfaces , Colloids , Polymers , Soft Matter , Surfactants , and Glassy Materials The Interplay Between Charge Transport and CO2 Capturing Mechanism in [EMIM][SCN] Ionic Liquid - A Broadband Dielectric Study The Interplay between Charge Tr'. Available at: https://doi.org/10.1021/acs.jpcb.9b03929.

Padhi, S., Priyadarsini, D. and Nayak, N.C. (2020) 'Materials Today : Proceedings Dielectric behaviour of ethylene vinyl acetate / cenosphere composites', *Materials Today: Proceedings* [Preprint], (xxxx). Available at: https://doi.org/10.1016/j.matpr.2020.02.693.

Pal, A.K. and Katiyar, V. (2017) 'Thermal degradation behaviour of nanoamphiphilic chitosan dispersed poly (lactic acid) bionanocomposite films', *International Journal of Biological Macromolecules*, 95, pp. 1267–1279. doi:10.1016/j.ijbiomac. 2016.11.024.

Park, J.W. *et al.* (2018) 'Evaluation of mechanical performance and flame retardant characteristics of biomass-based EVA composites using intumescent flame retardant technology', *Journal of the Korean Wood Science and Technology*, 46(2), pp. 189–201. Available at: https://doi.org/10.5658/WOOD.2018.46.2.189.

Parthasarathy, P. *et al.* (2022) 'Thermogravimetric analysis of camel dung, date stone, and their blend for pyrolytic, kinetic, and thermodynamic studies', *Cleaner Chemical Engineering*, 4(October), p. 100072. Available at: https://doi.org/10.1016/j.clce.2022.100072.

Patil, Y., Ku, X. and Vasudev, V. (2023) 'Pyrolysis Characteristics and Determination of Kinetic and Thermodynamic Parameters of Raw and Torrefied Chinese Fir', *ACS Omega* [Preprint], (2021). Available at: https://doi.org/10.1021/acsomega.3c04328.

Patwa, R. *et al.* (2019) *Kinetic modelling of thermal degradation and non-isothermal crystallization of silk nano-discs reinforced poly (lactic acid) bionanocomposites*, *Polymer Bulletin*. Springer Berlin Heidelberg. Available at: https://doi.org/10.1007/s00289-018-2434-7.

Pisal, M.H.M. *et al.* (2021) 'The role of zinc chloride in enhancing mechanical, thermal and electrical performance of ethylene vinyl acetate/carbonized wood fiber conductive composite', *Polymers*, 13(4), pp. 1–17. Available at: https://doi.org/10.3390/polym 13040600.

Poplavko, Y. (2021) *Broadband dielectric spectroscopy*, *Dielectric Spectroscopy of Electronic Materials*. doi:10.1016/b978-0-12-823518-8.00001-3.

Pracella, M. *et al.* (2016) 'Property tuning of poly(lactic acid)/cellulose bio-composites through blending with modified ethylene-vinyl acetate copolymer', *Carbohydrate Polymers*, 137, pp. 515–524. Available at: https://doi.org/10.1016/j.carbpol.2015.10.094.

Qian, Y., Jiang, K. and Li, L. (2019) 'Improving the flame retardancy of ethylene vinyl acetate composites by incorporating layered double hydroxides based on Bayer red mud', *E-Polymers*, 19(1), pp. 129–140. Available at: https://doi.org/10.1515/epoly-2019-0015.

Radhakumary, C. *et al.* (2003) 'Graft copolymerization of 2-hydroxy ethyl methacrylate onto chitosan with cerium (IV) ion. I. Synthesis and characterization', *Journal of Macromolecular Science - Pure and Applied Chemistry*, 40 A(7), pp. 715–730. Available at: https://doi.org/10.1081/MA-120021421.

Radhakumary, C. *et al.* (2005) 'Biopolymer composite of chitosan and methyl methacrylate for medical applications', *Trends in Biomaterials and Artificial Organs*, 18(2), pp. 117–124.

Radhakumary, C., Nair, P.D. and Mathew, S. (2005) 'Biopolymer Composite of Chitosan and Methyl Methacrylate Biopolymer Composite of Chitosan and Methyl Methacrylate for Medical Applications', (February 2015).

Rahaman, M., Chaki, T.K. and Khastgir, D. (2013) 'Polyaniline, ethylene vinyl acetate semi-conductive composites as pressure sensitive sensor', *Journal of Applied Polymer Science*, 128(1), pp. 161–168. Available at: https://doi.org/10.1002/app.38137.

Rumyantsev, A.M., Jackson, N.E. and Pablo, J.J. De (2021) 'Polyelectrolyte Complex Coacervates: Recent Developments and New Frontiers', pp. 155–176.

Sadeghifar, H. *et al.* (2017) 'Cellulose-Lignin Biodegradable and Flexible UV Protection Film', *ACS Sustainable Chemistry and Engineering*, 5(1), pp. 625–631. Available at: https://doi.org/10.1021/acssuschemeng.6b02003.

Saïed, N. and Aïder, M. (2014) 'Zeta Potential and Turbidimetry Analyzes for the Evaluation of Chitosan / Phytic Acid Complex Formation', 3(2), pp. 71–81. Available at: https://doi.org/10.5539/jfr.v3n2p71.

Sajjad, S. (2014) 'Synthesis and Evaluation of Chitosan-Polyaniline Copolymer in Presence of Ammonium Persulfate as Initiator', *Journal of Applied Chemical Research*, 8(1), pp. 47–54.

Santos, V.O. *et al.* (2020) 'Pyrolysis of acai seed biomass: Kinetics and thermodynamic parameters using thermogravimetric analysis', *Bioresource Technology Reports*, 12(August), p. 100553. Available at: https://doi.org/10.1016/j.biteb.2020.100553.

Sebastian, J. *et al.* (2015) 'Enhancement in the Electrical and Thermal Properties of Ethylene Vinyl Acetate (EVA) Co-Polymer by Zinc Oxide Nanoparticles', (July), pp. 79–91.

Sefadi, J.S. and Luyt, A.S. (2012) 'Morphology and properties of EVA/empty fruit bunch composites', *Journal of Thermoplastic Composite Materials*, 25(7), pp. 895–914. Available at: https://doi.org/10.1177/0892705711421806.

Sessini, V. *et al.* (2019) 'Melt-processing of bionanocomposites based on ethylene-co-vinyl acetate and starch nanocrystals', *Carbohydrate Polymers*, 208(December 2018), pp. 382–390. Available at: https://doi.org/10.1016/j.carbpol.2018.12.095.

Shahadat, M. *et al.* (2017) 'Historical perspective A critical review on the prospect of polyaniline-grafted biodegradable nanocomposite', *Advances in Colloid and Interface Science*, 249, pp. 2–16. Available at: https://doi.org/10.1016/j.cis.2017.08.006.

Sharma, S. *et al.* (2022) 'Effect of nanoadditives on the novel leather fiber/recycled poly(ethylene-vinyl-acetate) polymer composites for multifunctional applications: Fabrication, characterizations, and multiobjective optimization using central composite design',

Nanotechnology Reviews, 11(1), pp. 2366–2432. Available at: https://doi.org/10.1515/ntrev-2022-0067.

Shaw, A. V *et al.* (2019) 'The Dielectric Properties of PP-EVA-Organoclay Composites', pp. 42–45.

Shelenkov, P.G., Pantyukhov, P. V. and Popov, A.A. (2018) 'Highly filled biocomposites based on ethylene-vinyl acetate copolymer and wood flour', *IOP Conference Series: Materials Science and Engineering*, 369(1), pp. 2–7. Available at: https://doi.org/10.1088/1757-899X/369/1/012043.

Shelenkov, P.G., Pantyukhov, P. V. and Popov, A.A. (2020) 'Mechanical properties of superconcentrates based on ethylene-vinyl acetate copolymer and microcrystalline cellulose', *Materials Science Forum*, 992 MSF, pp. 306–310. Available at: https://doi.org/10.4028/www.scientific.net/MSF.992.306.

Shen, L. *et al.* (2019) 'Preparation and characterization of ethylene–vinyl acetate copolymer (EVA)–magnesium hydroxide (MH)–hexaphenoxycyclotriphosphazene (HPCTP) composite flame-retardant materials', *Polymer Bulletin*, 76(5), pp. 2399–2410. Available at: https://doi.org/10.1007/s00289-018-2500-1.

Shen, Y. *et al.* (2019) 'Solvent-free electrically conductive Ag/ethylene vinyl acetate (EVA) composites for paper-based printable electronics', *RSC Advances*, 9(34), pp. 19501–19507. Available at: https://doi.org/10.1039/c9ra02593f.

Shi, J. *et al.* (2020) 'Effect of graphene on thermal stability and mechanical properties of ethylene-vinyl acetate: A molecular dynamics simulation', *Materials Research Express*, 7(3). Available at: https://doi.org/10.1088/2053-1591/ab79cd.

Shirdel, S., Omrani, A. and Ehsani, M. (2017) 'Thermochimica Acta Non-isothermal degradation kinetics of Ethylene-Vinyl Acetate Copolymer nanocomposite reinforced with modi fi ed Bacterial Cellulose Nano fi bers using advanced isoconversional and master plot analyses', *Thermochimica Acta*, 655(May), pp. 87–93. Available at: https://doi.org/10.1016/j.tca.2017.06.014.

Singh, D.K. and Ray, A.R. (1998) 'Characterization of grafted chitosan films', *Carbohydrate Polymers*, 36(2–3), pp. 251–255. doi:10.1016/S0144-8617(97)00260-9.

Singh, G. *et al.* (2019) 'Pyrolysis kinetic study of waste milk packets using thermogravimetric analysis and product characterization', *Journal of Material Cycles and Waste Management*, 21(6), pp. 1350–1360. doi:10.1007/s10163-019-00891-9.

Soleimani, N., Vaseghi, A. and Loconte, V. (2019) 'Poliglusam Nanoparticles Activate T Cell Response in Breast Cancer Cell : an In Vivo and In Vitro Study Poliglusam Nanoparticles Activate T Cell Response in Breast Cancer Cell: an In Vivo and In Vitro Study', (July 2020). doi:10.1007/s10895-019-02423-y.

Sonia, A. and Priya Dasan, K. (2013) 'Celluloses microfibers (CMF)/poly (ethylene-co-vinyl acetate) (EVA) composites for food packaging applications: A study based on barrier and biodegradation behavior', *Journal of Food Engineering*, 118(1), pp. 78–89. Available at: https://doi.org/10.1016/j.jfoodeng.2013.03.020.

Stan, F., Stanciu, N.V. and Fetecau, C. (2017) 'Melt rheological properties of ethylene-vinyl acetate/multi-walled carbon nanotube composites', *Composites Part B: Engineering*, 110, pp. 20–31. Available at: https://doi.org/10.1016/j.compositesb.2016.10.071.

Stephy, A., Antony, A.M. and Francis, T. (2021) 'Thermal decomposition kinetics of melt-mixed ethylene-co-vinyl acetate – based bio-composites', *Materials Today Chemistry*, 21, p. 100544. Available at: https://doi.org/10.1016/j.mtchem.2021.100544.

Stephy, A., Antony, A.M. and Francis, T. (2023) 'Thermal Degradation Kinetics of Chitosan/Phytic Acid Polyelectrolyte Complex as Investigated by Thermogravimetric Analysis', *Journal of Polymers and the Environment*, 31(1), pp. 210–220. doi:10.1007/s10924-022-02621-z.

Subramanian, K. (2019) 'A Comprehensive Study on Thermal Degdradation of Selective Edible Vegetable Oils By Simultaneous Thermogravimetric and Differential Thermal Analyses', 11(9), pp. 3201–3209.

Sukhishvili, S.A., Kharlampieva, E. and Izumrudov, V. (2006) 'Where polyelectrolyte multilayers and polyelectrolyte complexes meet', *Macromolecules*, 39(26), pp. 8873–8881. Available at: https://doi.org/10.1021/ma061617p.

Sunny, M.C. *et al.* (2011) 'Porous composites of hydroxyapatite-filled poly[ethylene-co-(vinyl acetate)] for tissue engineering', *Polymer International*, 60(1), pp. 51–58. doi:10.1002/pi.2973.

Tarani, E. *et al.* (2021) 'Cold crystallization kinetics and thermal degradation of pla composites with metal oxide nanofillers', *Applied Sciences (Switzerland)*, 11(7). Available at: https://doi.org/10.3390/app11073004.

Taylor, P. *et al.* (no date) 'Journal of Macromolecular Science , Part A : Pure and Applied Chemistry Graft Copolymerization of 2-Hydroxy Ethyl Methacrylate onto Chitosan with Cerium (IV) Ion . I . Synthesis and Characterization Graft Copolymerization of 2-Hydroxy Ethyl Methacrylate', (November 2014), pp. 37–41. Available at: https://doi.org/10.1081/MA-120021421.

Thomas, A. *et al.* (2020) 'A kinetic analysis of the thermal degradation behaviours of some bio-based substrates', *Polymers*, 12(8). Available at: https://doi.org/10.3390/POLYM12081830.

Tirrell, M. (2018) 'Polyelectrolyte Complexes: Fluid or Solid?', pp. 532–533. Available at: https://doi.org/10.1021/acscentsci.8b00284.

Tiwari, A. and Singh, V. (2007) 'Synthesis and characterization of electrical conducting chitosan-graft-polyaniline', *Express Polymer Letters*, 1(5), pp. 308–317. Available at: https://doi.org/10.3144/expresspolymlett.2007.44.

Vyazovkin, S. *et al.* (2014) 'ICTAC Kinetics Committee recommendations for collecting experimental thermal analysis data for kinetic computations', *Thermochimica Acta*, 590, pp. 1–23. Available at: https://doi.org/10.1016/j.tca.2014.05.036.

Vyazovkin, S. and Sbirrazzuoli, N. (2006) 'Isoconversional kinetic analysis of thermally stimulated processes in polymers', *Macromolecular Rapid Communications*, 27(18), pp. 1515–1532. Available at: https://doi.org/10.1002/marc.200600404.

Wang, P. *et al.* (2021) 'Synergistic effect of EVA-GMA and nanofillers on mechanical and dielectric properties of polyamide', *Composites Communications*, 25(March), p. 100738. Available at: https://doi.org/10.1016/j.coco.2021.100738.

Wang, Y. *et al.* (2021) 'Stretchable and compressible conductive foam based on Cu nanowire/MWCNT/ethylene-vinyl acetate composites for high-mass-loading supercapacitor electrode', *Chemical Engineering Journal*, 417(February), p. 129176. Available at: https://doi.org/10.1016/ j.cej.2021.129176.

Wardhono, E.Y. *et al.* (2022) 'Modification of Physio-Mechanical Properties of Chitosan-Based Films via Physical Treatment Approach'.

Wojnarowska, M., Sołtysik, M. and Guzik, M. (2021) 'Socio-economic Importance of Biomaterials in the Transition to the Circular Economy Model', *SHS Web of Conferences*, 92, p. 05029. Available at: https://doi.org/10.1051/shsconf/20219205029.

Wu, W. *et al.* (2019) 'Significantly improved dielectric properties of polylactide nanocomposites via TiO2 decorated carbon nanotubes', *Composites Part A: Applied Science and Manufacturing*, 127(May). Available at: https://doi.org/10.1016/j.compositesa.2019.105650.

Xiao, N.Y. *et al.* (2020) 'Construction of EVA/chitosan based PEG-PCL micelles nanocomposite films with controlled release of iprodione and its application in pre-harvest treatment of grapes', *Food Chemistry*, 331(March), p. 127277. Available at: https://doi.org/10.1016/j.foodchem.2020.127277.

Xu, S. *et al.* (2021) 'Flame-retardant ethylene vinyl acetate composite materials by combining additions of aluminum hydroxide and melamine cyanurate: Preparation and characteristic evaluations', *Journal of Colloid and Interface Science*, 589, pp. 525–531. Available at: https://doi.org/10.1016/j.jcis.2021.01.026.

Yousef, S. *et al.* (2020) 'Pyrolysis kinetic behavior and TG-FTIR-GC–MS analysis of metallised food packaging plastics', *Fuel*, 282(July), p. 118737. Available at: https://doi.org/10.1016/j.fuel.2020.118737.

Yousef, S. *et al.* (2021) 'Pyrolysis kinetic behaviour of glass fibre-reinforced epoxy resin composites using linear and nonlinear isoconversional methods', *Polymers*, 13(10), pp. 1–18. Available at: https://doi.org/10.3390/polym13101543.

Yousef, S. *et al.* (2023) 'Pyrolysis Kinetic Behavior and Thermodynamic Analysis of PET Nonwoven Fabric', *Materials*, 16(18), p. 6079. Available at: https://doi.org/10.3390/ma16186079.

Yu, C. *et al.* (2020) *A review on the synthesis of graft copolymers of chitosan and their potential applications*, *International Journal of Biological Macromolecules*. Elsevier B.V. Available at: https://doi.org/10.1016/j.ijbiomac.2020.09.060.

Yuwawech, K., Wootthikanokkhan, J. and Tanpichai, S. (2015) 'SC', *Polymer Testing* [Preprint]. Available at: https://doi.org/10.1016/j.polymertesting.2015.09.007.

Zec, J. *et al.* (2018) 'Processing and characterization of UHMWPE composite fibres with alumina particles in poly(ethylene-vinyl acetate) matrix',

Journal of Thermoplastic Composite Materials, 31(5), pp. 689–708. Available at: https://doi.org/10.1177/0892705717718240.

Zhang, T. *et al.* (2014) 'Chitosan/phytic acid polyelectrolyte complex: A green and renewable intumescent flame retardant system for ethylene-vinyl acetate copolymer', *Industrial and Engineering Chemistry Research*, 53(49), pp. 19199–19207. Available at: https://doi.org/10.1021/ie503421f.

Zhang, X. *et al.* (2019) 'Pyrolytic behavior and kinetic of wood sawdust at isothermal and non-isothermal conditions', *Renewable Energy*, 142, pp. 284–294. Available at: https://doi.org/10.1016/ j.renene. 2019.04.115.

Zhang, X. (2021) 'Applications of kinetic methods in thermal analysis: A review', *Engineered Science*, 14, pp. 1–13. Available at: https://doi.org/10.30919/es8d1132.

Zhang, Z. *et al.* (2020) 'A facile and green strategy to enhance flame retardant and mechanical properties of poly (vinyl alcohol) simultaneously by introduction of bio-based polyelectrolyte complex formed by chitosan and phytic acid', *Dalton Transactions* [Preprint]. Available at: https://doi.org/10.1039/D0DT02019B.

Zhou, K. *et al.* (2016) 'Combination effect of MoS2 with aluminum hypophosphite in flame retardant ethylene-vinyl acetate composites', *RSC Advances*, 6(44), pp. 37672–37680. Available at: https://doi.org/ 10.1039/c6ra04861g.

Zimmermann, M.V.G. *et al.* (2014) 'Comparative study between poly(ethylene-co-vinyl acetate) - EVA expanded composites filled with banana fiber and wood flour', *Materials Research*, 17(6), pp. 1535–1544. Available at: https://doi.org/10.1590/1516-1439.269814.

Zou, D. *et al.* (2018) 'Phase Transformation and Thermal Decomposition Kinetics of a Mixed Rare Earth Concentrate', *ACS Omega*, 3(12), pp. 17036–17041. Available at: https://doi.org/10.1021/ acsomega. 8b01140.

Zubkiewicz, A. *et al.* (2020) 'Ethylene vinyl acetate copolymer/halloysite nanotubes nanocomposites with enhanced mechanical and thermal properties', *Journal of Applied Polymer Science*, 137(38), pp. 1–12. Available at: https://doi.org/10.1002/app.49135.

LIST OF PUBLICATIONS DURING THE COURSE OF PHD RESEARCH WORK

1. **Annie Stephy**, Ann Mary Antony, Tania Francis, Thermal Degradation Kinetics of Chitosan/Phytic Acid Polyelectrolyte Complex as Investigated by Thermogravimetric Analysis. *J. Polym. Environ.* **2023**, 31 (1), 210 - 220.https://doi.org/10.1007/s10924-022-02621-z.

2. **Annie Stephy**, Ann Mary Antony, Tania Francis, Thermal Decomposition Kinetics of Melt-Mixed Ethylene-Co-Vinyl Acetate – Based Bio-Composites. *Mater. Today Chem*. **2021**, 21, 100544. https://doi.org/10.1016/j.mtchem.2021.100544.

3. P. Bashpa, **Annie Stephy**, K. Bijudas, Tania Francis, Thermal degradation kinetics and solvent transport behavior of natural rubber composites filled with polyurethane rich shoe sole waste from footwear industry. *J. Therm. Anal. Calorim*. 148, 10871–10883 (**2023**).https://doi.org/10.1007/s10973-023-12425-5

4. **Annie Stephy**, Meril Shelly, Meril Mathew and Tania Francis, XRD and FESEM characterization of size controlled nanohydroxyapatite synthesized by wet precipitation technique. Full Paper: ISSN-2348-3369, Page No. 382-390

Book chapter

1. **Annie Stephy**, Neethumol Varghese, Minu Joys, Tania Francis, Ajalesh B. Nair, 2023, Application of UPR in marine applications, *Applications of Unsaturated Polyester Resins: Synthesis, Modifications, and Preparation Methods*, (pp 223-245), Elsevier. https://doi.org/10.1016/B978-0-323-99466-8.00017-4s

INTERNATIONAL/NATIONAL/STATE LEVEL CONFERENCES

1. Annie Stephy, Tania Francis, (**Oral Presentation**), International Conference of Advanced Materials (ICAM 24), Deva Matha College, Kuruvilangad. January 2024. (**Best Oral Presentation-Online**)

2. Annie Stephy, Tania Francis, (**Poster Presentation**) National Conference on Emerging Frontiers of Chemical Sciences (EFCS), Farook College, Calicut, January 2023

3. Annie Stephy has participated in the "Emerging Threat and Mitigation Opportunities in Environment, Healthcare and Security" organized by St Joseph's College, Devagiri and Intelligence Research Institute, San Diego, USA, July 2022.

4. ACS Science Talks; Science Connect: Langmuir (virtual), October 2020.

5. Annie Stephy, Tania Francis, (**Poster Presentation**), 107th Indian Science Congress, Bangalore, January 2020. (**Best Poster Award – Engineering Sciences**)

6. Annie Stephy, Tania Francis, (**Oral Presentation**) in Seminar on National Seminar on "Frontiers in Chemistry-FCS 2020", University of Calicut, January 2020.

7. National conference on "Biopolymers & Green Composites" (BPGC 2019- 6th Series) held at Kochi, January 2019

8. Annie Stephy Participated in the RUSA funded seminar "Conceptual Understanding in Quantum Mechanics" held at Department of Chemistry, St. Joseph's College (Autonomous) Devagiri, August 2019.

9. Annie Stephy, Tania Francis, (**Poster Presentation**) National Conference on "Emerging Frontiers in Chemical Sciences-EFCS" Farook College, Calicut, December 2019

10. Participated in the RUSA funded International Conference on "Frontiers of Material Science FOMS-19" held at Department of Physics, St. Joseph's College (Autonomous) Devagiri, December 2019

11. Annie Stephy, Tania Francis (**Oral Presentation**), Fourth Annual "Left of Boom Conference" held at San Diego State University in San Diego, California, May 2018

12. Annie Stephy, Meril Shelly, Tania Francis, participated in the International Conference on Emerging Frontiers in Chemical Sciences, Dept. of Chemistry, Farook College (Autonomous), Kozhikode, September, 2017.

13. Annie Stephy, Meril Shelly, Tania Francis, (**Oral Presentation**) in Seminar on National Seminar on "Frontiers in Chemistry", University of Calicut, March 2017.

14. Meril Shelly, Annie Stephy, Tania Francis, National Conference on Biopolymers and Green Composites BPGC 2017- 5^{th} in series, Centre for biopolymer science and technology (CBPST)- A unit of CIPET, Kochi, December 15-16, 2017